

**Two Novel Zebrafish Mutants Reveal Genes Necessary for
Neuronal and Muscle Function**

Jenna Lynnette Eckardt
Somerville, NJ

BS, The College of William and Mary, 2009

A Dissertation Presented to the Graduate Faculty
of the University of Virginia in Candidacy for the Degree of
Doctor of Philosophy

Department of Biology

University of Virginia
November, 2015

Table of Contents

Abstract	1
I. Introduction	3
The development of the CNS and peripheral nerve	3
<i>The domains of the spinal cord</i>	3
<i>The development of motor axons and oligodendrocytes</i>	4
<i>Myelination</i>	6
<i>The neural crest and its derivatives</i>	7
<i>The layers of a PNS nerve</i>	9
<i>Innervation at the muscle</i>	9
Origin of perineurial glia and their developmental function	11
<i>Motor ensheathing perineurium is CNS-derived</i>	12
<i>Interactions with other cell types</i>	12
<i>Perineurial signaling pathways</i>	13
ENU mutagenesis and mapping in zebrafish	14
<i>Mutagenesis screens</i>	15
<i>Mapping the mutation</i>	15
<i>Confirmation of the gene</i>	18
Development and clinical outlook of Duchenne Muscular Dystrophy	20
<i>The importance of the DAPC</i>	21
<i>Duchenne Muscular Dystrophy</i>	23
II. Methods for <i>ftl</i>^{vu268} and <i>ray</i>^{vu267} projects	25

<i>Fish husbandry</i>	25
<i>In vivo imaging</i>	25
<i>In situ RNA hybridization</i>	26
<i>Immunohistochemistry</i>	26
<i>Data quantification and statistical analysis</i>	27
<i>Bulk segregant analysis</i>	28
<i>Whole genome sequencing</i>	28
<i>Fine mapping</i>	28
<i>RT-PCR</i>	29
<i>Sectioning</i>	29
<i>Morpholino injections</i>	30
<i>Alcian blue Staining</i>	30
<i>Alkaline phosphatase stain</i>	30
<i>Ataluren treatment</i>	31
<i>Dantrolene and Gabapentin treatment</i>	31
<i>TUNEL</i>	31
III. Novel mutant (<i>ftl</i>)^{vu268} exhibits perturbed glial migration, differentiation, and survival	32
Introduction	32
Results	34
<i>The <i>ftl</i>^{vu268} mutation disrupts perineurial migration and is located on chromosome 17</i>	34
<i>Identification of the gene remains unanswered</i>	37

<i>Schwann cells fail to make myelin and undergo apoptosis</i>	42
<i>Oligodendrocytes are decreased but migration is unaffected</i>	45
<i>Motor neurons and their axons are not affected by the <i>ftl</i>^{vu268} mutation</i>	47
<i>Angiogenesis and brain development is perturbed</i>	49
Discussion	49
IV. The <i>ray</i>^{vu267} mutant defines a novel neuronal role for	53
<i>dystrophin</i> independent of muscle function	
Introduction	53
Results	57
<i>Identification of a novel mutant allele of dystrophin in zebrafish</i>	57
<i><i>ray</i>^{vu267} is a model of DMD</i>	74
<i>Loss of dystrophin leads to spinal motor nerve defects</i>	77
<i>Neural crest-derived cell populations are disrupted in <i>ray</i>^{vu267} embryos</i>	80
<i>Perturbed crestin expression occurs before muscle degeneration</i>	82
<i>Evaluating DMD drug therapies for their impact on</i>	86
<i>nervous system defects</i>	
Discussion	87
V. Discussion and Future Directions	91
Summary of <i>ftl</i>^{vu268}	91
Future Directions for <i>ftl</i>^{vu268}	92
Summary of <i>ray</i>^{vu267}	94
Future directions for <i>ray</i>^{vu267}	95
VI. References	99

Abstract

The peripheral nerve is a complex structure composed of several cell types that must interact and communicate to form a healthy nerve. The perineurium, which encloses multiple axon-Schwann cell bundles, is necessary for nerve protection and structural support, but many questions remain about its development. To that end, an ENU mutagenesis screen was performed in zebrafish using the transgene *Tg(nkx2.2a:megfp)*, a marker of perineurial glia. Two zebrafish mutants were identified in this screen: *failure to launch (ftl)^{vu268}* and *runaway (ray)^{vu267}*. These mutants have contrasting glial phenotypes: in *ftl^{vu268}* embryos, glia fail to migrate out of the spinal cord, and in *ray^{vu267}* embryos, the glia migrate ectopically and exhibit a highly branched morphology. These mutants were further characterized and mapping of their mutations was attempted using several techniques, including bulk segregant analysis, whole genome sequencing (WGS) and allele-specific PCR.

For *ftl^{vu268}*, the candidate list was narrowed to a handful of genes, but the gene was not identified. However, the newest zebrafish genome casts these previous efforts into doubt. Nevertheless, in these mutants we were still able to characterize severe glial defects, including fewer Schwann cells and oligodendrocytes and the absence of myelination in mutant larvae.

In *ray^{vu267}* embryos, the mutation was found to be located within the *dystrophin* gene on chromosome 1. Interestingly, we characterized many novel nervous system phenotypes in these mutants as well as in *sapje-like^{cl100}*

mutants, which have a different mutation in *dystrophin*. This study illustrates the importance of a healthy, functioning nervous system in muscle function of DMD patients. This dissertation reviews novel and unexpected aspects of the development of perineurial glia, and also provides a foundation for future work.

Chapter 1: Introduction

The development of the CNS and peripheral nerve

The vertebrate nervous system is a complex set of interacting groups of cells that are crucial for an individual to function properly. Its fundamental structure is constituted at the earliest stages of embryonic development. Following gastrulation, the neural plate forms as ectodermal cells dorsal to the notochord become more columnar in shape, and align in a plate. In mammals, this plate then bends and the cells converge into a tube, which eventually specializes into the brain and spinal cord (Karfunkel, 1973; Schoenwolf and Smith, 1990). In zebrafish, the process is similar, however the folding neural plate first forms a solid rod called the neural keel, and then hollows into a tube (Lowery and Sive, 2004; Papan and Campos-Ortega, 1994). This neural tube eventually develops into the brain and spinal cord.

The domains of the spinal cord

The brain and spinal cord are extensively patterned, both on the anterior-posterior axis and on the dorsal-ventral (D-V) axis, a process that is crucial to the development of many peripheral nerve components (Brown, 1981). The D-V patterning in the spinal cord is organized by opposing gradients of morphogens. The notochord expresses the morphogen *shh*, while *bmp4* and *wnt1/3a* are expressed in the overlying ectoderm (Echelard et al., 1993; Krauss et al., 1993).

The relative concentration of these factors induces the expression of various transcription factors in neural precursors, which interact to delineate domain boundaries. These transcription factors also specify unique cell populations (Briscoe et al., 2000). In the ventral spinal cord, a strong Shh signal instructs the cells to form a structure called the floor plate, which can be subdivided into three columns of cells, two lateral and one medial (Chiang et al., 1996; Ericson et al., 1996; Martí et al., 1995). The domain immediately dorsal to the floorplate is the pMN domain. Both domains are important for the development of the peripheral nerve (Figure 1-1 A).

The development of motor axons and oligodendrocytes

Motor neurons and oligodendrocyte precursor cells (OPCs) are specified from the same progenitor population of neural stem cells within in the pMN domain of the spinal cord (Richardson et al., 2000). For this reason, both cell types are labeled with the marker *olig2* (Zhou and Anderson, 2002). This process is temporally regulated: first neurons are produced, then later glia are produced. Motor neuron cell bodies remain within the pMN domain but send their axons through exit points called motor exit point (MEP) transition zones (TZ) and into the periphery, where they pathfind to their targets in the muscle (Figure 1-1 B).

Oligodendrocyte precursor cells undergo a complex developmental time course to reach maturity. OPCs are bipolar, highly migratory and proliferative cells, which can be identified by markers like *sox10*, *pdgfa* and *ng2* (Pfeiffer et al.,

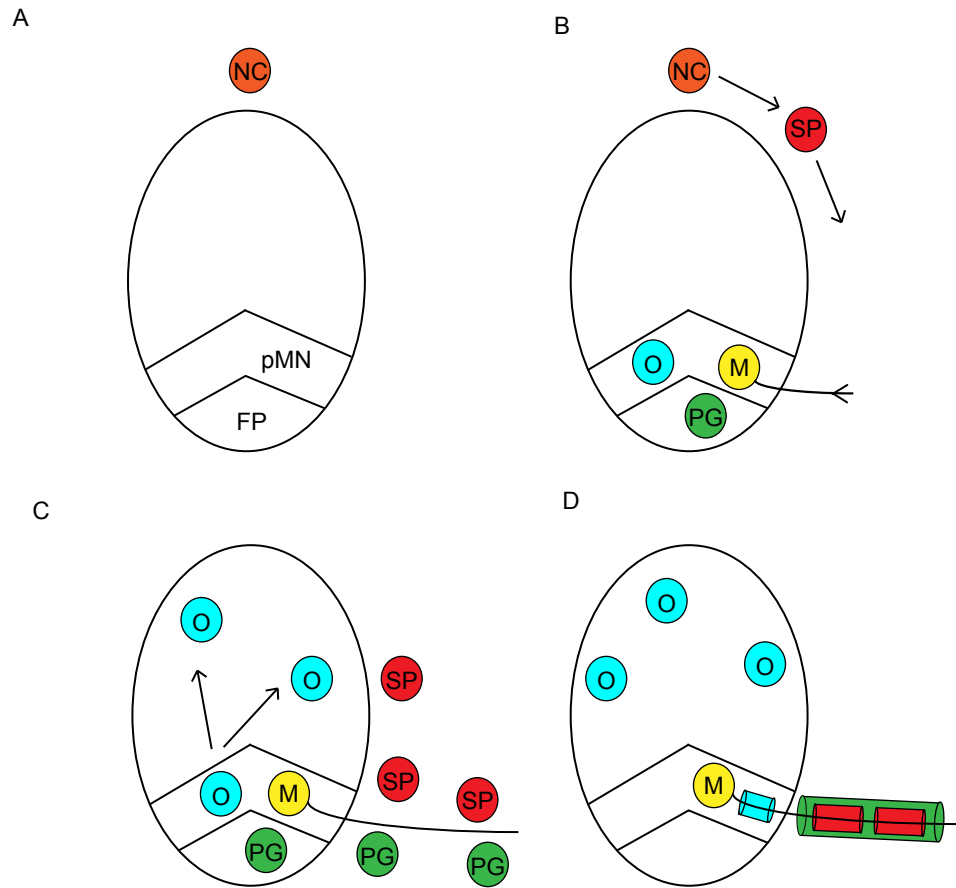


Figure 1-1: The development of the peripheral nerve. (A) First, the pMN domain and the floorplate (FP) are specified in the ventral spinal cord, and the neural crest (NC) is specified above the neural tube. (B) Neural crest cells migrate towards the MEP and differentiate into Schwann cells (SP). The oligodendrocytes (O) and motor neurons (MN) are specified in the pMN domain, and the neuron begins to extend its axon into the periphery. Perineurial cells (PG) are specified in the floorplate. (C) Oligodendrocytes migrate throughout the spinal cord. Perineurial glia exit the spinal cord, and Schwann cells associate with the axon. (D) Oligodendrocytes myelinate axons in the CNS. Schwann cells myelinate peripheral axons and then are wrapped by the perineurium.

1993; Kuhlbrodt et al., 1998; Nishiyama et al., 1996; Pringle and Richardson, 1993). After specification, these oligodendrocyte precursors migrate throughout the spinal cord (Figure 1-1 C) (Pfeiffer et al., 1993). Eventually these cells develop more elaborate processes and form stable connections with several different axons. They also change expression patterns, as mature oligodendrocytes express *mbp*, *mog*, and *plp*, which are key genes for the myelination process. Eventually they wrap their axons in layers of myelin sheath (Figure 1-1 D) (Baumann and Pham-Dinh, 2001).

Myelination

One of the most important functions of the oligodendrocyte is to wrap and insulate axons in myelin (Bunge, 1968). Axons carry information to and from the CNS using electrophysical signals called action potentials. When a neurotransmitter is taken up at the dendritic membrane, the cell experiences a wave of depolarization and then repolarization, eventually coming back to rest (Bernstein, 1868; Loewi and Navratil, 1926; Hodgkin, 1937). This wave travels down the membrane of the axon to the axon terminal, where it continues to transmit information through synapses onto other neurons or muscles (Hodgkin, 1937).

Action potentials on naked axons will travel slower than on axons that have been insulated by myelin, a lipid-rich, highly conductive substance. Myelin increases the resistance and lowers the capacitance of the action potential (Huxley and

Stämpfli, 1949). Myelin sheaths are not continuous but rather interspersed with short, unmyelinated regions called nodes of Ranvier, and the action potential can jump to these unmyelinated regions rather than travel all the way down the axon in a continuous but slower moving wave (Ranvier, 1878; Tasaki and Takeuchi, 1941, 1942; Huxley and Stämpfli, 1949). This process is called saltatory conduction and is crucial for motor nerve function.

In the CNS motor axons are wrapped by oligodendrocytes, but in the periphery, it is another type of glia, Schwann cells, that myelinate motor axons. Unlike oligodendrocytes, most Schwann cells are neural crest-derived (Le Douarin, 1986). However, recently it has been identified that a subpopulation of Schwann cells called MEP glia does not have neural crest origins, but rather are derived from CNS, migrate into the periphery through the TZ, and populate the motor nerve (Smith et al., 2014).

The neural crest and its derivatives

Besides the neural tube, the neural crest is the major contributor to the peripheral nervous system. At the same time that the neural tube is forming, outside of the CNS, the cell population between the dorsal neural tube and the epidermis forms the neural crest (Figure 1-1 A) (Hörstadius, 1950). The neural crest is pluripotent, highly migratory, and proliferative (Hörstadius, 1950; Bronner-Fraser and Fraser, 1988). Neural crest can be subdivided into 4 populations: cranial, trunk, vagal and sacral, and cardiac, each with its own migration and differentiation patterns.

Collectively, the neural crest differentiates into highly varied types of cells, including glia, neurons, melanocytes, cartilage, and muscle (Hörstadius, 1950). A subset of trunk neural crest cells takes the ventrolateral pathway through the somite, migrating along the edge of the spinal cord (Le Douarin and Teillet, 1974; Weston, 1963). At the MEP, they follow the axon growth cone as it searches out its target organ (Figure 1-1 B, C).

Regardless of origin, both Schwann cell populations follow the same differentiation path. One master signal in Schwann cell development is Neuregulin 1 (NRG1), which is produced by axons and is necessary for proper migration, proliferation, and differentiation of this cell type (Birchmeier and Nave, 2008; Meyer and Birchmeier, 1995). NRG1 signals to its receptors ErbB2 and ErbB3, which are expressed in Schwann cell precursors and are equally important for glial development (Lyons et al., 2005). Schwann cell precursors are highly migratory and proliferative cells that have only a loose association with the axon. As they differentiate into immature Schwann cells, they will sort into a 1:1 ratio with an axon. Eventually these cells become mature Schwann cells, which wrap and form myelin (Figure 1-1 D). Schwann cells will downregulate inhibitors of myelination, such as c-Jun (Parkinson et al., 2004). They also upregulate other important factors, such as Krox20, and Oct6, transcription factors which will trigger a cascade of myelin proteins (Jaegle et al., 2003; Topilko et al., 1994).

Not all axons will undergo myelination, which is correlated with axon size (Webster, 1971; Friede, 1972; Windebank et al., 1985). Unmyelinated axons will nevertheless be sorted into a close association with a nonmyelinating Schwann cell called a Remak bundle. Even nonmyelinating Schwann cells are important to the nerves as a source of trophic support for the axons. After nerve injury, they also play a major role in debris clearance and reinnervation (Nave, 2010).

The layers of the PNS nerve

The peripheral myelin sheath is surrounded by several additional layers of tissue besides Schwann cells. Ensheathing several axon-Schwann cell complexes is the perineurium. Composed of perineurial glia, which are derived from the lateral floorplate, these cells form a protective barrier that shields the axon from infectious agents or toxins in the blood (Akert et al., 1976a; Allt, 1969a; Bourne, 1968; Burkel, 1967a; Kucenas et al., 2008). In addition to the glia is connective tissue, called the endoneurium, which is also neural crest derived and located within the perineurium bundles (Joseph et al., 2004). Lastly, the nerve is surrounded by another layer of connective tissue, the epineurium, which adheres nerve fascicles together and forms the outermost portion of the nerve (Figure 1-2).

Innervation at the muscle

When the motor axon reaches its target muscle in the periphery, it synapses onto the muscle and forms what is called a neuromuscular junction (NMJ). These

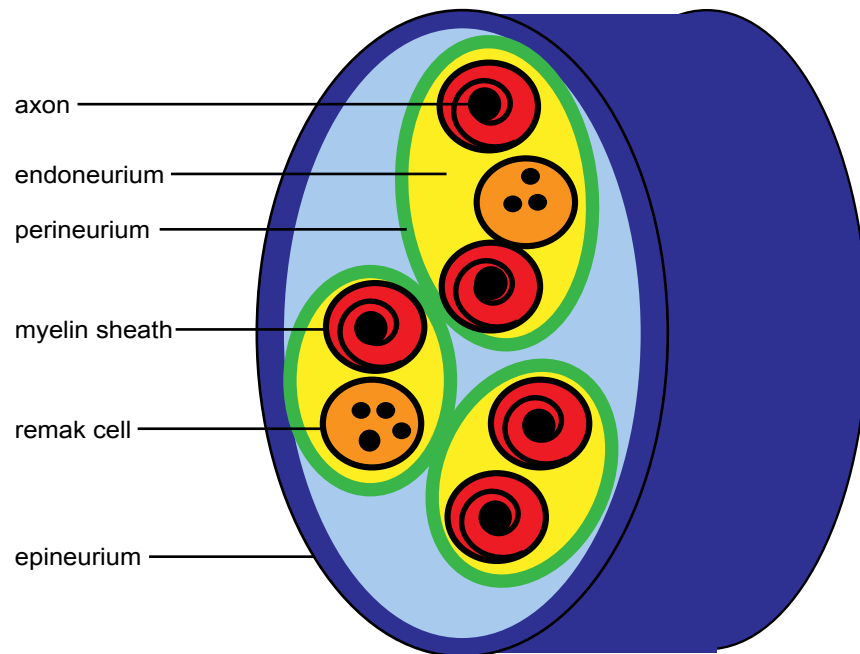


Figure 1-2: The anatomy of the mature peripheral nerve. Axons are wrapped by myelinating axons or nonmyelinating Schwann cells, called remak cells. These complexes are surrounded by a matrix of endoneurium. Several axon-Schwann cell bundles are ensheathed by a perineurium. Finally, multiple fascicles of perineurium are wrapped in the epineurium.

synapses release acetylcholine, which binds to nicotinic acetylcholine receptors (AChRs) on the sarcolemma, the muscle cell membrane (Dale et al., 1936; Changeux et al., 1970). The newly formed synapse is functional, but still must undergo a maturation process, which is reinforced by the activity of the axons itself (Misgeld et al., 2005). New synapses can be innervated by many axons, but pruning will occur to limit the axonal inputs to one (Wyatt and Balice-Gordon, 2003). Additionally, the entire structure of the postsynaptic endplate will change. The membrane invaginates into a highly folded structure, with the AChRs localized to the tops of the folds (Marques et al., 2000). Glia are important in NMJ formation as well, as perisynaptic Schwann cells are necessary for proper synapse formation and maintenance (Auld and Robitaille, 2003).

Origin of perineurial glia and their developmental function

The perineurium was first described by the anatomical studies of Henle in the nineteenth century. Studies of the nerve structure using EM have identified that the mature perineurium is composed of several rings of concentric flat cells that form tight junctions (Akert et al., 1976a; Allt, 1969a; Burkel, 1967a). Anatomical studies were also able to determine a function of the perineurium as a diffusion barrier to protect the nerve from toxins and infectious agents (Söderfeldt et al., 1973; Olsson, 1990). However, little is known regarding the development and molecular characterization of the perineurium.

Motor ensheathing perineurium is CNS-derived

More recently, a study in chick noted that the cells that formed the perineurium seemed to be derived from the mesenchyme surrounding the nerve, and Parmantier et al. postulated an epithelial to mesenchymal transition model in mice (Parmantier et al., 1999; Plessis et al., 1996). However, this was contrary to the origin of the analogous cells in *Drosophila*, in which they are specified in the ventral nerve cord (Sepp et al., 2000). Accordingly, Kucenas et al. found that the motor-ensheathing perineurial glia in zebrafish express the marker *nkx2.2a*. Using live imaging they observed that perineurial glia originate in the lateral floor plate of the spinal cord and migrate out into the PNS following the motor axons. Eventually these cells ensheath axon-Schwann cell complexes and form tight junctions, a hallmark of mature perineurium (Kucenas et al., 2008). This work has also been continued in mouse, which showed that *nkx2.2+* cells are CNS derived and have a similar importance in the development of the peripheral nerve (Clark et al., 2014). Therefore it has now been established that the perineurium is of ectodermal origin and that it is crucial for nerve function.

Interactions with other cell types

While the origin of the perineurium has been elucidated, questions remain as to how these cells interact with other glia and the axon. Preliminary evidence suggests that during embryonic development, neurons, Schwann cells and perineurial glia are mutually dependent on each other in order to form a functioning nerve fascicle (Kucenas et al., 2008). For example, in a study by

Kucenas et al., morpholino oligonucleotide knockdown of *nkx2.2a* was used to block specification of perineurial glia. In response, Schwann cells failed to wrap axons. Conversely, in the same study it was found that in mutant zebrafish without Schwann cells, perineurial glia were unable to exit the CNS or wrap motor axons (Kucenas et al., 2008). These results illustrate that both types of glia need reciprocal signaling to function. When this is not the case, motor nerve development is defective.

Initial studies also demonstrated that perineurial glia can influence the development of motor axons themselves. In the same study by Kucenas et al., inhibition of perineurial glial specification also impacted motor axon development. Using *in vivo* imaging, motor axons appeared stunted and defasciculated, motor axons exited ectopically, and some motor neuron cell bodies were seen to aberrantly follow their axons out into the periphery (Kucenas et al., 2008). This suggests that the perineurial glia may have a role in mediating the CNS/PNS transition zone.

Perineurial signaling pathways

Because of the limited body of work on perineurial glia, only a few signals have been shown to regulate these cells. The first two signals have not been shown to play a role during development, but rather on the perineurium in mature animals. The first is a Schwann cell-derived signal, Desert hedgehog

(Dhh). Schwann cells express *dhh* throughout development, and perineurial glia express its receptor, *patched*. In *dhh*^{-/-} adult mice, the perineurium is abnormally thin, and its characteristic tight junctions are not observed (Parmantier et al., 1999). The second of these signals identified is Ephrin signaling, used in the context of an injury model in adult animals. In this study, it was observed that perineurial glia regulate cell sorting of Schwann cells during the process of Wallerian degeneration using EphB2/EphrinB2 signaling. However, it is unknown if this signaling mechanism is used outside of the context of injury repair (Parrinello et al., 2010).

Only one regulator of perineurial glia during development has been identified. Binari *et al.* show that Notch is a regulator of both the migration and differentiation of perineurial glia. Notably, this same mechanism is not used in older animals that have undergone a peripheral nerve injury (Binari et al., 2013). In this same paper by Binari et al., Schwann cell development was also affected by Notch inhibition, despite the fact that Schwann cells do not use Notch signaling during the treatment period. These results concur that aberrant perineurial glia development has an effect on Schwann cell development (Binari et al., 2013).

ENU mutagenesis and mapping in zebrafish

Although preliminary studies on the perineurium have been informative, many questions about peripheral nerve development remain. Because perineurial glia

are poorly characterized cells, one of the best methods for identifying new factors involved in PNS nerve development is an N-ethyl-N-nitrosourea (ENU) mutagenesis screen using zebrafish.

Mutagenesis screens

Because of their large clutch sizes and short generation time, zebrafish have often been used for forward mutagenesis screens. The most effective way for inducing mutations in zebrafish is by using a chemical mutagen called ENU (Knapik, 2000). This is preferred because it is potent but its effects tend to be monogenic (Driever et al., 1996). In this procedure, mutagenized males (F0) are crossed to wild type females to create an F1 generation. The F1 fish are then outcrossed to create the F2 generation. Then, members of the F2 are incrossed amongst each to create the F3 generation. It is these fish that are used for preliminary screening, usually using morphology or genetic markers for particular cells of interest (Driever et al., 1996).

Mapping the mutation

Once the mutations have been undergone preliminary screening, they must be mapped to identify the genetic locus that is perturbed. The common method used to map these mutations in zebrafish is bulk segregant analysis. Before the mapping can begin, a map cross must be performed between two different wild type (WT) strains of zebrafish (Figure 1-3). A parent heterozygous for the mutation in an AB* background is outcrossed to a WT fish in a WIK background

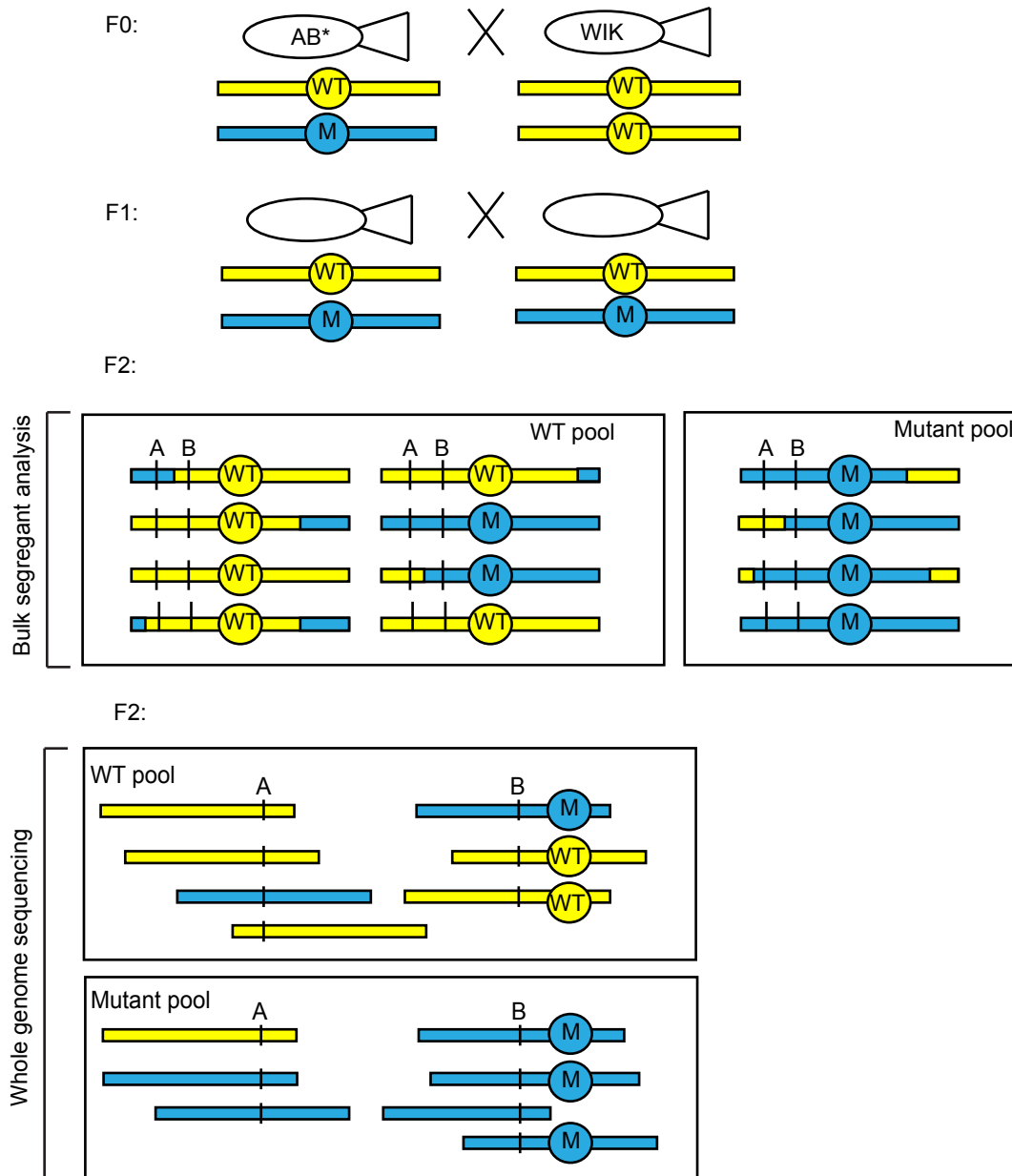


Figure 1-3: Comparison between bulk segregant analysis and whole genome sequencing methods. A heterozygote parent is outcrossed to a different WT line (F0). The progeny from this cross are grown up and heterozygotes are identified (F1). For both methods, these heterozygotes are identified as WT or mutant, pooled together, and the genomic DNA extracted. The WT pool will be composed of homozygotes and heterozygotes. In bulk segregant analysis, panels of primers for SSLP sites (A, B) are used to assess linkage throughout the genome. Recombination decreases as the SSLPs approach the SNP (A vs B). After whole genome sequencing, bioinformatic methods are used to call the SNPs (A and B) and calculate a homozygosity score, which is based on the ideal frequency of 100% in the mutant pool, 33% in the WT pool (modeled by SNP B).

(Knapik et al., 1996). The offspring of this pair are grown up and crossed together to identify new heterozygous carriers of the mutation. The newly genotyped fish are incrossed, and the offspring from these pairings are used for mapping purposes. This produces high levels of polymorphism, which is helpful for efficient mapping. This is because mapping techniques are based on identifying linkage between a polymorphic marker and the target locus, and fish from the same WT strain may have very few polymorphic markers (Knapik et al., 1996; Michelmore et al., 1991).

Pools of genomic DNA from mutant embryos and their WT (including both homozygous dominant and heterozygous) siblings are compared using large panels of primers which amplify regions of simple sequence length polymorphisms (SSLP) (Michelmore et al., 1991). Regions near the mutation will be genetically linked and show only one allele of the SSLP whereas other unlinked regions will show an equal representation of alleles (Figure 1-3). Although used successfully in the zebrafish community to identify many mutations, this method is laborious and time intensive.

Nevertheless, until recently, bulk segregant analysis was the best technique for mapping mutations in zebrafish. Recently, however, several studies using next generation sequencing approaches were published which provide a viable alternative. These studies outline protocols to utilize whole genome sequencing (WGS) of pooled genomic DNA from mutant and WT siblings to identify Single

Nucleotide Polymorphisms (SNP). By calculating the homozygosity score of these SNPs, it is possible to identify regions linked to the mutation (Leshchiner et al., 2012; Obholzer et al., 2012; Voz et al., 2012). This approach is much quicker than bulk segregant analysis, although also more expensive. It also requires more sophisticated bioinformatics skills to properly analyze the vast quantities of data produced. Alternatively, SNPTrack is a pipeline that takes raw sequencing data, analyzes it, and identifies regions of high homozygosity and the candidate SNPs within those regions (Figure 1-3) (Leshchiner et al., 2012).

Confirmation of the gene

There are several methods available in zebrafish for testing candidate genes, each with its own caveats. The easiest is a complementation test with another characterized mutant of that gene (Haffter et al., 1996). If a heterozygote of the unknown mutant is crossed with a heterozygote of the known mutant, and the offspring does not recapitulate the phenotypes of unknown mutant, then they do not affect the same gene (Fincham, 1966). This method is very strong, but it is only rarely that a mutant has been previously identified for the gene.

Attempting to phenocopy the effect of the mutation is another technique to test a candidate gene. In zebrafish, this can be done several ways. Traditionally an antisense oligonucleotide, called a morpholino, would be generated, which works by interfering with translation or splicing of the RNA (Summerton, 1999; Nasevicius and Ekker, 2000). Morpholinos are injected into the embryo at the

one cell stage, and are diluted to the point of impotence by 72 hpf, which is obviously problematic. Additionally, morpholinos have been shown to be prone to false positive results (Eisen and Smith, 2008). Recently newer methods of knocking out a gene have been developed, particularly the CRISPR method, which has the advantage of being stably integrated into the genome and inherited thereafter (Hwang et al., 2013; Jinek et al., 2012). This method is undoubtedly superior to morpholinos, but the F0 generation is highly mosaic, and thus should be crossed to the F1 or F2 generation for the best analysis, a process that takes months.

The third option for phenocopy is by treating embryos with a drug that is known to inhibit activity of the target gene. Drug treatment in zebrafish is very simple as it can be dosed in their water, and is absorbed into the body directly. This method is obviously highly dependent on the actual gene in question and the specificity of the drug. Additionally, it can be difficult to achieve a full knockout of activity, rather than just a knockdown, which might make interpretation of results difficult.

In contrast to phenocopy techniques, rescue of the mutation can also be tested. Again, rescue can be accomplished by treating mutant embryos with a drug that acts as an agonist to the gene, if available. This technique has the same qualifications mentioned above. A second method is injecting mutant embryos at the one cell stage with mRNA of the candidate gene (Zhang et al., 1998). Rescue of the mutant phenotype is strong evidence for the identity of the gene

Development and clinical outlook of Duchenne Muscular Dystrophy

In humans, loss of motor nerve function leads to various stages of disability. One disease that impacts the motor nerves is Duchenne Muscular Dystrophy (DMD), an x-linked condition that causes progressive degeneration of the muscle and eventually death. DMD is caused by mutations in *dystrophin*, a large, complex gene with many isoforms (Burghes et al., 1987; Monaco et al., 1986). The full-length gene consists of 79 exons, encoding a 14 kb transcript which will be translated a 427 kD protein (Tennyson et al., 1995). In addition to this transcript, several smaller isoforms have been identified in humans, which are denoted by the size of their respective protein products: *dp260*, *dp140*, *dp116*, and *dp71* (Ahn and Kunkel, 1993; Sadoulet-Puccio and Kunkel, 1996). Although many of the smaller transcripts are expressed at basal levels in the muscle, it is *dp427* that is the primary source of dystrophin in the myoseptum of skeletal muscle (Khurana et al., 1991; Sadoulet-Puccio and Kunkel, 1996). In contrast, the *dp260* isoform has a strong expression in the retina, and the *dp140* isoform is expressed in the brain and kidney (Lidov et al., 1995; D'Souza et al., 1995). The *dp116* isoform is associated with the PNS as it is predominately expressed in Schwann cells (Byers et al., 1993). Lastly, the *dp71* transcript is expressed at low levels in skeletal muscle but most abundantly in the brain and heart (Lederfein et al., 1993).

The structure of *dystrophin* is highly conserved across many organisms, including zebrafish. The full-length *dystrophin* was identified to have similar number of exons and expression patterns its mammalian homologues (Bolaños-Jiménez et al., 2001a, 2001b). However, as of yet only two of the alternative isoforms has been identified in zebrafish, *dp116* and *dp71* (Bolaños-Jiménez et al., 2001b; Jin et al., 2007). *dp71* was found to be expressed in the brain and retina, and at lower intensity in the myoseptum (Bolaños-Jiménez et al., 2001a, 2001b). Additionally, two zebrafish *dystrophin* mutants have been identified, *sapje*^{ta222a} and *sapje-like*^{cl100}, both of which display hallmarks of DMD, including muscle wasting and absence of Dystrophin protein at the myoseptum (Bassett et al., 2003; Guyon et al., 2009).

The importance of the DAPC

Dystrophin is a critical component of the dystrophin associated protein complex (DAPC), a complex localized to the sarcolemma that connects the actin cytoskeleton to the extracellular matrix (Arahata et al., 1988; Bonilla et al., 1988; Zubrzycka-Gaarn et al., 1988). In healthy muscle, the DAPC provides tensile strength to the sarcolemma, but in DMD the sarcolemma becomes torn and scarred, compromising muscle function (Ervasti and Campbell, 1991). The DAPC is also a signaling complex. Dystrophin associates with the transmembrane components α and β dystroglycan, which are receptors to extracellular Laminin and relay RAC1/JNK and ERK/MAPK signaling within the cell (Figure 1-4). Another component of the DAPC are the Syntrophin proteins, which are

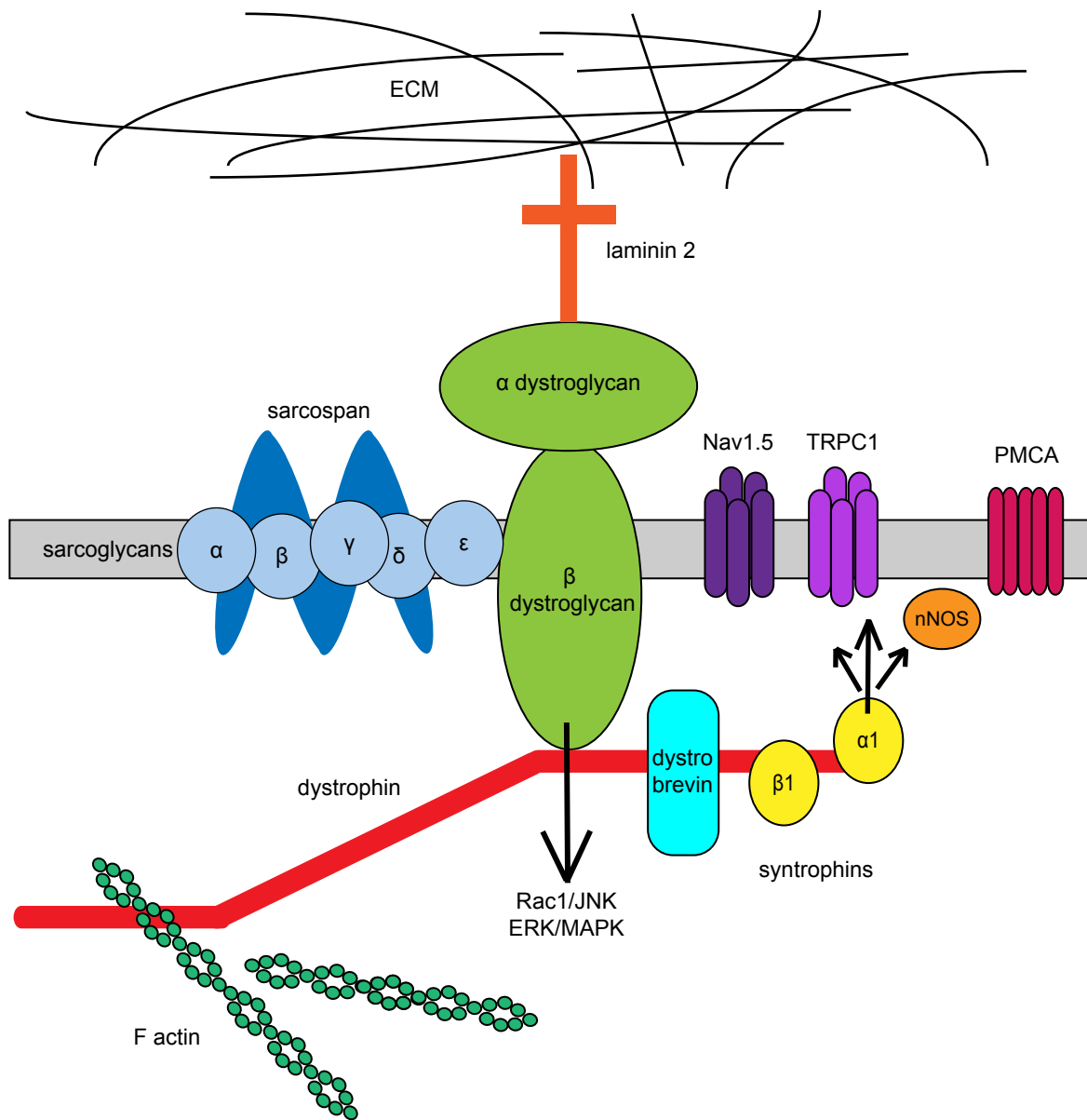


Figure 1-4: The DAPC is a signaling platform in the sarcolemma. The DAPC is composed of dystrophin, dystrobrevin, α and β dystroglycan, syntrophin $\alpha 1$ and $\beta 1$, sarcospan, and 5 sarcoglycans. Dystrophin binds to the actin cytoskeleton, and α dystroglycan binds to various ECM components. Laminin2 binding with α dystroglycan is mediated through β dystroglycan to activate RAC1 and JNK, and these members also mediate the ERK/MAPK pathway. $\alpha 1$ syntrophin anchors nNOS at the membrane, and acts in conjunction with PMCA to regulate nNOS activity. Syntrophin also maintains a complex of voltage-gated sodium and calcium channels associated with the DAPC, and is important for expression and function of these ion channels.

important for the function and anchoring of nNOS and voltage-gated sodium and calcium channels at the membrane (Figure 1-4). When Dystrophin is absent, the entire complex is destabilized, potentially disrupting signaling pathways. .

Duchenne Muscular Dystrophy

DMD patients display muscle weakness and motor deficits as young children, which progress into a more severe condition as they lose the ability to walk as adolescents. Patients develop secondary heart and respiratory symptoms, which are eventually fatal (McDonald et al., 1995). Although many clinicians consider DMD a disease of the muscle, many patients also suffer from some degree of mental impairment (Lidov, 1996). Not all mutations in *dystrophin* cause DMD, those that do not disrupt the reading frame cause Becker Muscular Dystrophy (BMD), a more mild condition (Ahn and Kunkel, 1993).

Currently, there are no effective treatments for DMD. Several potential methods of therapy are being developed and tested, each with its own caveats. Viral gene therapy has been proposed to substitute functional Dystrophin protein, however this technique raises safety concerns (Bowles et al., 2012). Exon skipping has also been developed, using small splice-blocking oligonucleotides to induce skipping of the defective exon. However, exon skipping can only result in a truncated protein and the patient would still suffer from milder BMD-type symptoms (Cirak et al., 2011; van Deutekom et al., 2007; Kinali et al., 2009). Lastly, drug-induced stop codon read-through is being developed, however only

about 15% of patients could benefit from this method. Clinical trials have shown that the drug Ataluren is able to restore Dystrophin in the muscle, but did not significantly improve the six-minute walk test (Finkel, 2010; Finkel et al., 2013; Welch et al., 2007). Many questions remain in our understanding of this disease.

In this dissertation, I present two novel zebrafish mutants, which strongly impact glia and nerve development in different ways. Chapter III introduces *ftl*^{vu268}, a mutant in which perineurial glia fail to migrate. I discuss progress towards mapping this mutation and also demonstrate a wide range of glial defects in these mutants. Chapter IV concerns the mapping and characterization of *ray*^{vu267}, a mutant that illuminates the close relationship between muscle and nervous system and emphasizes the key role that the nervous system plays in Duchenne Muscular Dystrophy.

Chapter II: Methods for *ftl*^{vu268} and *ray*^{vu267} projects

Fish husbandry

All animal studies were approved by the University of Virginia Institutional Animal Care and Use Committee. Zebrafish strains used in this study included *Tg(nkx2.2a:megfp)*^{vu17} (Kirby et al., 2006; Kucenas et al., 2008), *Tg(olig2:dsred2)*^{vu19} (Kucenas et al., 2008), *Tg(sox10:eos)* (Prendergast et al., 2012), *Tg(hb9:gfp)* (Sainath and Granato, 2013) and *Tg(sox10:mrfp)* (Kucenas et al., 2008). We also used the mutant line *sapje-like*^{cl100} (Guyon et al., 2009). Embryos were produced by pairwise matings, raised at 28.5°C in egg water, staged according to hours or days post fertilization (hpf and dpf, respectively) and embryos of either sex were used for all experiments described below (Kimmel et al., 1995). Embryos used for *in situ* hybridization, immunohistochemistry, and microscopy were treated with 0.003% phenylthiourea (PTU) in egg water to reduce pigmentation.

In vivo imaging

At 24 hpf, all embryos used for live imaging were manually dechorionated and transferred to egg water containing PTU to block pigment formation. At specified stages, embryos were anesthetized using 3-aminobenzoic acid ester (Tricaine), immersed in 0.8% low-melting point agarose and mounted on their sides in glass-bottomed 35 mm Petri dishes (Electron Microscopy Sciences). Images were captured using either 40x (NA 1.2) water immersion or 25x (NA 0.8) oil-

immersion objectives mounted on a motorized Zeiss AxioObserver Z1 microscope equipped with a Quorum WaveFX-X1 spinning disc confocal system (Quorum Technologies Inc.). For time-lapse imaging, Z image stacks were collected every 15 min for 15-24 hours. MetaMorph software was used to compile three-dimensional datasets and to create videos. Image adjustments were limited to contrast enhancement and level settings using MetaMorph software.

In situ RNA hybridization.

Larvae were fixed in 4% paraformaldehyde for 24 h, stored in 100% methanol at -20°C , and processed for *in situ* RNA hybridization. Plasmids were linearized with appropriate restriction enzymes and cRNA preparation was performed using Roche DIG-labeling reagents and SP6 RNA polymerase (New England Biolabs). After *in situ* hybridization, larvae were mounted on their sides in 0.8% low-melting point agarose on glass-bottomed 35 mm Petri dishes. Images were obtained using a Zeiss AxioCam CCD camera mounted on a Zeiss AxioObserver Z1 microscope equipped with Zeiss AxioVision software. All images were imported into Adobe Photoshop. Adjustments were limited to levels, contrast, color matching settings, and cropping.

Immunohistochemistry

Larvae were fixed in AB Fix (4% paraformaldehyde, 0.1% TritonX-100, 1x PBS) for 3 hours at 23°C , followed by a 5 minute wash with PBSTx (1% TritonX-100,

1x PBS), a 5 minute wash with DWTx (1% TritonX-100 in distilled water), a 5 minute wash with acetone at 23 °C and a 10 minute wash with acetone at -20 °C. Larvae were pre-blocked in 5% goat serum/PBSTx for 1 hour, then incubated in primary antibody for 1 hour at 23 °C and overnight at 4 °C. The primary antibodies used included mouse anti-acetylated tubulin (1:5,000, Sigma), rabbit anti-Sox10 (1:5000, (Binari et al., 2013)), mouse Mandra1 (1:200, Sigma), mouse anti-F59 (1:100, DHSB), rabbit anti-laminin, (1:100, Sigma), mouse anti-islet (1:100, DHSB), mouse anti-HuC (1:100, Molecular Probes). Larvae were washed extensively with 1x PBSTx and incubated in secondary antibody for 1 hour at 23 °C and overnight at 4 °C. Secondary antibodies used were Alexa Fluor 568 goat anti-rabbit, Alexa Fluor 568 goat anti- mouse, Alexa Fluor 647 goat anti-rabbit, and Alexa Fluor 647 goat anti-mouse (Invitrogen). Larvae were washed extensively with 1x PBSTx and stored in 50% glycerol/PBS at 4 °C until imaging. Larvae were mounted on their sides in 0.8% low-melting point agarose on glass-bottomed 35 mm Petri dishes and imaged using the confocal microscope described above. Image adjustments were limited to contrast enhancement and level settings using MetaMorph software and Photoshop.

Data quantification and statistical analysis

All graphically presented data represent the mean of the analyzed data or the percent of the total. Statistical analyses and graphing were performed with Excel software. The level of significance was determined by using an unpaired t test using a confidence interval of 95%.

Bulk segregant analysis

At 72 hpf, 50 WT or mutant embryos were identified and pooled. Genomic DNA from each pool was extracted using a Qiagen DNeasy Kit. PCR was performed with a panel of primers for 192 SSLPs spread across the genome. PCR reactions were run on a 2% agarose gel.

Whole genome sequencing

At 72 hpf, wild type (WT) and mutant embryos were identified by observing perineurial glia defects via confocal microscopy of *Tg(nkx2.2:megfp)* embryos. Genomic DNA from 50 WT and 50 mutant embryos was extracted and pooled using a Qiagen DNeasy Kit. Pooled DNA was sent to Hudson Alpha for genome amplification sequencing (WGS). DNA was sequenced on an IlluminaHiSeq 2500 platform with paired-end reads of 100 base pairs in length. Raw data was uploaded into the SNPtrack pipeline, (genetics.bwh.harvard.edu/snptrack/), which aligned the reads to the ZV9 genome, called the SNPs, and identified regions of high homozygosity.

Fine mapping

Individual DNA from 125 identified mutant or WT embryos was extracted using the HotSHOT lysis protocol and stored at -20 degrees (Meeker et al., 2007). SNP-specific PCR primers for genes within the regions of interest were designed (Ugozzoli and Wallace, 1991). PCR was performed and run a 1% agarose gel.

Presence of WT band in the mutant PCR reaction indicates crossing over, and eliminates the gene as a candidate. Genes were sequentially eliminated on either side of the region to narrow the window as far as possible.

RT-PCR

At 72 hpf, 50 WT or mutant embryos were identified and pooled. Total RNA was extracted according to Petersen and Freeman (Peterson and Freeman, 2009). RNA was transcribed into cDNA using the High Capacity cDNA Reverse Transcription Kit (Life Technologies). cDNA was purified with the QIAquick PCR Purification Kit (Qiagen). PCR was performed with primers designed to amplify desired regions of the DMD cDNA and run on a 1% agarose gel. PCR product was also sent to GeneWiz for Sanger sequencing. Sequencing results were aligned to the reference sequence on Ensembl using Serial Cloner.

Sectioning

Embryos which had been labeled with immunohistochemistry were embedded in 1.5% Agar/30% Sucrose. Blocks were incubated in 30% sucrose overnight at 4°C. Blocks were frozen by floating on 2-methylbutane chilled by liquid nitrogen. Larvae were sectioned transversely every 20 μ M with a cryostat microtome. Sections were mounted with Vectashield (Vector Laboratories) and imaged using confocal microscopy as described above.

Morpholino injections

Morpholino oligonucleotides (MO) were diluted in 2x Phenol red injection buffer. Embryos were injected with approximately 2nl at the one cell stage and raised until 72 hpf for analysis. Ryr3-like, Grem1, and FMN1 are start site morpholinos, while Thbs1 is a splice-blocking morpholino.

Gene name	Sequence	Injection concentrations
<i>ryr3-like</i>	GACCTGAATTCACCTGAACACTCAT	1.5 mM,-2.0mM
<i>grem1</i>	AGAAACGATCTGTGAAGCGTCCCAT	1.25 mM,-2.0mM
<i>fMN1</i>	AAGAAATCCTACTTGCTGGATCCAT	1.25 mM,-2.0mM
<i>thbs1</i>	CACACACACAGAAAATAATGTGGCC	1.25 mM,-2.0mM

Alcian blue Staining

Larvae were treated according to the protocol in *Imaging Blood Vessels in the Zebrafish* (Kamei et al., 2010). They were imaged using a Zeiss AxioCam CCD camera mounted on a Zeiss AxioObserver Z1 microscope equipped with Zeiss AxioVision software.

Alkaline phosphatase stain

72 hpf embryos were labeled with alkaline phosphatase according to the protocol published by Kamei et al. (Kamei et al., 2010). They were imaged using a Zeiss AxioCam CCD camera mounted on a Zeiss AxioObserver Z1 microscope equipped with Zeiss AxioVision software.

Ataluren treatment

Ataluren was dissolved in DMSO to create a stock solution of 0.5mM. This was then dissolved in egg water with PTU to achieve the desired concentration of 0.5uM and 0.1% DMSO. Control tests were performed with no treatment (only egg water and PTU) and also egg water with PTU and 0.1% DMSO. Embryos were exposed to the Ataluren solution from 24 to 72 hpf, when they were imaged live. Each embryo was numbered and individually fixed and stored for subsequent whole mount immunohistochemistry with the Mandra1 antibody.

Dantrolene and Gabapentin treatment

For both treatments, fish were exposed to drug at 5 hpf. Gabapentin (Sigma) was dissolved in egg water and DMSO to reach final concentration of 1% DMSO, 1mM Gabapentin. Dantrolene (Sigma) was dissolved in egg water to reach concentrations in the range of 10nM-500nM. Fish remained in drug treatment until 72 hpf, when they were imaged.

TUNEL

Sectioned embryos were labeled using ApopTag Plus *In Situ* Apoptosis Fluorescein Detection Kit (Millipore) and imaged using confocal microscopy as described above.

Chapter III: Novel mutant (*ftl*)^{*vu268*} exhibits perturbed glial migration, differentiation, and survival

Introduction

Proper nerve development is crucial for the health of the organism. In the case of the motor nerves, many different cell types interact to form a functioning nerve, including the Schwann cells, which increase conduction velocity, the endoneurium, a matrix of collagen rich connective tissue, the perineurium a protective sheath that surrounds each nerve fascicle, and the epineurium, the outer layer that ensheaths all the nerve fascicles into one fiber (Haller and Low, 1971; Akert et al., 1976b). Although all of these cell types are important for nerve function, very few studies have examined the outer layers of the nerve in any significant way.

The perineurium is a multilayered sheath of concentric layers of flat cells that are connected with tight junctions, which functions as the peripheral blood brain barrier. (Burkel, 1967b; Allt, 1969b; Akert et al., 1976b; Söderfeldt et al., 1973; Olsson, 1990). From electromicroscopy studies in chick and mouse it was previously believed that the perineurial cells were recruited from the surrounding mesenchyme in an mesenchymal-to-epithelial transition (Parmantier et al., 1999; Plessis et al., 1996). More recent studies in zebrafish have found that perineurial glia are *nkx2.2a*⁺ cells, which are specified within the spinal cord (Parmantier et al., 1999b; Kucenas et al., 2008; Clark et al., 2014). These cells migrate out of

the spinal cord through the MEP as they associate with the developing peripheral nerve (Kucenas et al., 2008). Perineurial glia have an important role in the formation of the nerve, as perturbation of these cells results in aberrant motor neuron and Schwann cell development (Clark et al., 2014; Kucenas et al., 2008). While these studies were informative as to the basic role of perineurial glia, very little is known about the development of this cell type and its association with other cells that compose the nerve.

To answer this question more fully, an ENU mutagenesis screen was performed to identify regulators of peripheral nerve development. Zebrafish were used for their small size and short generation time, as well as their amenability to imaging of early developmental events. A novel zebrafish mutant was identified, *failure to launch* (*ftl*)^{vu268}. This mutant, which displayed a smaller head and necrosis in the brain, was selected for its striking glial phenotype, the absence of perineurial glial migration.

Through further characterization I found that the perineurial glia are not the only cell type disrupted in these mutants. The *ftl*^{vu268} mutation causes perturbation of floorplate development, Schwann cell and oligodendrocyte cell death, and the absence of myelin. Although I saw perturbations in the development of many glial cell types, no differences were observed within the motor neurons. However, a non-neuronal phenotype was also observed in the perturbation of vascularization across the trunk. The mechanism by which these phenotypes are produced

remains unclear until the gene can be identified.

Many mapping strategies were used to identify the gene in which the *ftl*^{vu268} mutation is located. Bulk segregant analysis was performed, but this approach did not provide useful results. Instead, WGS was performed on pools of mutant and WT fish. The mapping pipeline SNPTrack was used to identify a region of chromosome 17 in which the mutated locus is located, and fine mapping was used to narrow that region to a 50 kb window, which contains fewer than ten genes. Several methods were used to narrow the list of possibilities even further, to only three possibilities. However, these efforts did not give enough conclusive evidence to identify the candidate gene from these final three candidates.

Importantly, in the intervening time, a newer version of the zebrafish genome has been released. This map rearranges the end of chromosome 17 significantly, even removing some genes from the map altogether. Clearly, this new map changes our interpretation of our results dramatically. To accurately identify this mutation, and fully understand its mechanism and effects, the WGS data will have to be realigned to the new reference genome and another round of fine mapping will have to be performed.

Results

*The *ftl*^{vu268} mutation disrupts perineurial migration and is located on chromosome*

17

Fish carrying the transgene *Tg(nkx2.2a:megfp)*, which labels perineurial glia, were exposed to ENU to trigger mutagenesis. These offspring were then crossed for several generations. Fish from the F3 generation were screened via confocal microscopy for developmental defects in *nkx2.2a*+ cells. Two mutant lines were identified in this screen, including *ftl^{vu268}*. Preliminary characterization identified a smaller, malformed head, and necrosis in the brain (Figure 3-1 A, B). In 48 hpf WT embryos, glia exit the spinal cord at regularly spaced intervals at the MEP, migrate along the motor nerve, and eventually ensheath it (Figure 3-1 C, arrowhead). In contrast, the *ftl^{vu268}* mutant identified from this screen was selected because of the absence of perineurial glial migration from the spinal cord at 48 to 72 hpf (Figure 3-1 D). Additionally, the floorplate of the fish, also labeled with *nkx2.2a*, is disorganized and abnormally wide in *ftl^{vu268}* mutants (bracket, Figure 3-1 D). The *ftl^{vu268}* mutation is lethal to the larvae, which die by 5 to 6 dpf.

The first method utilized to map the mutant locus was bulk segregant analysis. I used a library of primers amplifying 144 different short tandem repeats scattered throughout the zebrafish genome. Unfortunately, this method did not produce any informative results. I then used a different method, whole genome amplification sequencing. Fifty WT and mutant embryos were pooled; genomic DNA was extracted and sent to be sequenced. The sequencing was carried out in paired-end reads of 100 bp on an Illumina HiSeq 2500 platform. Raw data was uploaded onto the SNPTrack pipeline, which aligns the reads to the reference

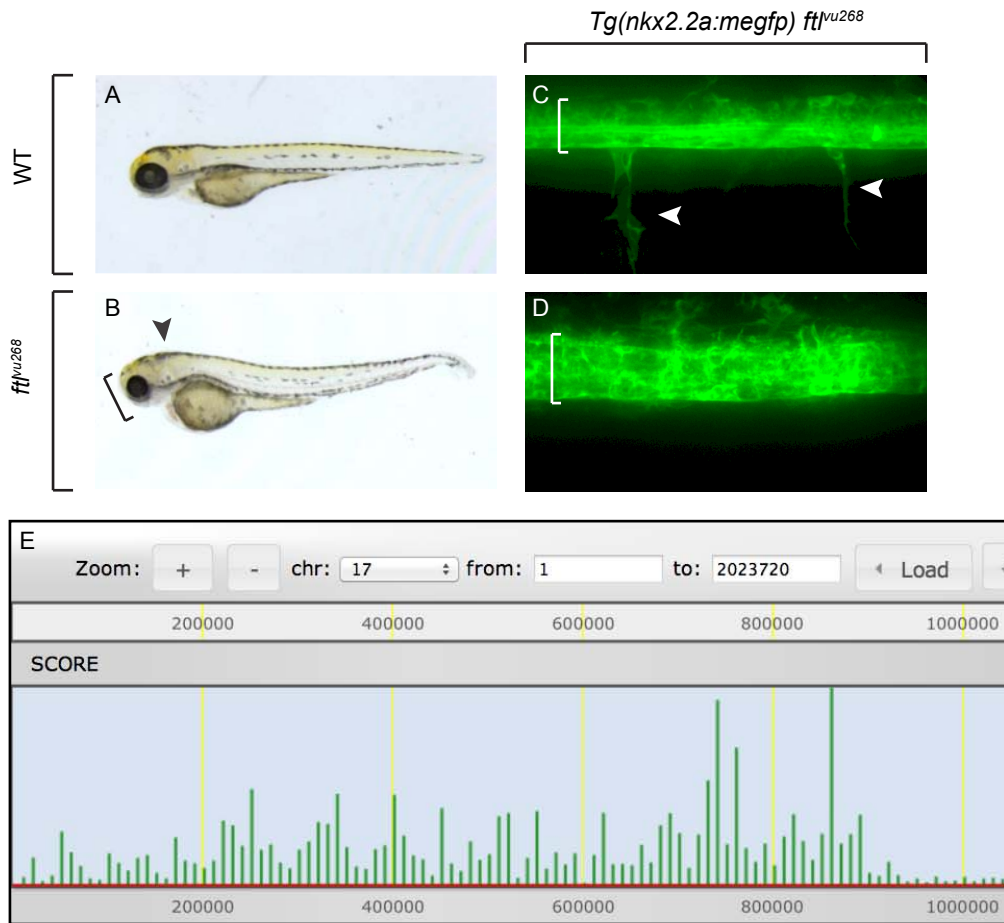


Figure 3-1: The *ftl^{vu268}* mutant perturbs glial development and is located on chromosome 17. Comparison of development between a 72 hpf WT fish (A) and a *ftl^{vu268}* mutant fish, showing smaller head (bracket) and necrosis in the brain (arrowhead, B). Transgenic *Tg(nkx2.2a:megfp)* fish from a *ftl^{vu268}* clutch were imaged at 72 hpf. WT siblings show regular exit of perineurial glia (arrowheads, C) while mutant siblings show the absence of glial migration and a larger, more disorganized floorplate (bracket, D). (E) SNPtrack identified a 1Mb region of chromosome 17, the green bars representing regions with a high homozygosity score.

genome and calls the SNPs. The reference genome used was ZV9. For each SNP, SNPTrack also calculates a homozygosity score. The ideal score is a SNP which is 100% represented in the mutant pool but only 33% represented in the WT pool (which is an unknown combination of homozygotes and heterozygotes). Then it identifies a chromosomal region where many of these highly ranked SNPs are clustered.

In the *ftl*^{vu268} mutant pool, SNPTrack identified only one region of high homozygosity, the first 1 Mb of chromosome 17 (Figure 3-1 E). Fine mapping, using allele-specific PCR, was able to narrow the region even further, to the window between 39 kb and 96 kb. Within this region are seven characterized genes and one uncharacterized gene. However, after focusing our search on splice site and nonsynonymous mutations, SNPTrack only identified highly ranked SNPs in only five of these genes: *thrombospondin 1 (thbs1)*, *cabz01118004.1*, *ryanodine receptor 3-like (ryr-3 like)*, *formin 1 (fmn1)*, and *gremlin 1 (grem1)* (Figure 3-2 A).

Identification of the gene remains unanswered

After investigating the literature on all of these genes, the highest ranked candidate on the list was *thbs1*, a glycoprotein that has been shown to be expressed in oligodendrocytes and astrocytes (Scott-Drew and French-Constant, 1997; Christopherson et al., 2005). This protein is generally involved in cell-cell or cell-matrix adhesions, but in the nervous system it has been shown to

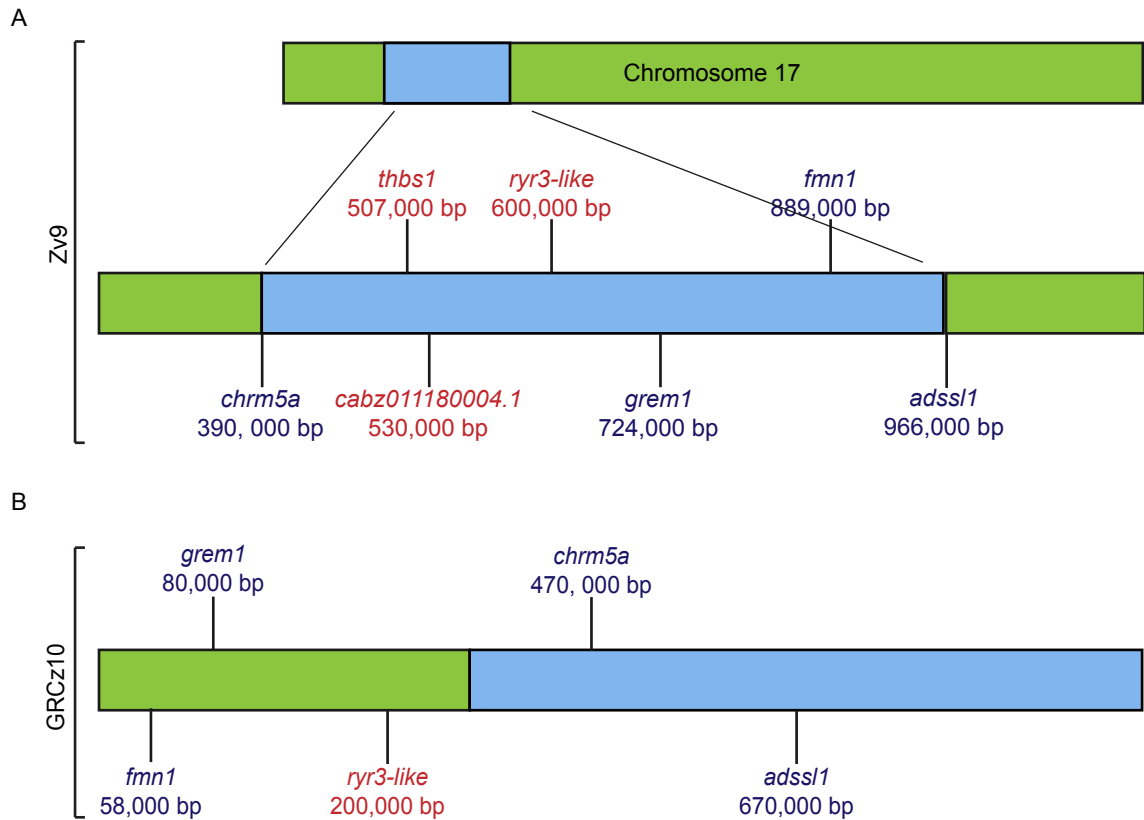


Figure 3-2: Fine mapping narrowed the region of *ftl*^{vu268} further, but was complicated by new genome. (A) SNPtrack identified a 1Mb region of chromosome 17, which was narrowed further to the region of 39 kb to 96 kb (in blue). Genes in red are candidates, genes in blue are eliminated. (B) Updated version of the map, showing the new location of genes in GRCz10.

promote oligodendrocyte migration and synaptogenesis (Scott-Drew and French-Constant, 1997; Christopherson et al., 2005; Xu et al., 2010).

From studies in other organisms, it is known that *fmn1* is an actin nucleator. In particular, *fmn1* has been shown to mediate actin polymerization during dendritogenesis and synaptogenesis in the mouse hippocampus (Kobielak et al., 2004; Simon-Areces et al., 2011). An *fmn1*-null mouse was observed to have limb bud deformity and increased levels of BMP (Zhou et al., 2009). This gene's role in neuronal development caused it to be ranked second highest in this list of candidate genes.

Little information is available about the gene *ryr3-like*, except for its putative 53-exon transcript. Because NCBI has characterized the gene as a pseudogene, it is questionable if the gene is functional at all, or how similar its function would be to other ryanodine receptor genes. The ryanodine receptor family is a class of calcium channels, some of which are expressed in the nervous system. *ryr3* has been shown to play a role in synaptic plasticity and learning as well as a mouse model of Alzheimer's disease (Balschun et al., 1999; Liu et al., 2014).

grem1 is a BMP antagonist that functions downstream of the Shh signaling pathway. Studies in mouse have shown that *grem1* that regulates organogenesis and body patterning. One study in zebrafish has also shown a role in signaling between Shh and Fgf8 (Nicoli et al., 2005). Unless Shh signaling is affected in

this mutant, which seems unlikely, it is ranked *grem1* as the least likely candidate out of the list of characterized genes.

Several methods were employed to narrow this list further. I decided to focus on the four characterized genes before tackling the uncharacterized gene. I consulted SNPfisher, a recently published database of SNPs found in highly inbred WT lines, and found some of my candidate SNPs in this list (Butler et al., 2015). Because these inbred, WT lines develop completely normally, any SNPs found in these lines are benign and do not cause the major perturbations of *ftl^{vu268}*. For this reason I was able to eliminate *fmn1* and *grem1* from contention.

In order to eliminate *ryr3-like*, I treated AB* embryos with Dantrolene, a ryanodine receptor inhibitor, which only mildly perturbed the glia. In some fish, the glial projections were thinner and in others the projections were large and blebbing (Figure 3-3 C, arrowhead). However, none of the fish exhibited widespread absence of glia migration or notable floorplate enlargement (Figure 3-3 A-D). Additionally, I designed a morpholino to test *ryanodine receptor 3-like*. In agreement with the drug treatment, the MO resulted in some cases of thinner perineurial projections, but did not phenocopy the *ftl^{vu268}* mutants, where the glia completely fail to exit (Figure 3-3 E, F). However, morpholinos are not without drawbacks, in particular the fact that they lose potency as the fish develop, and that they can have off target effects.

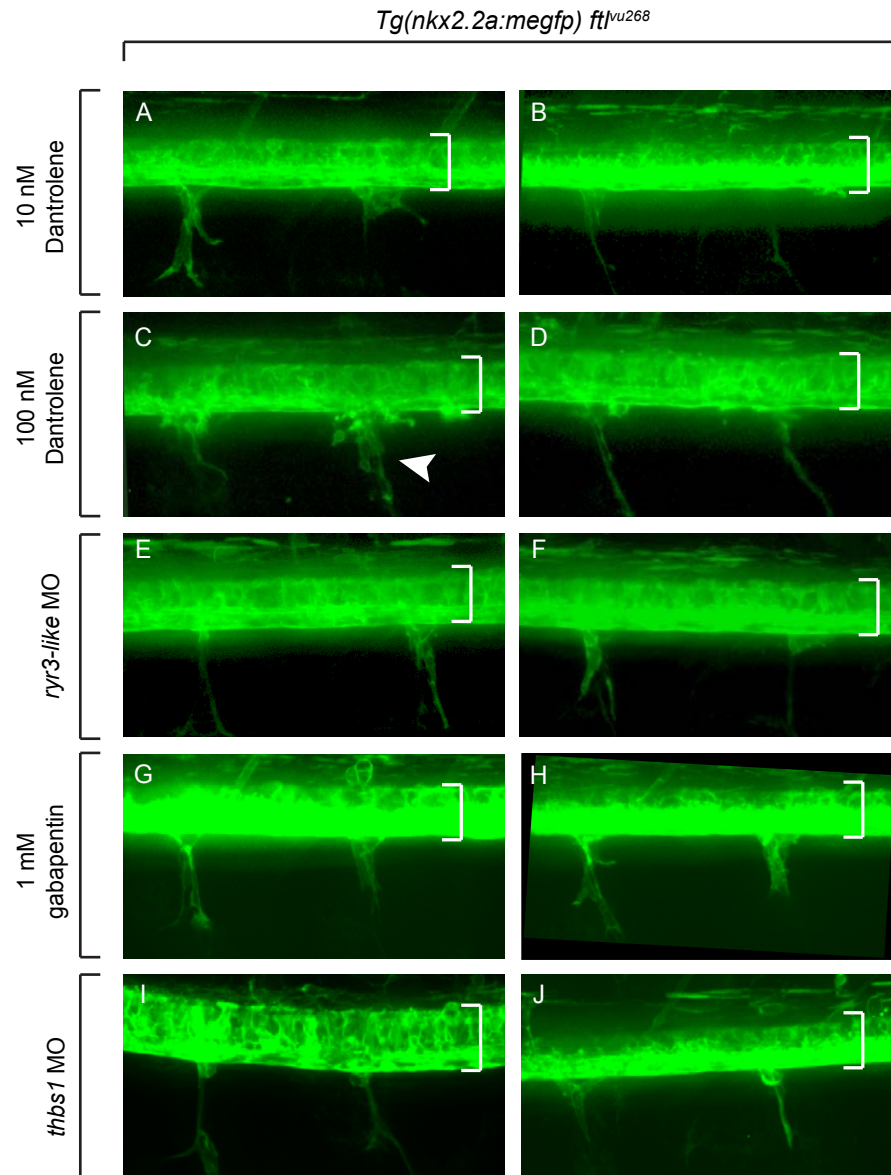


Figure 3-3: Inhibition of *ryr3-like* or *thbs1* perturbs glia mildly but does not phenocopy. Transgenic *Tg(nkx2.2a:megfp)* fish from a *ft^{lvu268}* clutch were MO-injected or drug treated and imaged at 72 hpf. Treatment with dantrolene, a ryanodine receptor inhibitor, induces thinner perineurial glia projections (B, D), but not in all fish (A, C) and occasionally causes blebbing glia (arrowhead, C). Injection with MO against *ryr3-like* produces some thinner projections but no floorplate defects (bracket, E,F). Treatment with 1mM gabapentin does not disrupt glia or floorplate (G,H). Injection with *thbs1* MO causes larger floorplate very infrequently (bracket, I), and also causes thinner glial projections (J).

I took a similar approach with my assessment of *thbs1*, attempting to phenocopy the mutation by injecting AB* embryos with a morpholino against *thbs1* (Figure 3-3 G, H). However, this did not perturb the floorplate or the glia. I also treated embryos with Gabapentin, an inhibitor of *thbs1* binding to the receptor $\alpha 2\delta-1$ (Eroglu et al., 2009). Rarely with this drug treatment a larger floorplate was observed, but glia still exited the CNS normally (Figure 3-3 I, J). A caveat to this experiment is that *thbs1* interacts with many other proteins besides the $\alpha 2\delta-1$ receptor, so this drug is affecting only some of the functions of *thbs1*.

In summary, neither *thbs1* nor *ryr3-like* were conclusively eliminated, and the uncharacterized gene *CABZ01118004.1* also remained in contention. At this point in the project a new genome assembly was released, GRCz10. This version significantly changed the orientation, location, and relative order of many of the candidate genes. It has also removed some genes from the chromosome 17 altogether. The GRCz10 alignment has moved *ryr3-like* a distance of 400,000 bp from its previous position, and *thbs1* is no longer mapped to the chromosome (Figure 3-2 B). This new reference assembly casts our previous fine mapping, which relies upon knowing the relative order of genes, into doubt. In the future, the raw WGS data will need to be re-aligned to this new reference genome and re-analyzed to identify this gene.

Schwann cells fail to make myelin and undergo apoptosis

It has been shown that the components of the peripheral nerve can be

interdependent on each other (Clark et al., 2014; Kucenas et al., 2008).

Therefore, once a perineurial glial phenotype had been characterized, the *ftl*^{vu268} mutants were assayed for other nervous system and glial defects. Using 72 and 96 hpf *ftl*^{vu268} embryos, an *in situ* hybridization for *myelin basic protein (mbp)* showed a complete lack of myelin in the mutants (Figure 3-4 D, E) compared to WT siblings (Figure 3-4, A, B). This indicates that the mutation is not just affecting the perineurial glia, but also the oligodendrocytes and Schwann cells.

To account for the absence of myelin, I looked more closely at the morphology of these glial cell types. I used live confocal microscopy of 72 hpf *ftl*^{vu268} fish, which are transgenic for *Tg(nkx2.2a:megfp)*, which labels perineurial glia and the floorplate, and for *Tg(sox10:mrfp)*, which labels oligodendrocytes and Schwann cells. I observed that the Schwann cells were present along the nerve, but had an unhealthy, blebbing appearance (Figure 3-4 F), which is not normally present in WT fish (Figure 3-4 C). Blebbing is frequently a sign of cell death.

Neural crest cell migration and numbers were evaluated using immunohistochemistry with antibodies for Sox10 and Tubulin on *ftl*^{vu268} embryos. Because *ftl*^{vu268} mutant siblings cannot be easily differentiated until 48 hpf, all assays performed on younger embryos are blind screens of *ftl*^{vu268} +/- x *ftl*^{vu268} +/- clutches. At 24 hpf, no difference in migration patterns was observed (Figure 3-4 G, H). The number of neural crest cells was counted as part of a blind screen of a mutant clutch, and no difference was found compared to an entirely WT clutch,

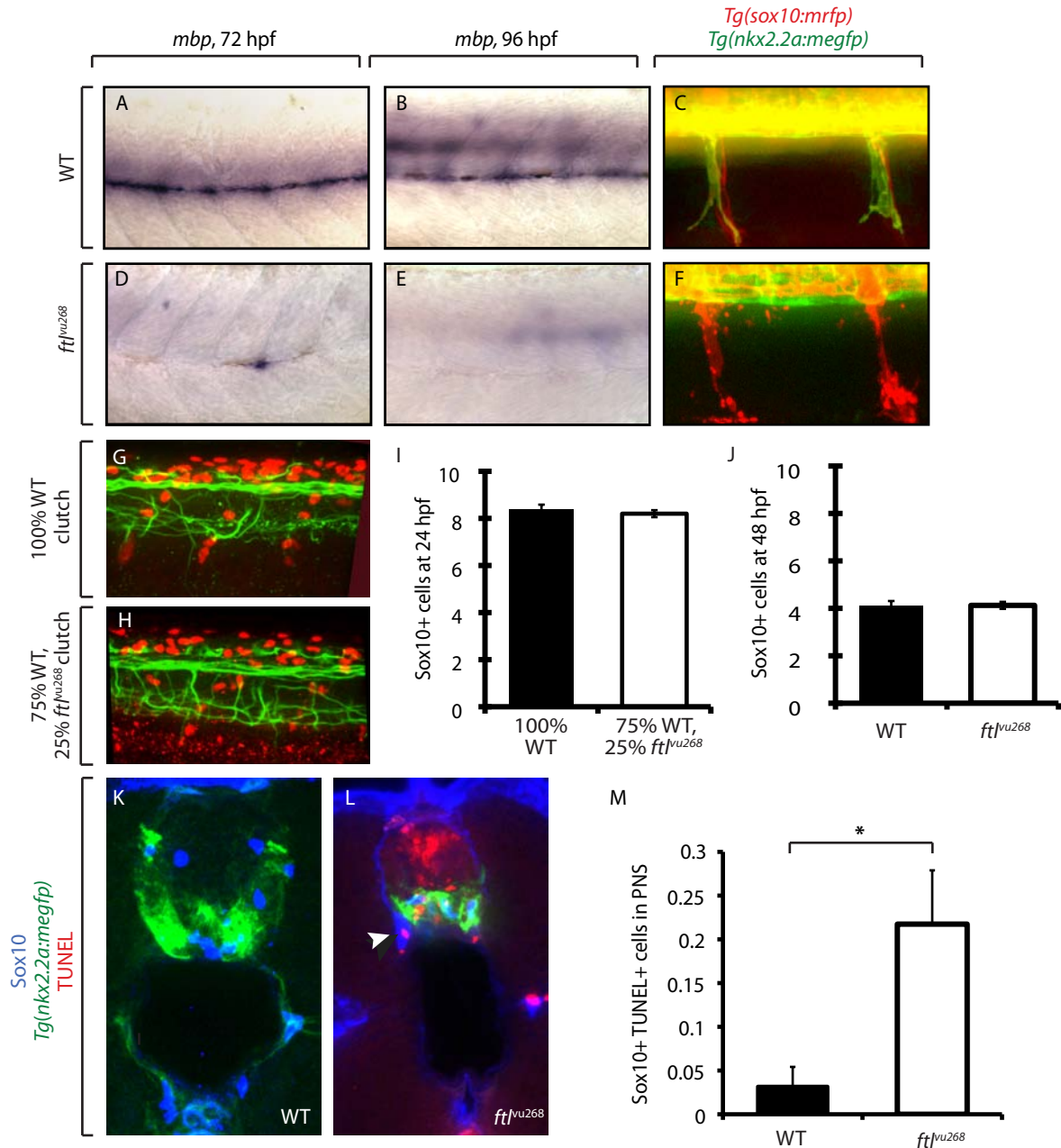


Figure 3-4: In *ftjvu268* mutant fish, Schwann cells develop normally until 72 hpf when they fail to make myelin and die. *In situ* for *mbp* on *ftjvu268* 72 hpf embryos. Mutants show near absence of stain at 72 hpf and 96 hpf along the lateral line (D, E) compared to WT sibling expression pattern (A, B). Transgenic *Tg(nkx2.2a:megfp)*, *sox10:mrfp* fish from a *ftjvu268* clutch imaged live at 72 hpf. WT siblings exhibit smooth sheaths of *sox10*+ cells (C) compared to blebbing in mutant embryos (E). Transgenic *Tg(nkx2.2a:megfp)* fish from a 100% WT clutch or a 75% WT 25% *ftjvu268* clutch labeled with Tubulin and Sox10 at 24 hpf and imaged. No difference observed in the streaming of neural crest cells (G, H). No difference was found in the number of Sox10+ cells along each nerve at 24 hpf (I) and 48 hpf (J). Transgenic *Tg(nkx2.2a:megfp)* fish from a *ftjvu268* clutch labeled with Sox10 and TUNEL at 72 hpf and imaged (K, L). Mutant fish had more TUNEL expression overall (L) and when co-labeled with Sox10 (arrowhead), a trend quantified in M (p value=0.002).

averaging 8 cells (Figure 3-4 I). Similarly, at 48 hpf, when mutant and WT siblings can be distinguished, no significant decrease in the number of Schwann cells was observed, both having approximately four cells per motor nerve (Figure 3-4 J). By this analysis, neural crest development is unperturbed before 48 hpf.

The blebbing morphology suggests that glia are dying at 72 hpf, so I used TUNEL labeling to assess for apoptosis in Sox10+ cells. I assayed for cell death in 72 hpf *Tg(nkx2.2a:megfp) ftl^{vu268}* mutant embryos and their WT siblings by labeling with TUNEL and Sox10, sectioning the larvae, and imaging the sections (Figure 3-4 K, L). I observed a significant increase in the number of Sox10+ cells in the periphery that were also labeled with TUNEL, from 0.03 to 0.2 dying cells per section (Figure 3-4 M). In summary, I conclude that in mutant embryos, neural crest cells are unperturbed before 48 hpf. At later stages, Schwann cells do not make myelin, but rather exhibiting a blebbing morphology and undergo apoptosis.

Oligodendrocytes are decreased but migration is unaffected

Because of the complete absence of myelin discussed above, I hypothesized that oligodendrocytes were affected as well as Schwann cells. I labeled *Tg(nkx2.2a:megfp) ftl^{vu268}* larvae with Sox10 at 48 hpf and 72 hpf, sectioned the embryos, and imaged the sections (Figure 3-5 A, B). After counting the number of Sox10+ cells within the CNS, I indeed found that the number of oligodendrocytes was decreased in mutant fish, from an average of 3 to 0.8 cells

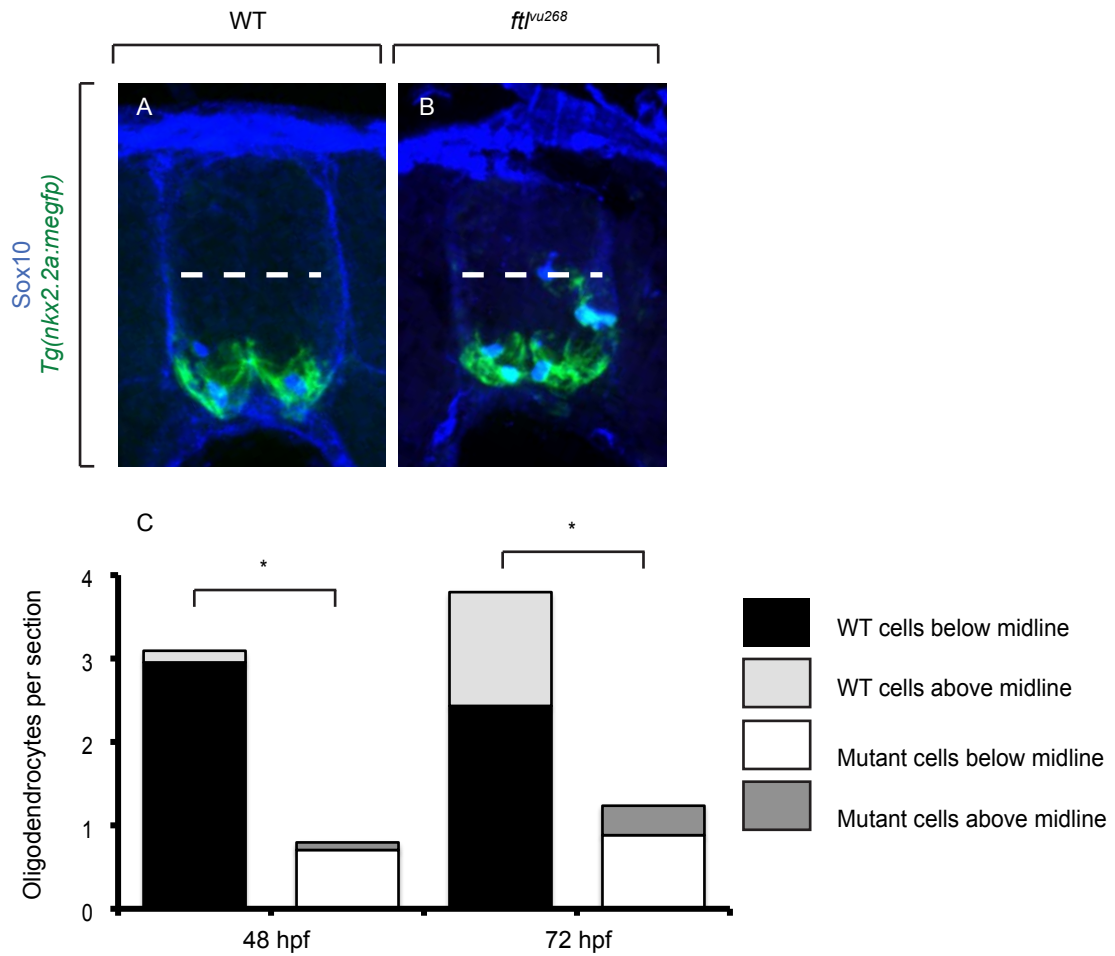


Figure 3-5: *ft/vu268* mutant fish have fewer oligodendrocytes but oligodendrocyte migration is not perturbed. Transgenic *Tg(nkx2.2a:megfp)* fish from a *ft/vu268* clutch were labeled with Sox10 at 72 hpf, sectioned, and imaged (A+B). At 48 hpf and 72 hpf, mutant fish had fewer oligodendrocytes overall (both p values = < 0.0001). The proportion of glia above the midline (dashed line) was not different from WT siblings (quantified in C).

per section at 48 hpf, and 3.8 to 1.2 cells per section at 72 hpf. I also tested for perturbations of oligodendrocyte migration. As I counted the number of Sox10+ cells in CNS, I also scored for whether they remained in the region below the midline, or had migrated to the dorsal region of the spinal cord. Although the overall number of oligodendrocytes was decreased, the proportion of oligodendrocytes in each region was not significantly different at 48 hpf or 72 hpf (Figure 3-5 C). This result suggests that while migration of perineurial glia is perturbed, not all cell migration within the CNS is affected.

Motor neurons and their axons are not affected by the ftl^{vu268} mutation

Previous studies have found that when perineurial glia were prevented from being specified using a Nkx2.2a morpholino, motor axons exited ectopically from the spinal cord (Kucenas et al., 2008). Accordingly, I hypothesized that motor axons would be perturbed in this ftl^{vu268} mutant as well. I assayed for neuronal perturbation using several methods. First, I labeled a 48 hpf *Tg(nkx2.2a:megfp)* mutant clutch with an antibody for Tubulin (Figure 3-6 A, B). In these embryos I measured the distance between two MEP in WT and mutant siblings, but found no difference in the spacing, at 105 μ M each (Figure 3-6 C). I also used these embryos to compare axon branching at 48 hpf, and this assay also found no difference between mutant fish and their WT siblings (Figure 3-6 D). The antibody for Islet, which in the CNS labels motor neurons and Rohan-Beard neurons, was used to label 24 hpf *Tg(nkx2.2a:megfp)* embryos, which were sectioned, and Islet+ cells counted (Figure 3-6 E, F). No significant difference

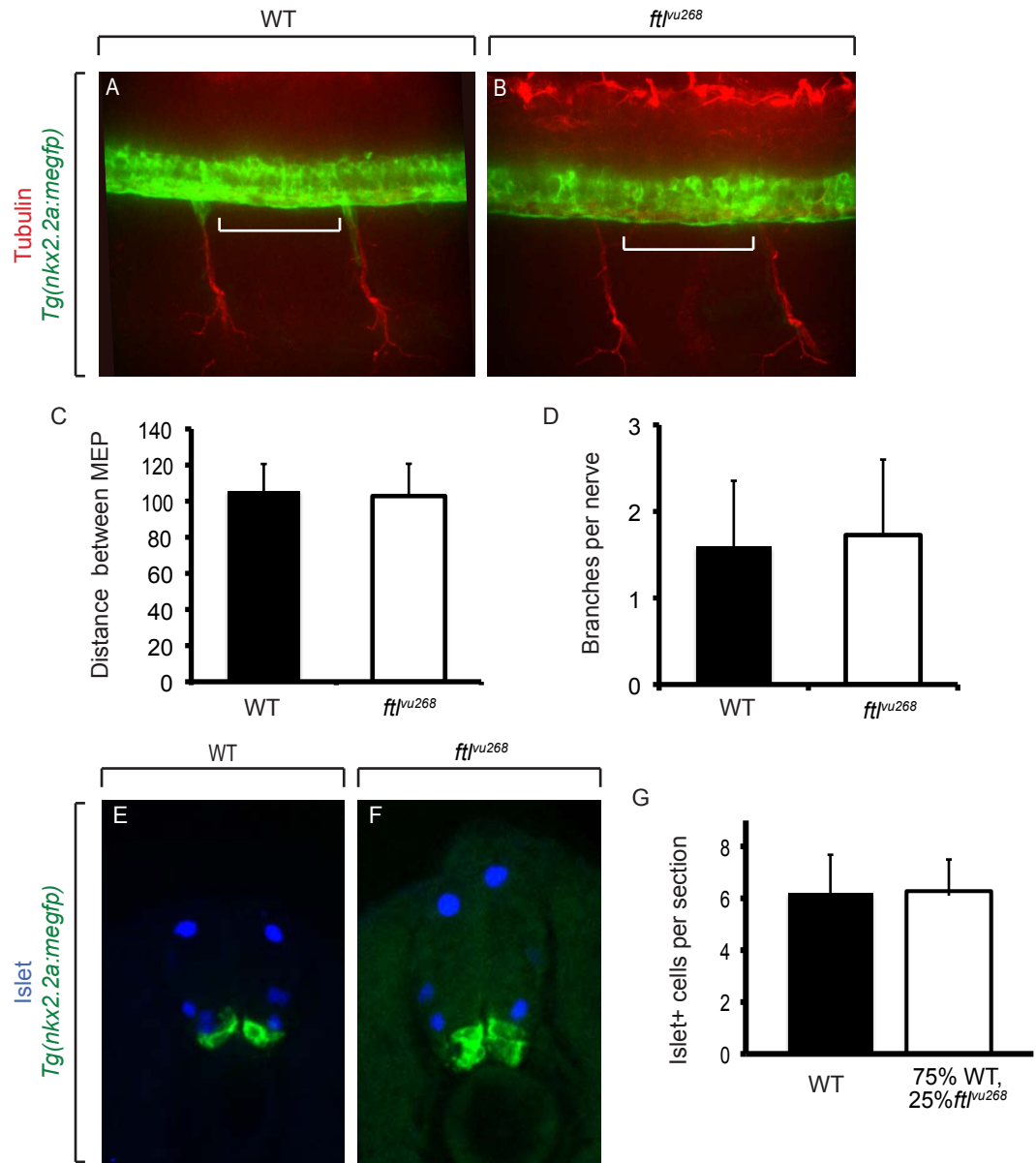


Figure 3-6: *ftl^{vu268}* mutant fish have no motor neuron defect. Transgenic *Tg(nkx2.2a:megfp)* fish from a *ftl^{vu268}* clutch were labeled with Acetylated Tubulin and imaged at 48 hpf. In WT (A) and mutant embryos (B) axons exit at each MEP and at regularly spaced intervals, which is quantified in μm (C). The average number of branches on each nerve before the horizontal myoseptum is also quantified (D). (E, F) Transgenic *Tg(nkx2.2a:megfp)* fish from a *ftl^{vu268}* clutch were labeled with Islet at 24 hpf, sectioned, and imaged. In a blind screen, no difference was observed in the number of Islet+ cells per section, which is quantified in (G).

was found from this assay between a 100% AB* clutch and a *ftl^{vu268}* clutch, both averaging approximately six cells per section (Figure 3-6 G). In sum, according to several measures of motor neuron development, these cells are not perturbed in *ftl^{vu268}* mutant fish.

Angiogenesis and brain development is perturbed

There are some non-gliial phenotypes in *ftl^{vu268}* fish that were characterized as well. In attempts to eliminate other candidate genes, I assayed for vascular development using an alkaline phosphatase stain in 72 hpf fish, focusing on the vessels across the yolk sac (arrowheads, Figure 3-7 A, B). I found that mutant embryos were more likely to have limited or absent vascularization. Decreased vascularization increased significantly from 8% to 59%, and absent vascularization increased significantly from 0% to 26% (Figure 3-7 C). Also, I used *in situ* hybridization for *pax3* on 48 hpf *ftl^{vu268}* embryos and found that mutant larvae had a distinctly different expression pattern in the head than WT larvae. This *in situ* clarifies that the brain structures affected by this mutation includes the telencephalon, optic tectum, and cerebellum (arrowheads, Figure 3-7 D, E).

Discussion

The lack of motor neuron perturbation is an interesting result. Currently there is no way to distinguish perineurial glia precursors within the spinal cord from other neuronal cells, such as interneurons, which are also labeled with *nkx2.2a*. This

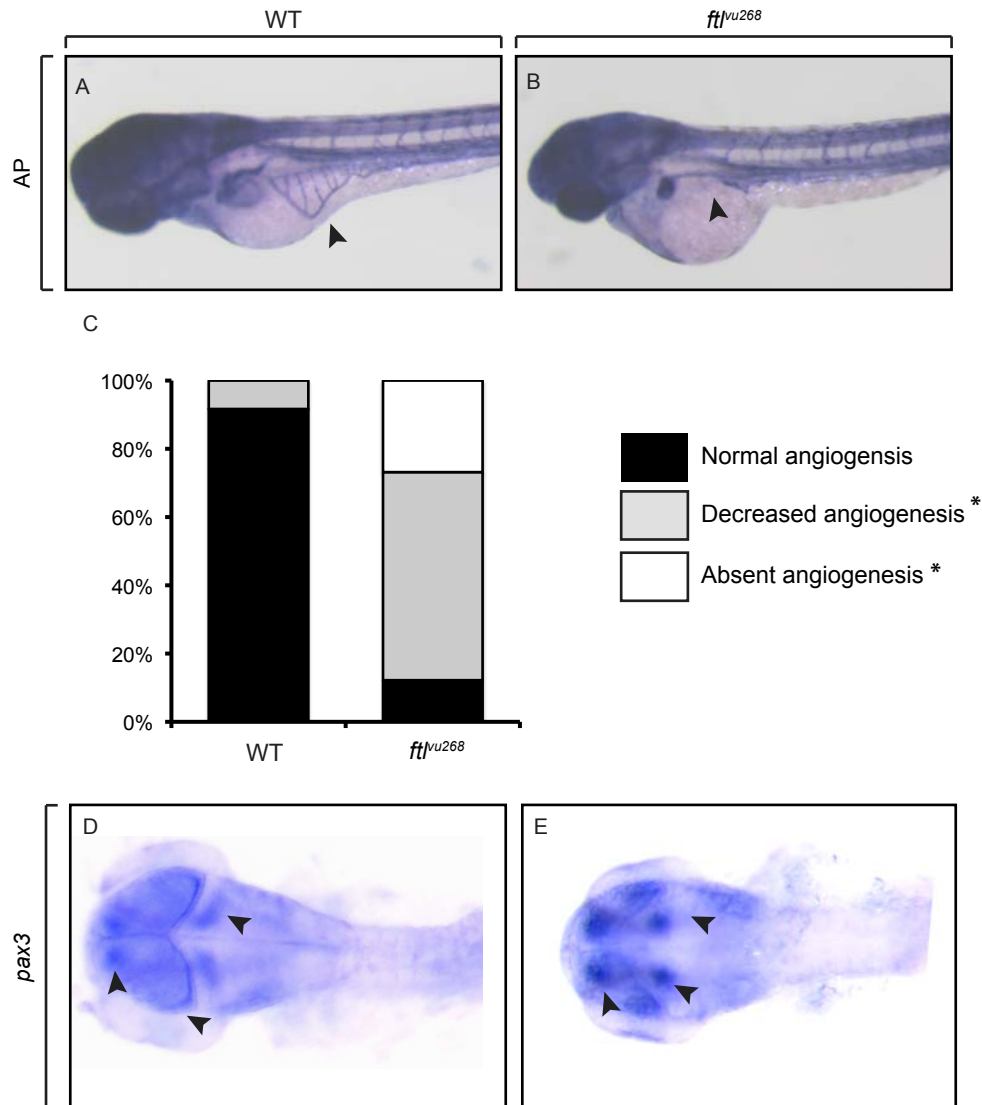


Figure 3-7: *ftl^{vu268}* mutant fish have decreased angiogenesis and a brain-patterning defect. Fish from a *ftl^{vu268}* clutch were labeled with alkaline phosphatase at 72 hpf and imaged. In the trunk, decreased or completely absent angiogenesis was observed in mutant fish (arrowheads, A, B). This trend was quantified in C. The proportion of fish that have absent or decreased angiogenesis was calculated to be significantly different (p values= 0.008 and <0.0001 , respectively). At 48 hpf fish from a *ftl^{vu268}* clutch were labeled with *pax3* and imaged. Differences in expression pattern were observed in the telencephalon, optic tectum, and cerebellum (arrowheads, D, E).

raises the question about the nature of this mutation- whether the glia are ever specified, or if they are present but only unable to migrate out of the spinal cord. To be consistent with previous results, my findings suggest that perineurial glia are in fact specified within the spinal cord of *ftl^{vu268}* mutants, and despite failing to migrate, they can still regulate motor axon development, unlike the *nkx2.2a* morphants.

This project will not be complete without identifying the gene in which the *ftl^{vu268}* mutation is located. A reliable alignment of chromosome 17 is crucial for the success of mapping this gene. This is one disadvantage to working with zebrafish, a model organism that is not as well studied as others. Assuming this recent alignment is correct, the raw data will have to be completely re-analyzed. At this point, the SNPTrack pipeline does not even allow data to be analyzed with the GRCz10 genome, meaning that another method of analysis must be found.

While the *ftl^{vu268}* mutation remains unmapped, I still have characterized a very interesting but inconsistent role for this gene. Importantly, the mutation does not affect all glial cell types in the same manner. In perineurial glia, cell migration is perturbed. However, in Schwann cells and oligodendrocytes, migration appears normal, but differentiation into mature, myelinating glia is affected and cell death occurs. The floorplate is larger and more disorganized, which can be explained by an excess of perineurial glia stalling within the spinal cord, but this is only conjecture. There are other cells in the floorplate, such as interneurons, that

could also be affected.

The manner in which vascularization is also regulated by this gene is not clear. It is not unusual that a factor can affect both neuronal and vascular development. Interestingly, *thbs1* has been identified to inhibit angiogenesis in the context of tumors and injury, but it was also eliminated from the newest version of chromosome 17 (Lawler, 2002). It is clear that the mutation has effects both in the CNS and the periphery. Although the Schwann cells and oligodendrocytes represent two halves of the nervous system, they frequently draw on the same master regulator genes, such as *sox10*, and *nrg1*, even if the role for that gene is not exactly the same in both cell types. This study illustrates that the *ftl*^{*vu268*} mutation has the same overarching effect, its perturbation resulting in the absence of myelin and glial cell death across the nervous system.

Chapter IV: The *ray*^{vu267} mutant defines a novel neuronal role for *dystrophin* independent of muscle function

Introduction

All vertebrate organisms rely on efficient neural transmission for locomotion. Spinal motor nerves, composed of axons and their associated glia and connective tissue, are essential for the coordinated contraction and relaxation of muscle fibers, which are essential for organism survival and reproduction. In Duchenne Muscular Dystrophy, progressive muscle wasting is thought to ultimately lead to the degeneration of the nerves that innervate it. Interestingly, prior to this degeneration, several previous studies conclude that motor conduction velocity (MCV) in DMD patients is normal. However, there is also evidence in the literature that supports that in some cases of DMD, MCV is significantly slower (Cruz Martinez and Lopez Terradas, 1990; Al-Ani et al., 2001; Anderson et al., 2002). Although motor nerves have been physiologically assessed in DMD, little is known about the development and maintenance of spinal motor nerves and their components in patients with this disease.

DMD is an X-linked recessive disorder caused by mutations in the *dystrophin* gene. Patients with DMD exhibit motor deficits as young children, which become more severe as they age. Most will become bedridden and die in their thirties from secondary complications such as respiratory or cardiac difficulties (McDonald et al., 1995). Many patients also show some level of mental

impairment (Anderson et al., 2002; Lidov, 1996). Currently, there are no treatments for DMD, although several therapies are in various stages of clinical trials. These include viral gene therapy, oligomers designed to trigger exon skipping and drug treatments that promote early stop codon read-through (Bowles et al., 2012; Cirak et al., 2011; Finkel et al., 2013; Goemans et al., 2011; Kinali et al., 2009).

Dystrophin is a key component of the DAPC that links the actin cytoskeleton within the sarcolemma to the ECM and physically reinforces the membrane under the strain of regular motor activity (Cohn and Campbell, 2000). The DAPC is also a platform for many different types of signaling events coming in and out of the cell, such as calcium and sodium homeostasis, nitric oxide synthetase, and MAPK and JNK signaling (Constantin, 2014). Therefore, a mutation in *dystrophin* would disrupt the entire complex and impact signaling going in and out of the cell, potentially also affecting the surrounding cellular environment.

Using an ENU forward mutagenesis screening approach in zebrafish to identify novel modulators of spinal motor nerve development, we identified mutants for one allele, designated as *ray*^{vu267}. These fish were phenotypically indistinguishable from wild type embryos at 48 hpf, but by 72 hpf, had smaller jaws, disrupted pigmentation and evidence of muscle fiber degeneration. Closer analysis revealed that motor nerve development was also perturbed, with perineurial glia exiting the spinal cord ectopically and an increased number of

Schwann cells. Using whole genome sequencing and bulk segregant analysis, we mapped this mutation to a region on chromosome one that includes the *dystrophin* gene. Complementation testing with a known *dystrophin* mutant allele, *sapje-like*, recapitulated these nervous system and muscle defects and confirmed *ray*^{vu267} as a novel mutant allele of *dystrophin*.

Here, I show using *in vivo* time-lapse imaging and molecular characterization, that mutations in *dystrophin* not only cause muscle phenotypes consistent with DMD, but also cause severe nervous system patterning defects. This is not unique to *ray*^{vu267} mutants, but seems to be a general property of *dystrophin* mutants, as I observed similar effects in *sapje-like*. These neuronal and glial phenotypes are observable well before the traditional muscle atrophy attributed to this disease, and are therefore independent of muscle wasting.

Understanding of these phenotypes cannot be complete without consideration of the multiple transcripts of the *dystrophin* gene. This chapter also discusses difficulties in assessing the relative effects of this mutation on *dmd* transcript isoforms, *dp427* and *dp71*. In humans, *dystrophin* produces many alternative transcripts, with various unique expression patterns. Dystrophin is present in many non-muscle locations, including brain, spinal cord, Schwann cells, and the kidney. In zebrafish, only two isoforms besides full-length *dystrophin* have been identified: *dp116* and *dp71* (Bolaños-Jiménez et al., 2001b; Jin et al., 2007). Previous research in zebrafish and other organisms has shown that *dp71* is

expressed at low levels in the myotome and much more strongly in the CNS (Bolaños-Jiménez et al., 2001a). However, *dp71* only differs very slightly from the *dp427* transcript. Our *in situ* hybridization results in similar expression levels between muscle and brain, in a pattern very similar to the *dp427* probe, which casts doubt on their specificity.

Nevertheless, we can conclude that some version of the *dmd* transcript and protein is absent from the myotome. The mechanism by which this perturbation can influence the development of glia and motor axons outside of the muscle is unclear. The position of Dystrophin in the DAPC of the sarcolemma means it could influence the ECM by destabilizing the signaling pathways routed through the DAPC. However, this effect on the peripheral ECM does not explain the mechanism by which oligodendrocytes or motor neurons within the CNS are being affected. I also have not yet determined whether this mutation is autonomous or nonautonomous, which is another important aspect of this mutation.

Currently, there are several therapies in clinical trials aimed at treating DMD. However, many of these therapies are yielding mixed results, which suggests that our understanding of the role of dystrophin in DMD is incomplete. Our data support the hypothesis that *dystrophin* mutations have a much broader impact than just on muscle maintenance, which should be considered when developing therapies.

Results

Identification of a novel mutant allele of dystrophin in zebrafish

Although we know the anatomical details of the components of the peripheral nerve, we know very little about the mechanisms that govern the development of some of these cell populations. To identify novel modulators of perineurial glial development, an ENU forward genetic screen was conducted in zebrafish. This screen utilized the *Tg(nkx2.2a:megfp)*, which use *nkx2.2a* regulatory sequences to drive expression of membrane-tethered EGFP in lateral floor plate cells, oligodendrocyte progenitor cells, and perineurial glia.

Characterization of the *ray*^{*vu267*} mutants was performed by myself in collaboration with two lab technicians, Rebecca Nash and Vani Hariharan. By screening families from this screen using this transgene, we identified mutants for one allele, designated as *ray*^{*vu267*}, that were phenotypically indistinguishable from wild type embryos at 48 hpf, but by 72 hpf, had smaller jaws, disrupted pigmentation and evidence of muscle fiber degeneration (Figure 4-1 A, B). When we assayed perineurial glial and motor nerve development, we observed that in contrast to wild type larvae, where perineurial glia exited the spinal cord at regularly spaced MEP and tightly ensheathed developing spinal motor nerves (Figure 4-1 E), *nkx2.2a*+ perineurial glia and *olig2*+ motor axons exited the spinal cord ectopically and had unusual morphologies in *ray*^{*vu267*} larvae at 72 hpf (Figure 4-1 G).

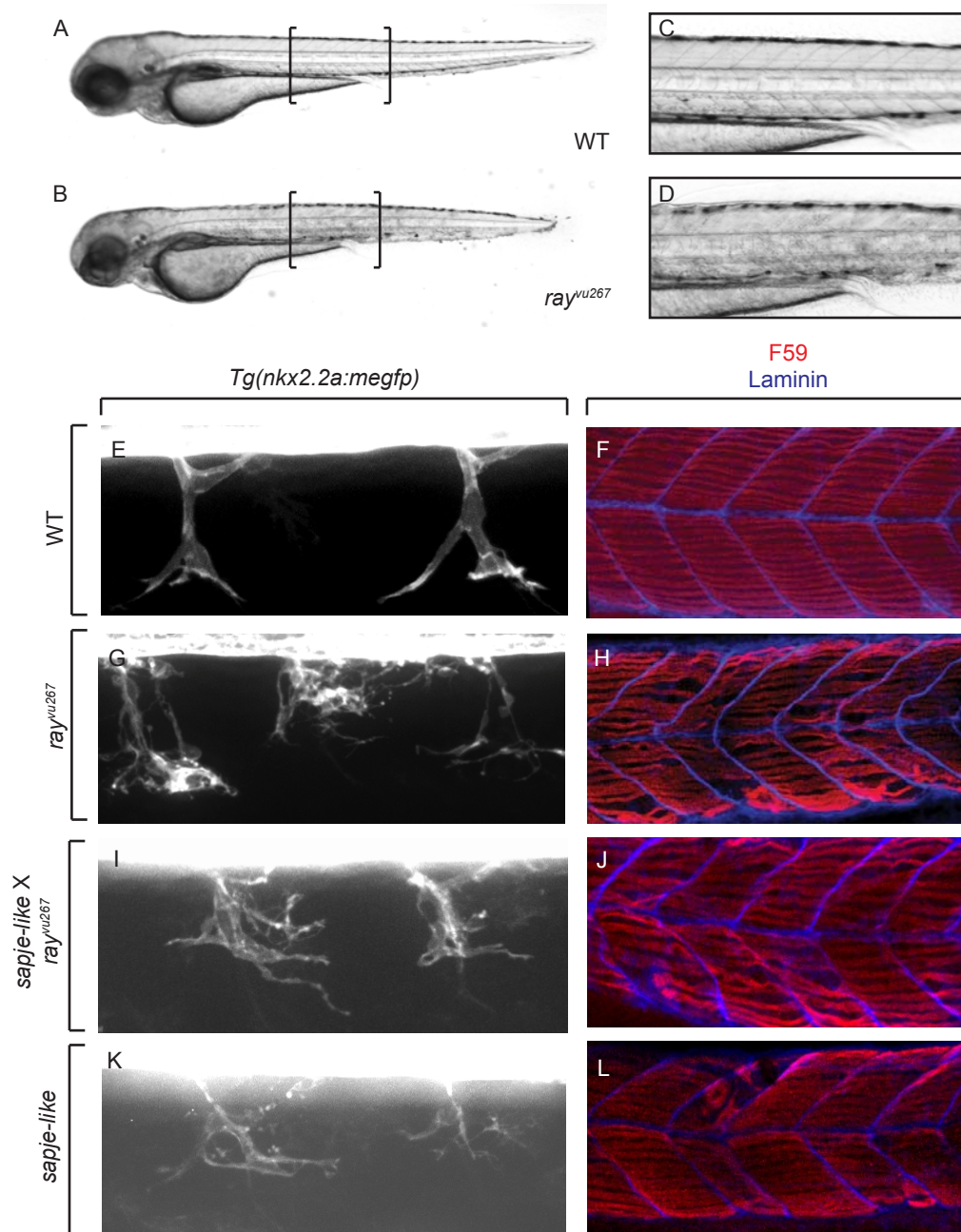
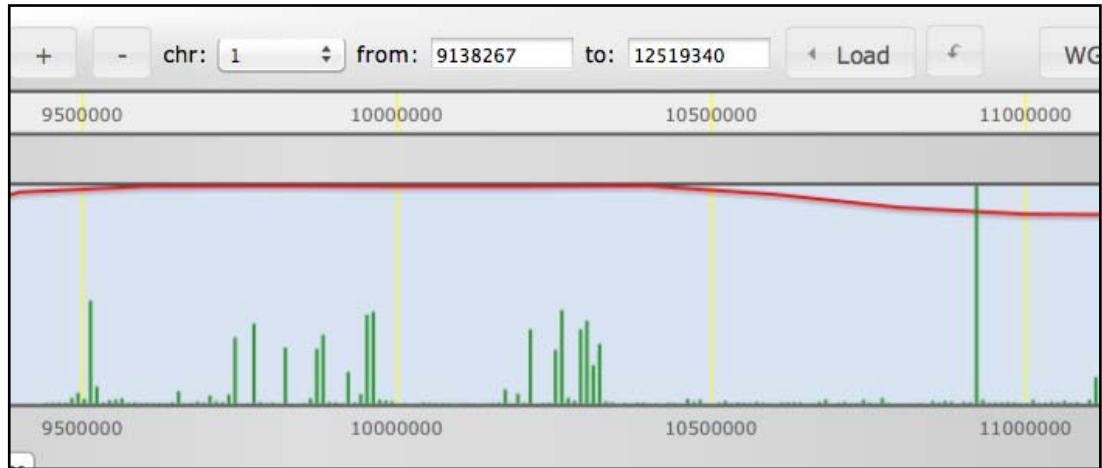


Figure 4-1: The *ray^{vu267}* mutation causes perineurial and muscle defects, and is located in *dystrophin*. 72h images of WT (A) and *ray^{vu267}* fish (B), with magnified view of muscle lesions in mutant fish compared to WT siblings (C, D). Transgenic *Tg(nkx2.2a:megfp)* fish from a *ray^{vu267}* clutch were imaged at 72 hpf. Glia exit in smooth sheaths at regularly spaced intervals in WT siblings (E). In mutant fish, the morphology is finely branched and they exit ectopically (G). A *ray^{vu267}* clutch labeled with F59 and Laminin at 72 hpf. In the WT sibling, the F59 and Laminin labeling is organized into straight, parallel lines (F). In the mutant, Laminin is wavy and the F59 fibers are patchy and disorganized (H). Transgenic *Tg(nkx2.2a:megfp) ray^{vu267} +/-* fish were crossed to *sapje-like +/-* fish. 72 hpf fish from this clutch display the perturbed glial phenotype (I). Transgenic *Tg(nkx2.2a:megfp) sapje-like* fish at 72 hpf display the perturbed glial phenotype (K). A 72 hpf *ray^{vu267} X sapje-like* clutch and a *sapje-like* clutch were labeled with F59 and Laminin and imaged. One fourth exhibits the disorganized labeling pattern (J, L).

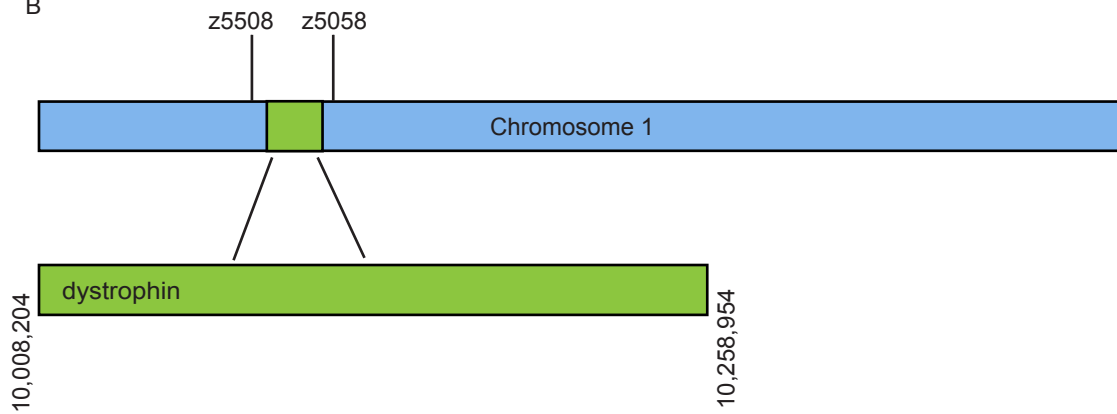
In order to map this mutation, I referred to the results of WGS and fine mapping performed by Nash. Genomic DNA from fifty WT and *ray*^{vu267} mutants was isolated and pooled, and WGS was performed using an IlluminaHiSeq 2500 with 100 base pair paired-end reads. The raw data was uploaded into the SNPtrack pipeline (genetics.bwh.harvard.edu/snptrack/), which aligns the reads to the reference genome, Zv9, and calls SNPs. SNPtrack also compares homozygosity of SNPs in the mutant pool to the WT pool, which is used to find a window of high homozygosity, within which the mutation is likely located. This limited the search to a 12 MB region on chromosome one (Figure 4-2 A).

To narrow the region further, the mutated loci responsible for this phenotype was located between z markers z5508 and z5058, a region of 2MB (Figure 4-2 B). One candidate gene in this region that immediately became relevant was *dystrophin*, as the mutants had evidence of muscle degeneration by 72 hpf, which has previously been described for other *dystrophin* mutant alleles (Figure 4-2 B). Because *ray*^{vu267} mutant embryos eventually display signs of muscle atrophy, we labeled mutant and sibling embryos at 72 hpf with antibodies to F59 and Laminin, which labels slow muscle myosin and basal lamina. In control embryos, muscle fibers labeled with F59 were highly organized, ran parallel to each other and all connected at the myosepta (Figure 4-1 F). In contrast, in *ray*^{vu267} mutant embryos, F59 labeling revealed patches of disorganized muscle fibers that often failed to connect to the myosepta (Figure 4-1 H). These data led

A



B



C

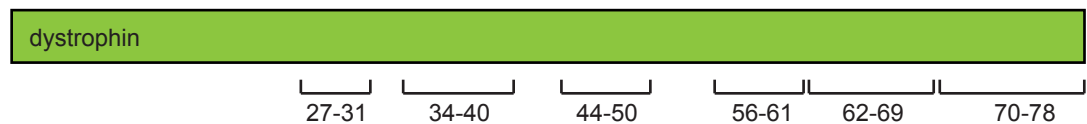


Figure 4-2: The mutation was mapped to a region containing *dmd*, and RT PCR was used to assay for pseudoexons. (A) SNPTrack identified a 2 MB region on chromosome 1 which had high levels of homozygosity (green bars). (B) Using fine mapping, this region was narrowed to the window between z5508 and z5058, which includes *dmd*. (C) Candidate SNPs within *dmd* were found to be located in 6 clusters of introns (brackets). (D) RT PCR and sequencing was used to test these six regions for pseudoexons. Excluding low quality results at the beginning and end of each sequence (purple boxes), and sequencing artifacts (blue circle) no insertions or pseudoexons were observed in the comparison between pooled WT DNA and pooled mutant DNA. Some single base pair changes were observed but they do not cause splice errors, frameshifts, or early stops.

D

Alignment of Sequence 1: M pool 27-31 F with Sequence 2: WT pool 27-31 F

Similarity : 744/881 (84.45 %)

Seq_1	1	NNNNNNNNNNNNNNNNNN--N--CCCGCGGCCCATGATGCCCTGAAGGCAGAAGCTGGAT	56
Seq_2	1	NNNNNNNNNNNNNNNNNNNGNNC'CCCGCGGCCCATGATGCCCTGAAGGCAGAAGCTGGAT	60
Seq_1	57	GTTTTGACTTCTAACTACCAGCGCCTGTGCAGCCGACTCGATGGAAAATGCAAGACTTTA	116
Seq_2	61	GTTTTGACTTCTAACTACCAGCGCCTGTGCAGCCGACTCGATGGAAAATGCAAGACTTTA	120
Seq_1	117	GAGGAAGTGTGGGCATGCTGGTGTGAGCTGCTGTCTTATTTGGAGTTGGAGAATGCCTGG	176
Seq_2	121	GAGGAAGTGTGGGCATGCTGGTGTGAGCTGCTGTCTTATTTGGAGTTGGAGAATGCCTGG	180
Seq_1	177	ATGGACCTACTTGAAAAGAACTTGATGAAACGGAAGGGCTTCAAGGAGGCATAGAGGAA	236
Seq_2	181	ATGGACCTACTTGAAAAGAACTTGATGAAACGGAAGGGCTTCAAGGAGGCATAGAGGAA	240
Seq_1	237	ATTGAAGAAGCTTTGACTTCTTTAGACACCATGATTAGAGAGCATCCTGAATACAACCGT	296
Seq_2	241	ATTGAAGAAGCTTTGACTTCTTTAGACACCATGATTAGAGAGCATCCTGAATACAACCGT	300
Seq_1	297	AACCAGATACGTGAATTAGCGCAGACCCTGATGGATGGCCGAGTCCCTGGATGAGCTCATC	356
Seq_2	301	AACCAGATACGTGAATTAGCGCAGACCCTGATGGATGGCCGAGTCCCTGGATGAGCTCATC	360
Seq_1	357	CACAAAAGGTGGAGGACTACAACACACGCTGGGATGAACTGATGCAAAGGGCTTCACAA	416
Seq_2	361	CACAAAAGGTGGAGGACTACAACACACGCTGGGATGAACTGATGCAAAGGGCTTCACAA	420
Seq_1	417	AGGCGCCAGCAGCTGGAGAAGAGCTTGCATTGGGCCCAGGAGAACGACAAAACCTGCGT	476
Seq_2	421	AGGCGCCAGCAGCTGGAGAAGAGCTTGCATTGGGCCCAGGAGAACGACAAAACCTGCGT	480
Seq_1	477	CTCATTCAGGACTCTCTGAACACCACTGACCGACATCTGACCGCTTACATAGCAGATGGC	536
Seq_2	481	CTCATTCAGGACTCTCTGAACACCACTGACCGACATCTGACCGCTTACATAGCAGATGGC	540
Seq_1	537	ATAGACGCTGCACAGATACCACAGGAAGCACAGAAAATTCAGACTGAGTTGAACGGCCAT	596
Seq_2	541	ATAGACGCTGCACAGATACCACAGGAAGCACAGAAAATTCAGACTGAGTTGAACGGCCAT	600
Seq_1	597	GAG--GNNNNNCTGGATGAANNCCACTCTACTGNTTCCGAACTTNCNGNNNACNNNGTG	654
Seq_2	601	GAGNNANNNNNNGANGNANNNAATTCACCAGTTCNAACTTGCCNNTNACCNGAGANC	660
Seq_1	655	NNAGCNGNCNTTNTCCCTTCNTNAGCTATGTANCGTNNCATGNCCNCNCNTGTANNTNA	714
Seq_2	661	TCTGCGCCTTTCNACCTTCNNGNNGTACNCTNNNNNANANCTC'NNNNNNNNNNNCGC	720
Seq_1	715	GTAAAGTTCNGAAAAGNANN'CNNGNGTCTAGNCNNTCNCNGNGTGCNANGAAANCTC---	771

Seq_2	721	<pre> ::: : : : : : : : : : : : : : : : NNNNGNNNGNAGNTCNNNCNCTCNGGCTTNCNNATCCNCNNNACCCCTCCNNN-CANGCC </pre>	779
Seq_1	772	<pre> CTTNTCAGCTGNNANNNCATCGGTCAANTCCTTTGANTANNTAC-CNCNNGTNGNNNNNG : : : : : : : : : : : : : : : </pre>	830
Seq_2	780	<pre> GACCCCTGCNCATCTT----CNGNATC-TAT---TNNCTTGAGTCCNNA-GCCGANTCTC </pre>	830
Seq_1	831	<pre> NNCCNCNCNTTTTGTGGNANANNTCATCNNNANNGANCNCNNNTGNNN : : : </pre>	881
Seq_2	831	<pre> ACNCNN----- </pre>	836

Seq_2	721	 CCTCCACATTTAGACCGTCTGACATTCAGCTTTCTCCANACAACCTGAGCAGAATCGATG	780
Seq_1	778	ACCTCAACATGAGATGGAGGCTTCTGCAGATCTCCATTGANGAGCATCTGAGTCAGCTGA	837
Seq_2	781	: : : : : : ACCTCAACATGANATGGANGCTTCTGCANATCTCCATTGANGANCATCTGANTCAGCTGA	840
Seq_1	838	CCACAGCCTTTAAGGACTTGNGANCCCTCTCAGANN	873
Seq_2	841	: CCN-----	843

Alignment of Sequence 1: WT pool 62-69 F with Sequence 2: M pool 62-69 F

Similarity : 854/932 (91.63 %)

Seq_1	1	NNNNNNNNNNNNNNNNNNNN--TN-NNNNTACT-AT-AT--C-NTCNCNGAGNNAACAN	52
Seq_2	1	NNNNNNNNNNNNNNNNNNNNCNGCCGCCACAGATGANCCAGTGGCCNAGGTCACAN	60
Seq_1	53	CNTGTNGNNACCACCCAAAGATGGNAGAANNNNNNCNGNCATTATGGGATCTCAACAACG	112
Seq_2	61	NNNGGG---ACCACCCAAAGATGGCAGAACTNTNNCAGTCATTAGCGGATCTCAACAACG	117
Seq_1	113	TGCGGTTCTCGGCATACAGGACGGCAATGAAGCTCAGACGAATGCCGAAAGCCCTCTGTT	172
Seq_2	118	TGCGGTTCTCGGCATACAGGACGGCAATGAAGCTCAGACGAATGCAGAAAGCCCTCTGTT	177
Seq_1	173	TGGATCTTCTGAGCATGCCTGCAGCCTGTGAAGCCTTTGATCAGCACAATCTCAAACAGA	232
Seq_2	178	TGGATCTTCTGAGCATGCCTGCAGCCTGTGAAGCCTTTGAGCAGCACAATCTCAAACAGA	237
Seq_1	233	ACGAGCAGTTCATGGACATCGTGCAGGTGATCAACTGTCTGACCAGCATCTACGACCGTC	292
Seq_2	238	ACGAGCAGTTCATGGACATCGTGCAGGTGATCAACTGTCTGACCAGCATCTACGACCGTC	297
Seq_1	293	TGGAGCACCACCACAGCAGCCTGGTCAACGTGCCTCTCTGTGTGGACATGTGTCTCAACT	352
Seq_2	298	TGGAGCAGCAGCACAGCAGCCTGGTCAACGTGCCTCTCTGTGTGGACATGTGTCTCAACT	357
Seq_1	353	GGCTGCTCAACGTTTACGATACAGGACGAGCTGGGAAGATTCGTACCCATCCTTCAAAA	412
Seq_2	358	GGCTGCTCAACGTTTACGATACAGGACGAGCTGGGAAGATTCGTACCCATCCTTCAAAA	417
Seq_1	413	CAGGAATAATCTCTTTGTGCAAAGCTCACCTTGAAGATAAGTACAGATTTTATTTTCNAG	472
Seq_2	418	CAGGAATAATCTCTTTGTGCAAAGCTCACCTTGAAGATAAGTACAGATTTTATTTTCGAG	477
Seq_1	473	AGGTGGCCAGTGCCACAGGCTTCTGTGACCAGCGGCCTCGGCCTCCTCCTGCATGATG	532
Seq_2	478	AGGTGGCCAGTGCCACAGGCTTCTGTGACCAGCGGCCTCGGCCTCCTCCTGCATGATG	537
Seq_1	533	CCATTCANATCCCCAGGCAGCTGGGTGAAGTGGCGTCTTACNGAGGGAGCAATATTGAGC	592
Seq_2	538	CCATTCAGATCCCCAGGCAGCTGGGTGAAGTGGCGTCTTTCGGAGGGAGCAATATTGAGC	597
Seq_1	593	CCANTGTGCGCAACTGCTTTTCAGTTCGCCAATAACAAACCGGAGTTAGAGGCTTCAGTCT	652
Seq_2	598	CCAGTGTGCGCAGCTGCTTTTCAGTTCGCCAATAACAAACCGGAGTTAGAGGCTTCAGTCT	657
Seq_1	653	NCCTGGACTGGATGCNTTTACAACCCNNNTCNATGGTTTGNNTTCTGTCTTCANCGTG	712
Seq_2	658	TCCGGACTGGATGCGTTTAGAACCTCAGTCGATGGTTTGGCTTCTGTCTTCACCGTG	717
Seq_1	713	TAGCGGCCGCTGAGACANCAAACCACCANGCTAANTGCNNCATTGTGAANGNANTGCCT	772

to the hypothesis that *dystrophin* was the mutated loci in *ray*^{vu267}. To confirm this hypothesis, complementation testing was used with an established *dystrophin* mutant, *sapje-like*. In a heterozygous cross of *ray*^{vu267} and *sapje-like*, 25% of the embryos from the resulting cross had both muscle degeneration as well as aberrant and ectopic perineurial glial migration (Figure 4-1 I, J). Additionally, *sapje-like* mutants alone also exhibited the glial and muscle phenotypes (Figure 4-1 K, L). Therefore, we conclude that *ray*^{vu267} is a new mutant allele for *dystrophin*.

To determine the exact nature of the mutation within *dystrophin*, we used SNPTrack to call the highest ranking candidate SNPs within the *dystrophin* gene. Intriguingly, we found no evidence of nonsense mutations, alterations in start or stop codons or splice site mutations. Instead, our analysis revealed approximately 70 SNPs that fall deep within introns. While this is unusual, some DMD patients have been shown to have deep intronic SNPs in *dystrophin*, which can cause pseudoexons, or the inappropriate splicing of intronic sequence into mRNA, and subsequently cause frameshifts or early stop codons (Homolova et al., 2010; Khelifi et al., 2011). I tested for pseudoexons using RT-PCR. I amplified cDNA from mRNA harvested from WT and *ray*^{vu267} embryos. Once low quality results at either end of the sequence and clear artifacts were excluded, this cDNA did not reveal the inclusion of any pseudoexons or frameshift mutations. Some single base pairs were altered, but did not cause frameshifts,

splice changes, or early stops, and thus were not investigated further (Figure 4-2 D).

Originally I hypothesized that perturbation of non-coding RNA might be an explanation for this mutation. However, all candidate SNPS are also intronic to non-coding RNAs. Although these SNPS do not cause pseudoexons in coding transcripts, it is possible they do create pseudoexons in non-coding RNA. This possibility has not been tested, nor is it certain how the function of non-coding RNA might be altered. Some non-coding RNA products of the human *DMD* locus have been shown to regulate *DMD* expression (Bovolenta et al., 2012).

ray^{vu267} is a model of DMD

ray^{vu267} mutant larvae have the characteristic muscle defects that have previously been associated with mutations in *dystrophin*, including gradual accumulation of muscle lesions, increasingly severe locomotor impairment, and eventual death (Bassett et al., 2003; Guyon et al., 2009). However, there are other hallmarks observed in DMD patients and in animal models harboring mutations in *dystrophin*, including the absence of *dystrophin* mRNA and protein in the muscle (Bassett et al., 2003; Guyon et al., 2009). To determine if *ray^{vu267}* mutant embryos share these common characteristics with other DMD models, I assayed *dystrophin* mRNA and protein levels at 24 hpf. At this stage, there are no obvious morphological differences between *ray^{vu267}* and *sapje-like* mutant embryos and their siblings. Therefore, all experiments before 48 hpf use blind screens of entire

clutches collected from *ray*^{vu267} +/- x *ray*^{vu267} +/- and a *sapje-like* +/- x *sapje-like* +/- crosses. Using *in situ* hybridization, Hariharan and I observed that *dystrophin* mRNA expression is evident at the myosepta in only 75% of all embryos assayed, in both *ray*^{vu267} and *sapje-like* clutches (Figure 4-3 A-D). Later in development, at 72hpf, we found that identified WT siblings retained *dmd* expression whereas it was absent in the *ray*^{vu267} and *sapje-like* mutants (Figure 4-3 E-H).

Dystrophin protein expression was also tested using whole mount antibody labeling with an antibody specific for dystrophin, Mandra1. I observed that protein was absent from the myotomes of 25% of embryos from *ray*^{vu267} and *sapje-like* clutches at 24 hpf (Figure 4-3 M-P). Notably, *dmd* protein persisted in the CNS of mutant embryos (arrowheads, Figure 4-3 N, P). At 72hpf, Mandra1 labeling was absent in the muscle of *ray*^{vu267} and *sapje-like* mutant larvae (Figure 4-3 Q-T). Interestingly, at this age it is easiest to appreciate that Mandra1 is expressed within the spinal cord in WT fish, and persists in *ray*^{vu267} and *sapje-like* mutant fish (arrowheads, Figure 4-3 Q-T). Expression in the CNS is confirmed by sectioning the Mandra1-labeled 72 hpf embryos (Figure 4-3 U, V). From this data, I conclude that the disruption of *dystrophin* in *ray*^{vu267} is very similar to *sapje-like*. I also determine that our novel mutant allele, *ray*^{vu267} is a mutant allele of *dystrophin* and a model of DMD.

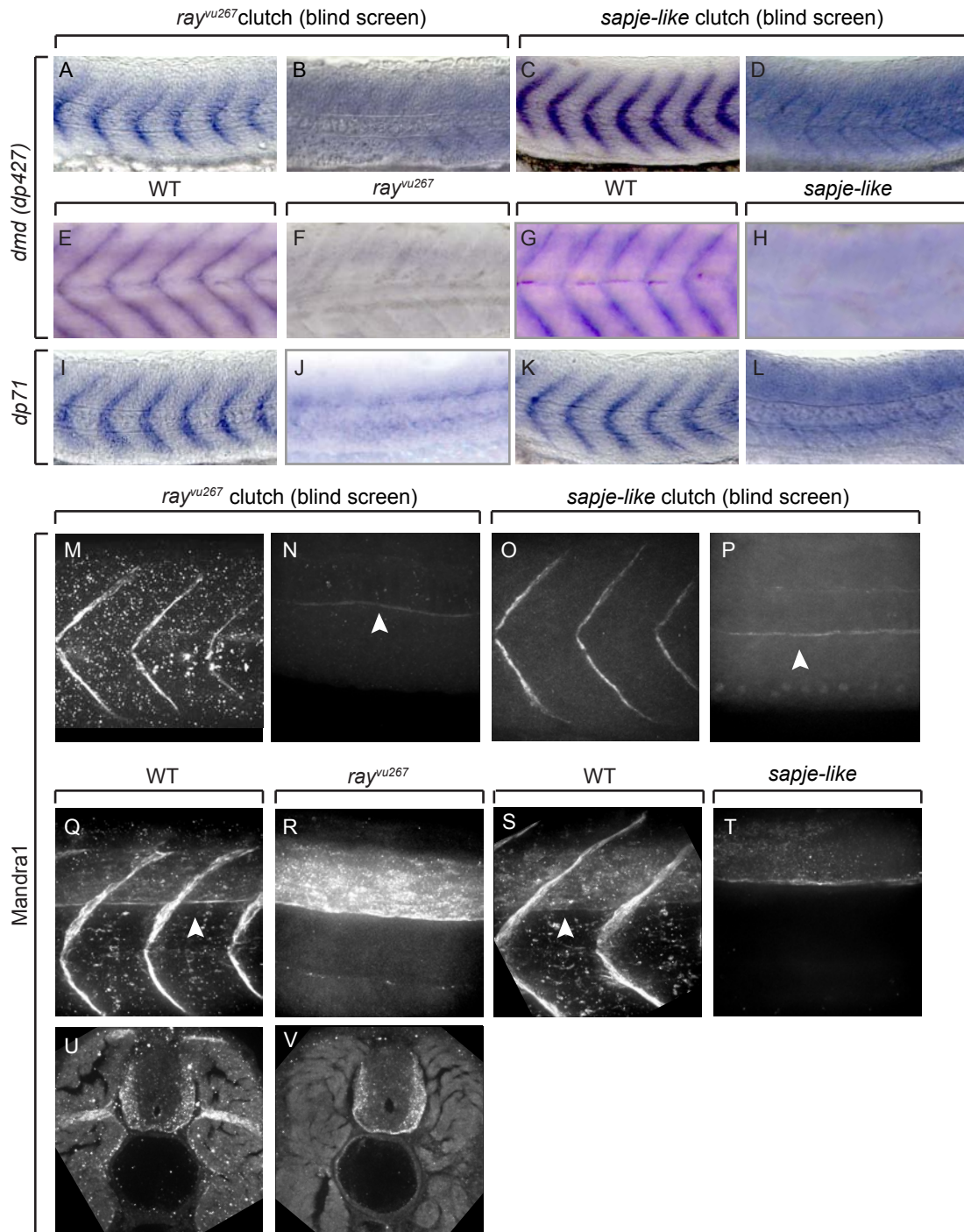


Figure 4-3: Similar to *sapje-like*, expression of *dmd* is perturbed in *ray^{vu267}*. A 24 hpf *ray^{vu267}* clutch was labeled with *dmd* and imaged. 75% of the clutch shows muscle expression (A), but 25% does not (B). The same is seen in *sapje-like* (C, D). At 72 hpf, *dmd* expression is observed in WT siblings (E, G) but not *ray^{vu267}* or *sapje-like* (F, H). At 24 hpf, a *ray^{vu267}* clutch and a *sapje-like* clutch were labeled with *dp71*, and myotome expression was only observed in 75% of the clutch (I-L). At 24 hpf Mandra1 labels myoseptum in 75% of *ray^{vu267}* clutch (M) but is absent in 25% of clutch (N). Mandra1 labels 75% of *sapje-like* clutch (O) but it absent in 25% of the clutch (P). Mandra1 label persists in the spinal cord (arrowhead, N, P). At 72 hpf, Mandra1 labels myoseptum and spinal cord in WT siblings (Q, S) but not *ray^{vu267}* fish (R) or *sapje-like* fish (T) except in the spinal cord. 72 hpf sectioned embryos show Mandra1 labeling in the CNS and muscle of WT siblings (U), but only in the CNS in *ray^{vu267}* fish (V).

One remaining question in regards to this project is identifying which isoforms of *dmd* are affected by the *ray*^{vu267} mutation. *dp71* and *dp427* differ by less than 20 nucleotides, making distinguishing between them technically difficult. It has been shown previously that the Mandra1 antibody recognizes the protein products of all dystrophin transcripts. The Rendon lab had previously developed an *in situ* probe for both isoforms which they believed was specific (Bolaños-Jiménez et al., 2001a). However, in our hands the *dp71* probe does not recapitulate their results, particularly the difference in expression levels between CNS and muscle. In 24 hpf *ray*^{vu267} and *sapje-like* clutches, *dp71* is expressed strongly in the muscle, but is absent in 25% of embryos labeled (Figure 4-3 I-L). However, it has been shown in other organisms that *dp71* is more predominant in the nervous system, therefore I lean towards the hypothesis that this probe is not specific, and that most neuronal expression is from *dp71* and not full-length *dystrophin*.

Loss of dystrophin leads to spinal motor nerve defects

In addition to the muscle defects that are characteristic of DMD, *ray*^{vu267} mutant embryos also have significant nervous system defects. We initially identified these mutants in our screen because of their perineurial glial migration defects. Previous work in the lab has demonstrated that perineurial defects can be the result of perturbed Schwann cell development and can cause defects in Schwann cells and motor axons (Kucenas et al., 2008). To clarify what other cell types were affected, I first set out to characterize two other major glial populations, Schwann cells in the PNS and OPCs in the CNS. For this reason, I

utilized experiments begun by Nash, which characterize other motor nerve components. Immunohistochemistry with an antibody specific to Sox10 was used to label 72 hpf WT and *ray*^{vu267} mutant larvae which were transgenic for *Tg(nkx2.2:meGFP); Tg(sox10:mRFP)* (Figure 4-4 A-D). At this stage, in WT larvae, there are an average of five Sox10⁺ peripheral glia along spinal motor nerve roots and ten cells along the lateral line. In contrast, in *ray*^{vu267} mutants, there was a significant increase in this cell population with mutants having an average of eight Sox10⁺ peripheral glia along the motor nerve and twelve Sox10⁺ peripheral glia along the lateral line. (Figure 4-4 E, F). Similarly, in sectioned embryos labeled with a Sox10 antibody, a significant increase was observed in the number of Sox10⁺ OPCs within the spinal cord, with WT and *ray*^{vu267} mutants averaging nine and twelve, respectively (Figure 4-4 K-I).

To determine if these glial populations were differentiating, we used *in situ* hybridization to assay for the presence of *myelin basic protein (mbp)*. At 72 hpf, we observed high levels of *mbp* along spinal motor nerves, the posterior lateral line nerve and in white matter tracts in the spinal cord (Figure 4-4 J, L). In contrast, in *ray*^{vu267} mutant larvae, we observed delayed *mbp* expression within the CNS (arrowhead, Figure 4-4 K) and weaker, patchy *mbp* expression along the lateral line (Figure 4-4 M). From these data, we hypothesize that *dystrophin* is required for glial development. However, whether this requirement is direct or indirect, will be investigated below.

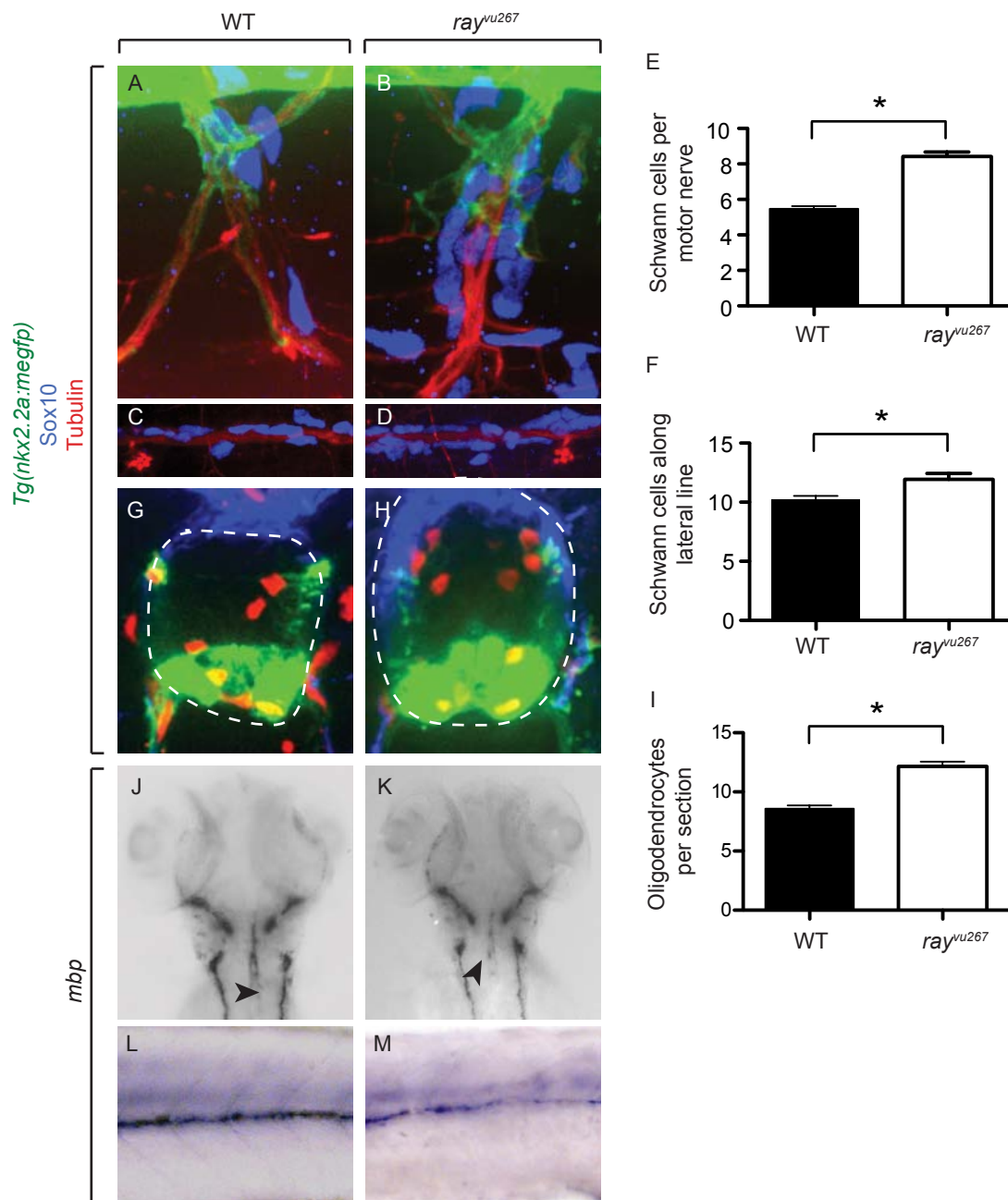


Figure 4-4: Schwann cells and oligodendrocytes are perturbed in *ray^{vu267}*. At 72 hpf, *Tg(nkx2.2a:megfp)* fish from a *ray^{vu267}* clutch were labeled with Sox10 and Tubulin. Mutant fish have more Sox10+ cells along the motor nerve (A, B) and lateral line (C, D), which is quantified in E (p value=<0.0001) and F (p value= .004). At 72 hpf, *Tg(nkx2.2a:megfp)* fish from a *ray^{vu267}* clutch were labeled with Sox10 and Tubulin and sectioned. There are more oligodendrocytes in the mutants, which are quantified in M (p value= < 0.0001). 72 hpf *ray^{vu267}* fish were labeled with probe for *mbp* (G-J). Mutant fish have delayed *mbp* expression pattern within CNS (H, arrowhead) and weaker, inconsistent expression along the lateral line (J).

Because of the glial defects we observed, we hypothesized that *ray*^{vu267} mutant embryos would also have motor axon pathfinding defects, as perturbed perineurial glial development can lead to ectopic motor axon exit from the spinal cord (Kucenas et al., 2008). To assess motor axon exit from the spinal cord and pathfinding, I referred to data collected by Nash, who performed live imaging of *Tg(nkx2.2a:megfp);Tg(olig2:dsred2)* *ray*^{vu267} fish. In WT fish at 72 hpf, motor axons exit the spinal cord at regularly spaced intervals (Figure 4-5 A). However, in mutant fish the motor axons can be seen exiting the spinal cord in the same ectopic position as the perineurial glia (Figure 4-4 B). Additionally, when I used *Tg(hb9:egfp)* embryos to assess axons development, I found that WT axons appear to have one major branch at the horizontal myoseptum at 48 hpf (Figure 4-5 C). However, in *ray*^{vu267} mutant embryos, I frequently observed random branching, and percent of total embryos with the WT branching pattern is decreased significantly from 80% to 40% (Figure 4-5 D, E). These experiments reveal how all components of the peripheral nerve, axons and glia, are disrupted in *ray*^{vu267} mutant embryos.

Neural crest-derived cell populations are disrupted in ray^{vu267} *embryos*

The *ray*^{vu267} mutant embryos not only have Schwann cell defects, they also have smaller heads at 72 hpf. Because Schwann cells and craniofacial cartilages are neural crest-derived structures, I sought to determine if other neural crest derivatives were affected by the loss of *dystrophin*. Therefore, I consulted previous neural crest characterization performed by Nash. Bright field

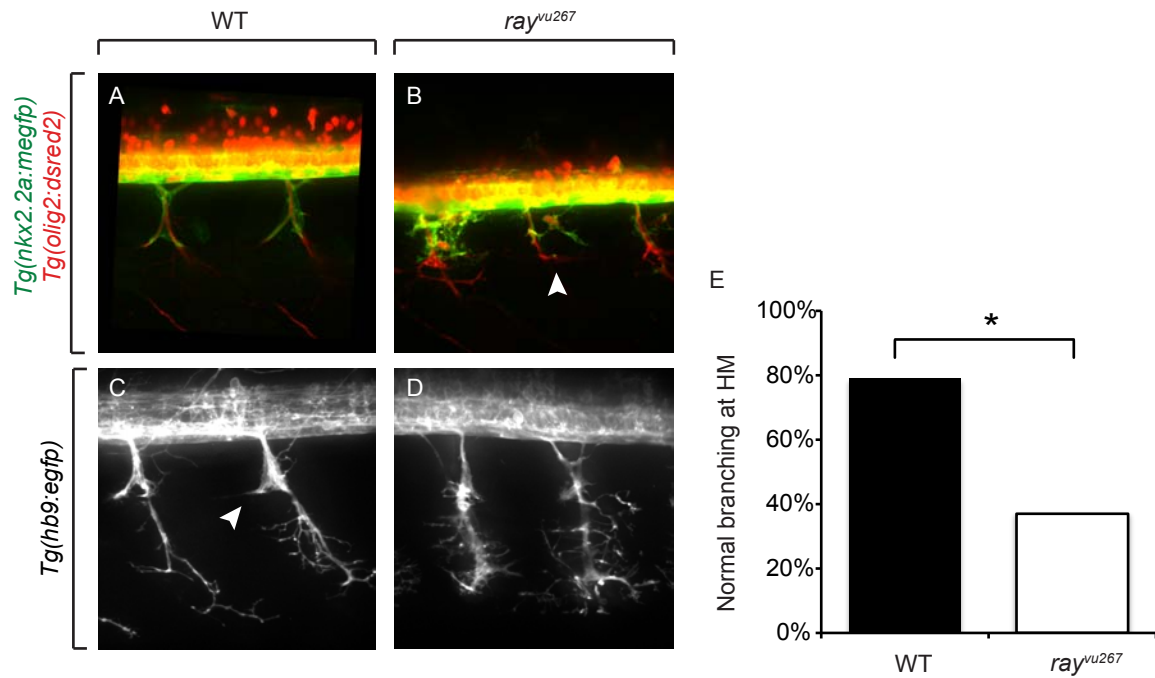


Figure 4-5: Motor axons are ectopic and defasciculated in *ray^{vu267}*. At 72 hpf, *Tg(nkx2.2a:megfp, olig2:dsred2)* fish from a *ray^{vu267}* clutch were imaged to observe ectopic, defasciculated motor axons in the mutants (A, B, arrowhead). At 48 hpf, a *Tg(hb9:egfp)* *ray^{vu267}* clutch was imaged and branching appears random (D) in the mutants, compared to a large, main branch at the horizontal myoseptum (C, arrowhead). This difference is quantified to be significant (E, p value= 0.00026).

microscopy was used to observe that melanocytes, which are derived from trunk neural crest, are disorganized in *ray*^{vu267} fish at 72 hpf, rather than being arranged into stripes (Figure 4-6 A, B). To assess craniofacial cartilage and bone, which is derived from cranial neural crest, Alcian blue staining was performed on 5 dpf embryos. This staining shows that cartilage in the skull of mutant fish develops incorrectly: namely that the jaw is smaller overall, the hyoid arch is inverted, and pharyngeal arches 3-7 are absent (Figure 4-5 C, D). Lastly, transgenic *Tg(nkx2.2:meGFP)* fish were labeled at 72 hpf with HuC, to mark dorsal root ganglia, Sox10, to show Schwann cells, and Tubulin, to label motor axons. This assay revealed that mutant fish have a greater number of DRG cell bodies, another derivative of the trunk neural crest population (stars, Figure 4-6 E, F). It is clear that *dystrophin* is required for development of not just the muscle but broadly across the nervous system and neural crest.

Perturbed crestin expression occurs before muscle degeneration

Because many neural crest derivatives are affected by *ray*^{vu267} mutation, I used an *in situ* for *crestin* to assess neural crest migration patterns. At 24 hpf, a blind screen of the clutch from a *ray*^{vu267} heterozygote cross shows that one fourth of the clutch have a diffuse staining pattern instead of being organized into streams (Figure 4-7 A, B). Similarly, in live confocal images of *Tg(nkx2.2:meGFP)*; *Tg(sox10:mRFP)* fish at 24 hpf, one fourth of the clutch have impaired neural crest streaming (arrowhead, Figure 4-7 C, D).

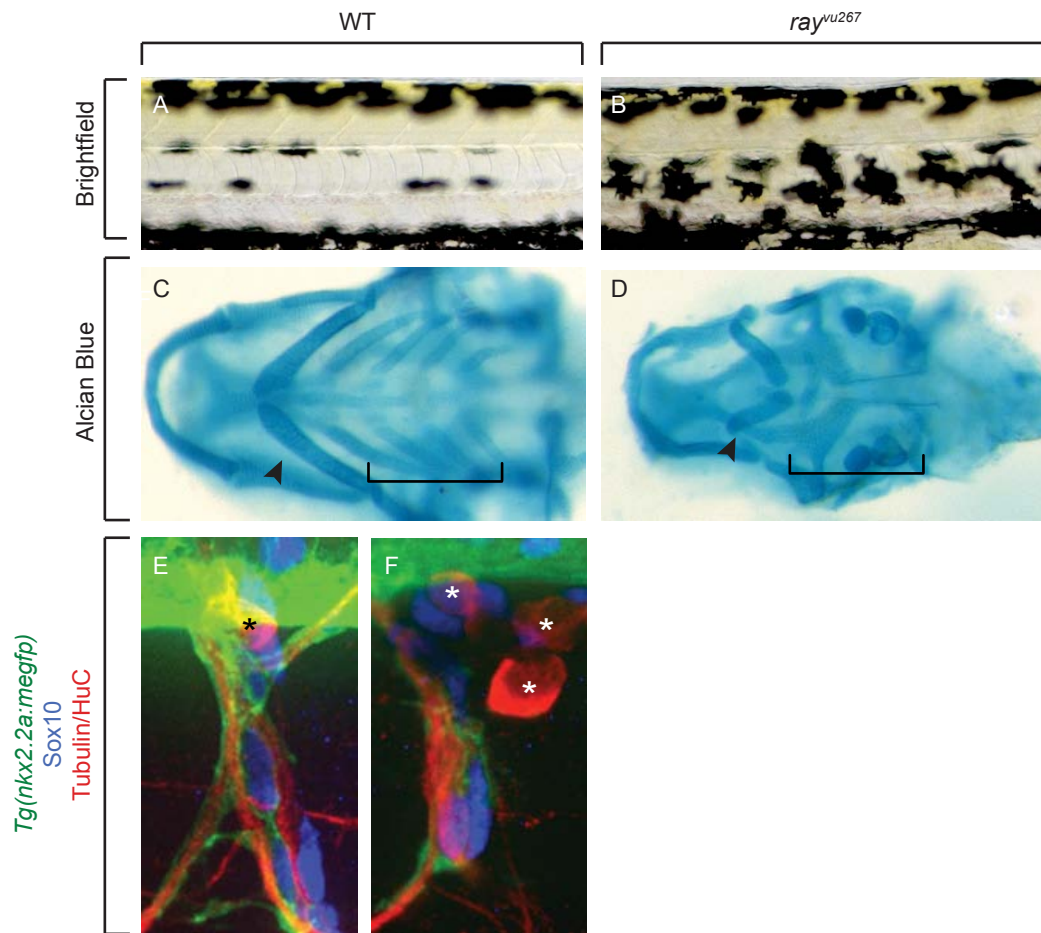


Figure 4-6: Neural crest derived populations are perturbed in ray^{vu267} . Brightfield image of 72 hpf fish shows ectopic location of melanocytes in mutant larvae (B), which form straight lines in WT (A). 4 dpf fish labeled with alcian blue, which shows a smaller jaw, inverted hyoid arch (arrowhead), and the absence of pharyngeal arches 3-7 (bracket, C, D). At 72 hpf, $Tg(nkx2.2a:megfp)$ fish from a ray^{vu267} clutch were labeled with HuC, Tubulin, and Sox10. More DRG neurons were observed in the mutants (F, stars) than in WT (E, star).

To more accurately observe this phenomenon, I used time lapse imaging of *Tg(sox10:mRFP)* embryos from AB* and *ray*^{vu267} clutches. From 20-36 hpf, I observed a Sox10+ cells migrating ectopically rather than associating with the two streams of neural crest cells on either side (arrowhead, Figure 4-7 I). However, I also observed similar phenomena in AB* fish (arrowhead, Figure 4-7 H). At such a rare frequency, this non-streaming migration is developmentally appropriate.

The rare ectopic migration of a few cells is not consistent with the *crestin in situ* results above, which showed a complete absence of migratory streams. Because the *in situ* labeling still appears strong dorsal to the spinal cord, we assayed whether neural crest cells were stuck above the spinal cord in mutant fish, even before they began to migrate. In a blind screen of a 24 hpf *Tg(hb9:egfp)* *ray*^{vu267} clutch, fish were labeled with Sox10 antibody (Figure 4-7 E, F). Sox10+ cells dorsal to the spinal cord were counted and compared to WT fish, but no difference was seen, both having an average of 30 cells. Accordingly, I hypothesize that neural crest cells downregulate *crestin* expression earlier than usual in mutant fish, but that this does not perturb their streaming along the motor nerves.

Importantly, this neural crest defect occurs before muscle degeneration can be observed. The relative timeline of the muscle phenotype and this neural crest phenotype bring into question our understanding of DMD. When patients seek

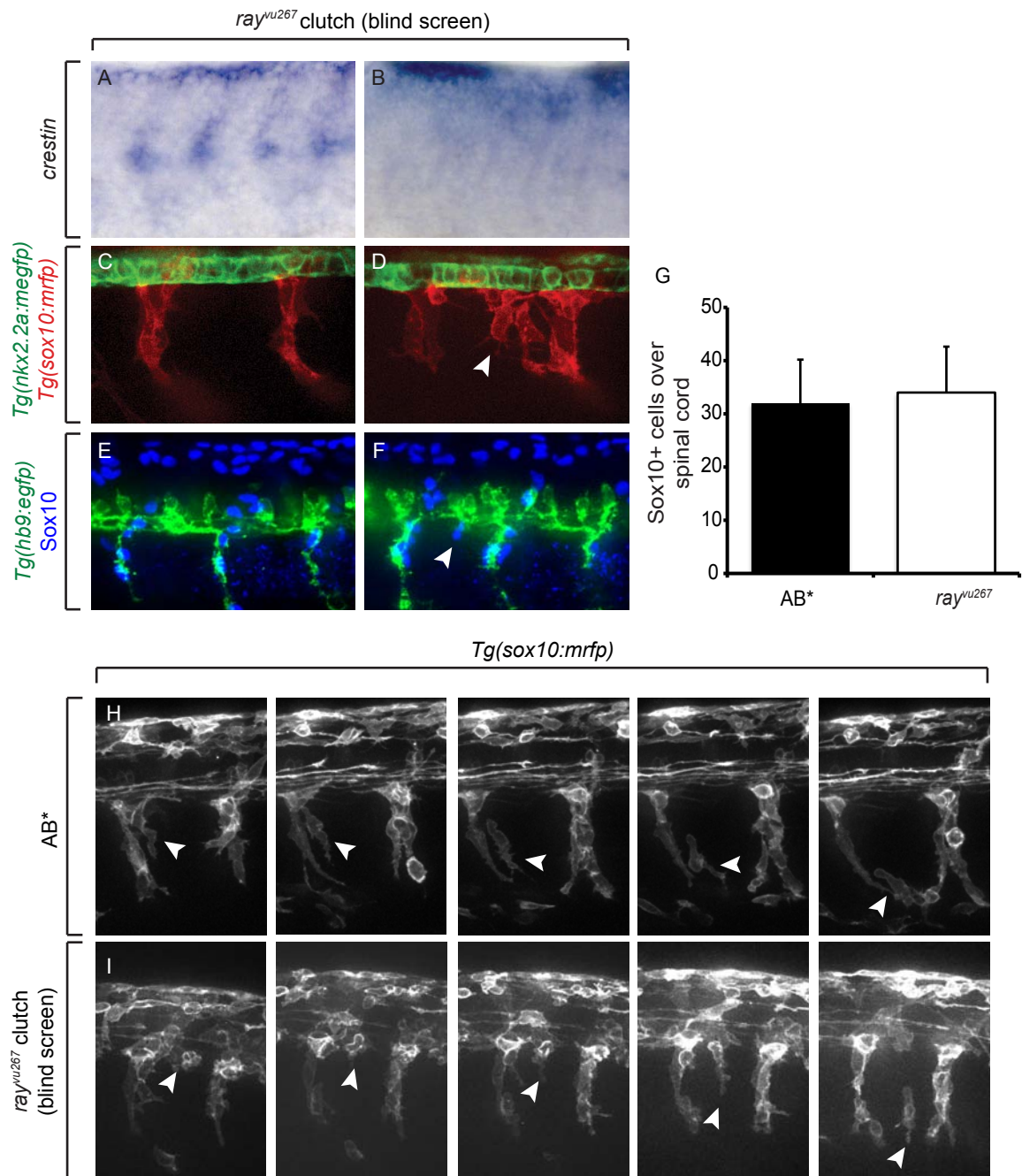


Figure 4-7: *ray^{vu267}* mutant fish have perturbed *crestin* expression but not a neural crest migration defect. Blind screen of 24 hpf *ray^{vu267}* clutch labeled with *crestin* shows perturbed expression pattern (A,B). At 24 hpf, blind screen of a *Tg(nkx2.2a:megfp, sox10:mrfp)* *ray^{vu267}* clutch shows perturbation in Sox10+ cell migration (arrowhead, C, D). 24 hpf blind screen of a *Tg(hb9:egfp)* *ray^{vu267}* clutch labeled with Sox10. No differences were observed Sox10+ cell migration patterns (E, F) or number of Sox10+ cells dorsal to the spinal cord compared to a WT clutch (G). Timelapse of embryos from a *Tg(sox10:mrfp)* *ray^{vu267}* clutch from 20 hpf to 36 hpf shows rare misdirected migration (arrowhead, I). Misdirected migration is also seen in timelapse of AB* fish (arrowhead, H).

treatment for muscle symptoms they also have hidden nervous system symptoms, which need to be treated as well.

Evaluating DMD drug therapies for their impact on nervous system defects

Currently, no effective treatment exists for DMD patients, however there are several types of therapies being evaluated. These include gene therapy, exon skipping, and stop codon read-through (Bowles et al., 2012; Cirak et al., 2011; Finkel et al., 2013; Goemans et al., 2011; Kinali et al., 2009). Stop codon read-through can be induced by treatment with the drug Ataluren. This drug reached phase 2b clinical trials with mixed results. It was able to restore Dystrophin protein in the muscle but did not improve the patients' six minute walk test. In the United States the drug was dropped from research, however it has since gained market authorization in Europe (Peltz et al., 2013).

Ataluren has never been tested for its ability to rescue nervous system defects. In light of the strong effect of *dmd* mutation on the nervous system, Hariharan and I treated *ray*^{vu267} fish with Ataluren and assessed its ability to rescue these previously described nervous system defects. Ataluren was dissolved in DMSO and then applied to the egg water to reach the desired concentration. A clutch of *ray*^{vu267} fish were raised in this egg water solution from 24 hpf to 72 hpf. These fish were transgenic for *Tg(hb9:gfp)* in order to assay motor axons at the same time as Dystrophin. At 72 hpf they were imaged live to observe motor axon and Schwann cell phenotypes, and then they were immediately fixed and labeled with

Mandra1 antibody. Each fish was stored individually in a 128 well plate in order to track nervous system phenotype with muscle phenotype.

In untreated *Tg(hb9:gfp) ray^{vu267}* clutches, WT siblings display strong Mandra1 expression in the muscle and healthy axons (Figure 4-8 A, F) while in mutant larvae the dystrophin is absent and axons are defasciculated (Figure 4-8 B, G). In Ataluren treated clutches, many fish exhibit both Mandra1 expression at the myotome and healthy, fasciculated axons (Figure 4-8 C, H). In some embryos, presumptive mutant siblings, Mandra1 expression is rescued but the blebbing appears along the axons and branching seems random (Figure 4-8 D, I). Lastly, in rare cases, Mandra1 expression is not retained, and axons appear highly defasciculated (Figure 4-8 E, J).

Mandra1 expression in AB* embryos is normally present in 100% of the clutch, and Ataluren treatment rescues this significantly, from 67% to 90% (Figure 4-8 K). However, the percent of larvae with a normal nervous system is only slightly increased from 60% to 66%, which is not significant. Ataluren treatment was able to restore Dystrophin localization to the muscle in most cases. However, muscle rescue is not sufficient for DMD patients without a functioning nervous system to control these muscles and coordinate complex motor activity. This casts doubt on the efficacy of Ataluren as a therapy for DMD.

Discussion

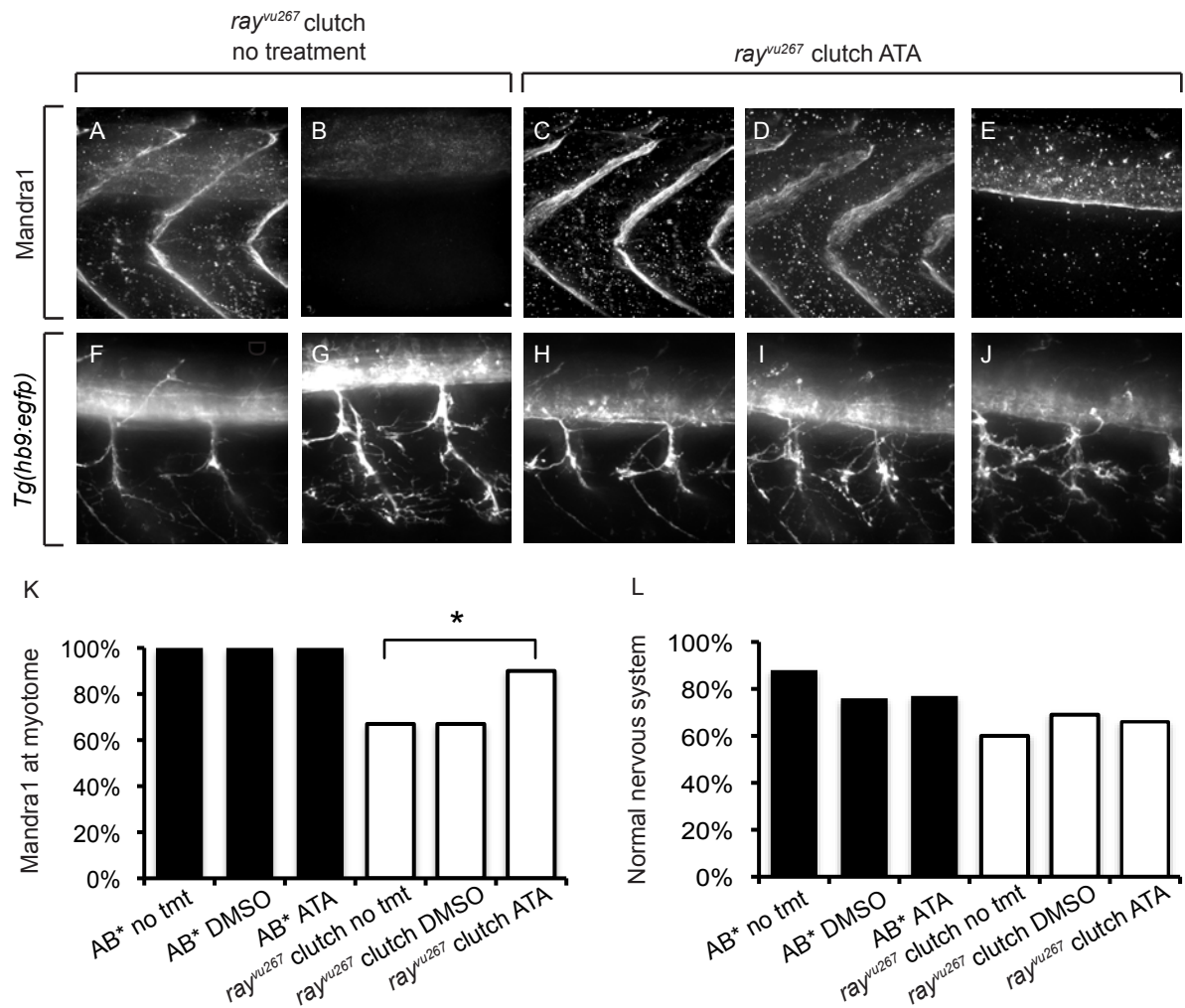


Figure 4-8: Ataluren rescues dystrophin in muscle of *ray^{vu267}* fish but not the nervous system. At 72 hpf, *Tg(hb9:egfp)* fish from a *ray^{vu267}* clutch were labeled with Mandra1. Untreated WT siblings express dystrophin in the muscle (A) and have a healthy nervous system (F) while mutants show an absence of Mandra1 (B) and defasciculated axons (G). In drug treated clutches, presumptive WT siblings display the presence of Mandra1 (C) and normal axons (H). In presumptive mutants, Mandra1 is rescued in most cases (D), but the axons remain defasciculated (I). In rare cases Mandra1 is not rescued (E) and the nervous system is highly perturbed (J). Data quantification illustrates the significant increase in dystrophin labeling in Ataluren-treated mutant clutches compared to untreated clutches (K, p value= 0.038). Ataluren treatment does not produce significant change in the nervous system (L).

An ENU mutagenesis screen for zebrafish mutants with defects in glial development has provided a novel link between the muscle gene *dystrophin* and nervous system development. I find that *ray*^{vu267} fish have established phenotypes of *dystrophin* mutations, such as muscle degeneration, absence of *dmd* RNA, and the absence of Dystrophin protein. However, mutant fish also have phenotypes in many different cell types- not just perineurial glia, but also motor axons, Schwann cells, oligodendrocytes, melanocytes, and cartilage. Additionally, some of these phenotypes were recapitulated in *sapje-like* fish, which suggests that this link is a common result of *dystrophin* perturbation.

DMD is a lethal degenerative condition of the muscle. Some progress has been made in developing treatments for this condition, particularly with exon skipping, gene therapy, and drug induced read-through of early stops (Kinali et al., 2009; Goemans et al., 2011; Cirak et al., 2011; Bowles et al., 2012; Finkel et al., 2013). However, clinical trials of these approaches have only had limited success (Fairclough et al., 2013). None of these studies addresses the concern that ameliorating muscle degeneration might not affect nervous system phenotypes. However, by the time patients first seek treatment for muscle weakness, their nervous system has been developing aberrantly as well. Therefore, potential therapeutic approaches to DMD cannot limit themselves to muscle.

This project provides a foundation for future studies from the lab studying dystrophin in more detail. Many questions remain open for now. For example, it

will be important to find a reliable method for differentiating between *dp427* and *dp71* expression. In the future, staining with double FISH may provide greater resolution between the two probes. Western blot could also tell us if the overall expression levels in the fish are affected, although it would not tell us where they are expressed. It would also be informative to determine whether the *ray*^{vu267} mutation is cell autonomous or not. This would clarify the mechanism of action, which is still unclear.

Another key question that remains open is the identification of the SNP. Although a complementation test has confirmed that the SNP is located in the *dmd* gene, we were unable to identify the specific SNP involved. All of the highest-ranking SNPs from the WGS are located within introns of full length *dmd*. We investigated whether intronic SNPs might be creating pseudoexons in the transcripts, but did not find any evidence of this. An alternative hypothesis is that the SNP is interfering with a regulatory element, such as a transcription factor binding site in the intron, which would not result in pseudoexon but would affect transcription. Understanding the type of mutation and its effect on the *dystrophin* gene would deepen our understanding of how this mutation is acting.

Chapter V: Discussion and Future Directions

In this dissertation I have outlined two similar parallel projects: the identification and characterization of two zebrafish mutants, *ftl*^{vu268} and *ray*^{vu267}. Both mutants were selected from the same ENU mutagenesis screen. This dissertation highlights some of the advantages and disadvantages of the forward genetics approach. Forward genetics can elucidate a completely novel genetic role. Without the *ray*^{vu267} mutant, there was little evidence to suggest that *dystrophin* would play such a strong role in the development of the nervous system. Conversely, the difficulties of the *ftl*^{vu268} project show that mapping a mutation is an undertaking with uncertain payoff. There is a tradeoff of risks and benefits to this method.

Summary of *ftl*^{vu268}

In Chapter 3, I have discussed my findings in regards to the *ftl*^{vu268} mutant. This project remains unfinished, partially due to the unreliable nature of zebrafish genomic alignment. This mutant exhibits a broad range of phenotypes, affecting each cell types in a different way. Within the CNS, perineurial glia fail to exit, the floorplate is wider and disorganized, and there are fewer oligodendrocytes, which fail to make myelin. In the PNS, Schwann cells have a blebbing morphology and also fail to myelinate, eventually undergoing apoptosis. No differences in motor neuron cell bodies or axons were observed, however, a decrease in angiogenesis was also observed. Without having identified the gene in which the

mutation is located, it is difficult to speculate on a mechanism that might explain these phenotypes.

Future Directions for *ftl^{vu268}*

Both projects leave opportunities for further study. In the *ftl^{vu268}* investigation, the fundamental issue of the candidate gene must be resolved. This goal should be accomplished with reanalysis of the raw WGS data, mapped to the newest zebrafish genome. At the moment, resources for analyzing this type of data in zebrafish are scarce. SNPtrack seemed to work relatively well, but as of this report, the platform does not allow alignment to GRCz10.

When that is accomplished, it is likely that fine mapping will be used to narrow the region. Some of previous fine mapping data may be able to be reused in light of this new analysis, but it is impossible to predict. Once we believe we have narrowed the region sufficiently, we will have to take confirmatory measures. These will be different depending on the gene and the tools available to us, but will probably include complementation, rescue, or phenocopy assays.

An additional aspect of the *ftl^{vu268}* mutants that is important to appreciate is the characterization of perineurial glia as they remain in the spinal cord. Both perineurial glia and interneurons are *Nkx2.2a+*, which is the only marker shown to label perineurial glia. However, recent efforts in the lab have developed a protocol for transient transgene injection, which results in mosaic labeling of the

floorplate, to study perineurial development before 48 hpf. Careful analysis of time-lapse data of these fish has provided other developmental hallmarks of glial precursors, such as a pattern of cell division and filapodial exploration of the PNS. I expect this technique can also be used with the mutants to assess the proliferation, migration, and cell death of perineurial glia in mutant embryos.

In the context of cell migration through the MEP, oligodendrocytes should also be considered. Although these cells normally remain within the CNS, in many circumstances, OPCs have been observed to migrate to the PNS. For example, in the absence of Schwann cells, it has been shown that oligodendrocytes not only exit the spinal cord, they wrap motor nerves in central myelin (Kucenas et al., 2009; Smith et al., 2014). Therefore, because *ftl^{vu268}* mutants have fewer Schwann cells, I hypothesize that oligodendrocytes will exit. This can be tested with time lapse imaging of *Tg(olig2:dsred2)* or *Tg(sox10:mrfp; nkx2.2aa:megfp)* *ftl^{vu268}* mutant larvae.

Another area of interest in *ftl^{vu268}* is the MEP glia in, a population of Schwann cells derived from the CNS, which exclusively myelinate the motor nerve. MEP glia have been shown to exit the CNS after 48 hpf, the same time period in which Schwann cells begin to show perturbation. Moreover, they exit the CNS through the same transition zone that perineurial glia also use to migrate into the periphery (Smith et al., 2014). If the TZ in *ftl^{vu268}* fish is perturbed, causing the perineurial cells to be contained, then the MEP glia may also be restricted to the

CNS. If they do exit the CNS, it would be interesting to assess whether MEP glia and neural crest-derived Schwann cells are dying at the same rate. MEP glia can be identified by use of a photoconvertible transgene *Tg(sox10:eos)*, which labels all Sox10+ cells green until converted by UV exposure into red. Exposing the entire fish to UV light at 48hpf allows the two populations to be easily distinguished, the neural crest-derived Schwann cells in red, and the MEP glia in green. Better understanding of the function of the transition zone will help clarify the mechanism by which the *ftl^{vu268}* mutation is acting.

Summary of *ray^{vu267}*

Chapter 4 presents a more complete study of the *ray^{vu267}* mutant and the role of *dystrophin* in zebrafish development. The importance of *dystrophin* in muscle development is well known, and accordingly this mutant exhibits an absence of *dystrophin* in the muscle. However, I have identified a novel role in neuronal development as well, which is observed in both *ray^{vu267}* and *sapje-like*. The *ray^{vu267}* mutant has ectopic perineurial exit and defasciculated axons. Additionally, there is a significant increase in the number of oligodendrocytes and Schwann cells. This mutant also displays defects in structures derived from the neural crest, such as melanocytes and cartilage. Some of these phenotypes have been observed before muscle begins to degenerate, in particular the disruption in *crestin* labeling at 24 hpf. Lastly, these mutants were shown to only partially respond to Ataluren treatment, which rescued Mandra1 in the muscle but did not

rescue the nervous system phenotypes. This project introduces a new DMD mutant in zebrafish and illustrates a new function for *dystrophin*.

Future directions for *ray*^{vu267}

Although more complete, the *dystrophin* study has several unresolved questions. One of the most pressing is the examination of the *dmd* transcripts, as their role in this mutant remains unclear. Because of the widespread functions of *dystrophin* throughout the body, it is hard to understand the mechanism without understanding which transcript is affected. Fluorescent *in situ* is one technique that might provide more clarity in expression pattern than traditional *in situ* hybridization. Western blot would also allow us to assess the overall expression of various transcripts, however, the western blot protocol is uncommon and difficult to perform using zebrafish.

It would be informative to test for nervous system perturbation in other models of DMD. Besides zebrafish mutants of *dystrophin*, there are mutants in other organisms as well, including the *mdx* mouse. In mice, mutations in *dmd* are not sufficient to recapitulate the severity of the human disease, instead it has been found that a combination *dmd* null with *utrophin* null is the best model (Deconinck et al., 1997). Testing the *mdx/utr* null mice for similar nervous system defects would be informative. Although live confocal imaging in mice is not feasible, antibody labeling with Sox10, S100, Tubulin, and α -bungarotoxin at various developmental time points would be valuable.

Another lingering question is the identity of the SNP and its affect on *dystrophin* expression. Understanding the SNP will illuminate our understanding of the consequences of this mutation. This SNP is located beyond the exons, yet I have shown that splicing and exon boundaries seem to be preserved in the mutants. I hypothesize that the SNPs are affecting a regulatory region, such as an enhancer or silencer, which would result in changes in expression. However, the many large introns of *dmd* will make this identification difficult.

Identification of the type of mutation will also enhance our understanding the mechanism by which Ataluren can achieve rescue. Ataluren is believed to function by suppressing premature stop codons, which lead to nonsense mediated decay, the cause of many diseases (Peltz et al., 2013). However, I have eliminated the possibility that the *ray*^{vu267} mutation is generating an early stop codon. Yet there was an effect on Dystrophin expression in the muscle of *ray*^{vu267} fish. One study has looked more closely at Ataluren and suggested that the initial assay used to test read-through, a luciferase assay, could have been biased by the fact that Ataluren has an inherent inhibitory affect on luciferase activity. This study uses a different assay to assert that Ataluren does not promote read-through (McElroy et al., 2013). A follow up test, with gentamycin, which has also shown to induce premature stop codon read-through, could be attempted (Pichavant et al., 2011).

Ataluren is not the only therapy in clinical trials. Although only about 15% of DMD patients have a mutation that causes an early stop, 83% of mutations are suitable for treatment with a method called exon skipping (Fairclough et al., 2013). Exon skipping is based on the reading frame rule of *dystrophin*: mutations that preserve the reading frame typically result in mild Becker's muscular dystrophy, while disrupting the reading frame of *dystrophin* leads to more severe DMD. Therefore, except for the critical N and C terminal domains, excising an exon to preserve the reading frame would still have a positive effect on DMD patient symptoms. Antisense oligonucleotides are used to interfere with splicing and remove the exon containing the mutation and restore the reading frame (van Deutekom et al., 2007). However, because the *ray*^{vu267} mutation is intronic, and does not affect splicing, it would not be a good candidate to test the efficacy of this therapy. We could, however, use *sapje-like* to evaluate this method, as they carry a splice mutation in that results in a reading frame error.

This project illustrates the limitations to studies on DMD in a clinical setting. Some previous studies have shown cognitive impairments, IQ deficit, and neuron loss in the brains of DMD patients, but this could easily be explained solely by a *dp71*-mediated mechanism (Anderson et al., 2002; Daoud et al., 2009). The fact that the *ray*^{vu267} mutation affects glia in the PNS suggests that *dp71* cannot be solely responsible.

Additionally, these studies of patients do not evaluate the impact of *dystrophin* on the nervous system during the process of development, which is understandably difficult to accomplish given the etiology of the disease. Some older studies attempted to address this question in model organisms. One group found that transplanted spinal cords from dystrophic chick embryos were able to induce higher levels of thymidine kinase, a hallmark of dystrophic muscle (Rathbone et al., 1975). A second group found a decrease in the number of myelinated axons in dystrophic mice that was significant from p0 and was observed before muscle fiber loss was detected, at three weeks (Montgomery and Swenarchuk, 1977). However, much of the recent studies have focused on the disease as originating in the muscle, and evaluated nervous system in older patients or animals. It is probable that in boys with DMD, serious defects are developing at earlier ages than previously believed, and not solely in the muscle.

In this dissertation I have outlined two similar parallel projects: the identification and characterization of two zebrafish mutants, *ftl*^{vu268} and *ray*^{vu267}. Both mutants were selected from the same ENU mutagenesis screen. This dissertation highlights some of the advantages and disadvantages of the forward genetics approach. The difficulties of the *ftl*^{vu268} project show that mapping a mutation is an undertaking with uncertain payoff. However, without the *ray*^{vu267} mutant, there was little evidence to suggest that *dystrophin* would play such a strong role in the development of the nervous system. Forward genetics has the power to elucidate a completely novel genetic role.

References

- Ahn, A.H., and Kunkel, L.M. (1993). The structural and functional diversity of dystrophin. *Nat. Genet.* 3, 283–291.
- Akert, P.K., Sandri, C., Weibel, E.R., Peper, K., and Moor, H. (1976a). The fine structure of the perineural endothelium. *Cell Tissue Res.* 165, 281–295.
- Allt, G. (1969a). Ultrastructural features of the immature peripheral nerve. *J. Anat.* 105, 283–293.
- Anderson, J.L., Head, S.I., Rae, C., and Morley, J.W. (2002). Brain function in Duchenne muscular dystrophy. *Brain* 125, 4–13.
- Al-Ani, F.S., Hamdan, F.B., and Shaikhly, K.I. (2001). In situ measurements of muscle fiber conduction velocity in Duchenne muscular dystrophy. *Saudi Med. J.* 22, 259–261.
- Arahata, K., Ishiura, S., Ishiguro, T., Tsukahara, T., Suhara, Y., Eguchi, C., Ishihara, T., Nonaka, I., Ozawa, E., and Sugita, H. (1988). Immunostaining of skeletal and cardiac muscle surface membrane with antibody against Duchenne muscular dystrophy peptide. *Nature* 333, 861–863.
- Auld, D.S., and Robitaille, R. (2003). Perisynaptic Schwann cells at the neuromuscular junction: nerve- and activity-dependent contributions to synaptic efficacy, plasticity, and reinnervation. *Neurosci. Rev. J. Bringing Neurobiol. Neurol. Psychiatry* 9, 144–157.

Balschun, D., Wolfer, D.P., Bertocchini, F., Barone, V., Conti, A., Zuschratter, W., Missiaen, L., Lipp, H.P., Frey, J.U., and Sorrentino, V. (1999). Deletion of the ryanodine receptor type 3 (RyR3) impairs forms of synaptic plasticity and spatial learning. *EMBO J.* *18*, 5264–5273.

Bassett, D.I., Bryson-Richardson, R.J., Daggett, D.F., Gautier, P., Keenan, D.G., and Currie, P.D. (2003). Dystrophin is required for the formation of stable muscle attachments in the zebrafish embryo. *Development* *130*, 5851–5860.

Baumann, N., and Pham-Dinh, D. (2001). Biology of Oligodendrocyte and Myelin in the Mammalian Central Nervous System. *Physiol. Rev.* *81*, 871–927.

Bernstein, D.J. (1868). Ueber den zeitlichen Verlauf der negativen Schwankung des Nervenstroms. *Arch. Für Gesamte Physiol. Menschen Tiere* *1*, 173–207.

Binari, L.A., Lewis, G.M., and Kucenas, S. (2013). Perineurial Glia Require Notch Signaling during Motor Nerve Development but Not Regeneration. *J. Neurosci.* *33*, 4241–4252.

Birchmeier, C., and Nave, K.-A. (2008). Neuregulin-1, a key axonal signal that drives Schwann cell growth and differentiation. *Glia* *56*, 1491–1497.

Bolaños-Jiménez, F., Bordais, A., Behra, M., Strähle, U., Sahel, J., and Rendón, A. (2001a). Dystrophin and Dp71, two products of the DMD gene, show a different pattern of expression during embryonic development in zebrafish. *Mech. Dev.* *102*, 239–241.

Bolaños-Jiménez, F., Bordais, A., Behra, M., Strähle, U., Mornet, D., Sahel, J., and Rendón, A. (2001b). Molecular cloning and characterization of dystrophin and Dp71, two products of the Duchenne Muscular Dystrophy gene, in zebrafish. *Gene* 274, 217–226.

Bonilla, E., Samitt, C.E., Miranda, A.F., Hays, A.P., Salviati, G., DiMauro, S., Kunkel, L.M., Hoffman, E.P., and Rowland, L.P. (1988). Duchenne muscular dystrophy: Deficiency of dystrophin at the muscle cell surface. *Cell* 54, 447–452.

Bourne, G.H. (1968). *The structure and function of nervous tissue* (New York: Academic Press).

Bovolenta, M., Erriquez, D., Valli, E., Brioschi, S., Scotton, C., Neri, M., Falzarano, M.S., Gherardi, S., Fabris, M., Rimessi, P., et al. (2012). The DMD Locus Harbours Multiple Long Non-Coding RNAs Which Orchestrate and Control Transcription of Muscle Dystrophin mRNA Isoforms. *PLoS ONE* 7, e45328.

Bowles, D.E., McPhee, S.W., Li, C., Gray, S.J., Samulski, J.J., Camp, A.S., Li, J., Wang, B., Monahan, P.E., Rabinowitz, J.E., et al. (2012). Phase 1 Gene Therapy for Duchenne Muscular Dystrophy Using a Translational Optimized AAV Vector. *Mol. Ther.* 20, 443–455.

Briscoe, J., Pierani, A., Jessell, T.M., and Ericson, J. (2000). A homeodomain protein code specifies progenitor cell identity and neuronal fate in the ventral neural tube. *Cell* 101, 435–445.

- Bronner-Fraser, M., and Fraser, S.E. (1988). Cell lineage analysis reveals multipotency of some avian neural crest cells. *Nature* 335, 161–164.
- Brown, A.G. (1981). *Organization in the Spinal Cord: The Anatomy and Physiology of Identified Neurones* (Springer Science & Business Media).
- Bunge, R.P. (1968). Glial cells and the central myelin sheath. *Physiol. Rev.* 48, 197–251.
- Burghes, A.H.M., Logan, C., Hu, X., Belfall, B., Worton, R.G., and Ray, P.N. (1987). A cDNA clone from the Duchenne/Becker muscular dystrophy gene. *Publ. Online* 30 July 1987 Doi101038328434a0 328, 434–437.
- Burkel, W.E. (1967a). The histological fine structure of perineurium. *Anat. Rec.* 158, 177–189.
- Burkel, W.E. (1967b). The histological fine structure of perineurium. *Anat. Rec.* 158, 177–189.
- Butler, M.G., Iben, J.R., Marsden, K.C., Epstein, J.A., Granato, M., and Weinstein, B.M. (2015). SNPfisher: tools for probing genetic variation in laboratory-reared zebrafish. *Dev. Camb. Engl.* 142, 1542–1552.
- Byers, T.J., Lidov, H.G.W., and Kunkel, L.M. (1993). An alternative dystrophin transcript specific to peripheral nerve. *Nat. Genet.* 4, 77–81.

Changeux, J.P., Kasai, M., and Lee, C.Y. (1970). Use of a snake venom toxin to characterize the cholinergic receptor protein. *Proc. Natl. Acad. Sci. U. S. A.* 67, 1241–1247.

Chiang, C., Litingtung, Y., Lee, E., Young, K.E., Corden, J.L., Westphal, H., and Beachy, P.A. (1996). Cyclopia and defective axial patterning in mice lacking Sonic hedgehog gene function. *Nature* 383, 407–413.

Christopherson, K.S., Ullian, E.M., Stokes, C.C.A., Mallowney, C.E., Hell, J.W., Agah, A., Lawler, J., Mosher, D.F., Bornstein, P., and Barres, B.A. (2005). Thrombospondins are astrocyte-secreted proteins that promote CNS synaptogenesis. *Cell* 120, 421–433.

Cirak, S., Arechavala-Gomez, V., Guglieri, M., Feng, L., Torelli, S., Anthony, K., Abbs, S., Garralda, M.E., Bourke, J., Wells, D.J., et al. (2011). Exon skipping and dystrophin restoration in patients with Duchenne muscular dystrophy after systemic phosphorodiamidate morpholino oligomer treatment: an open-label, phase 2, dose-escalation study. *The Lancet* 378, 595–605.

Clark, J.K., O'keefe, A., Mastracci, T.L., Sussel, L., Matise, M.P., and Kucenas, S. (2014). Mammalian Nkx2.2+ perineurial glia are essential for motor nerve development. *Dev. Dyn.* 243, 1116–1129.

Cohn, R.D., and Campbell, K.P. (2000). Molecular basis of muscular dystrophies. *Muscle Nerve* 23, 1456–1471.

Constantin, B. (2014). Dystrophin complex functions as a scaffold for signalling proteins. *Biochim. Biophys. Acta* 1838, 635–642.

Cruz Martinez, A., and Lopez Terradas, J.M. (1990). Conduction velocity along muscle fibers in situ in Duchenne muscular dystrophy. *Arch. Phys. Med. Rehabil.* 71, 558–561.

Dale, H.H., Feldberg, W., and Vogt, M. (1936). Release of acetylcholine at voluntary motor nerve endings. *J. Physiol.* 86, 353–380.

Daoud, F., Candelario-Martínez, A., Billard, J.-M., Avital, A., Khelifaoui, M., Rozenvald, Y., Guegan, M., Mornet, D., Jaillard, D., Nudel, U., et al. (2009). Role of Mental Retardation-Associated Dystrophin-Gene Product Dp71 in Excitatory Synapse Organization, Synaptic Plasticity and Behavioral Functions. *PLoS ONE* 4, e6574.

Deconinck, A.E., Rafael, J.A., Skinner, J.A., Brown, S.C., Potter, A.C., Metzinger, L., Watt, D.J., Dickson, J.G., Tinsley, J.M., and Davies, K.E. (1997). Utrophin-dystrophin-deficient mice as a model for Duchenne muscular dystrophy. *Cell* 90, 717–727.

van Deutekom, J.C., Janson, A.A., Ginjaar, I.B., Frankhuizen, W.S., Aartsma-Rus, A., Bremmer-Bout, M., Dunnen, J.T. den, Koop, K., van der Kooi, A.J., Goemans, N.M., et al. (2007). Local Dystrophin Restoration with Antisense Oligonucleotide PRO051. *N. Engl. J. Med.* 357, 2677–2686.

Le Douarin, N.M. (1986). Cell line segregation during peripheral nervous system ontogeny. *Science* 231, 1515–1522.

Le Douarin, N.M., and Teillet, M.A. (1974). Experimental analysis of the migration and differentiation of neuroblasts of the autonomic nervous system and of neurectodermal mesenchymal derivatives, using a biological cell marking technique. *Dev. Biol.* 41, 162–184.

Driever, W., Solnica-Krezel, L., Schier, A.F., Neuhauss, S.C., Malicki, J., Stemple, D.L., Stainier, D.Y., Zwartkruis, F., Abdelilah, S., Rangini, Z., et al. (1996). A genetic screen for mutations affecting embryogenesis in zebrafish. *Development* 123, 37–46.

Echelard, Y., Epstein, D.J., St-Jacques, B., Shen, L., Mohler, J., McMahon, J.A., and McMahon, A.P. (1993). Sonic hedgehog, a member of a family of putative signaling molecules, is implicated in the regulation of CNS polarity. *Cell* 75, 1417–1430.

Eisen, J.S., and Smith, J.C. (2008). Controlling morpholino experiments: don't stop making antisense. *Development* 135, 1735–1743.

Ericson, J., Morton, S., Kawakami, A., Roelink, H., and Jessell, T.M. (1996). Two Critical Periods of Sonic Hedgehog Signaling Required for the Specification of Motor Neuron Identity. *Cell* 87, 661–673.

Eroglu, Ç., Allen, N.J., Susman, M.W., O'Rourke, N.A., Park, C.Y., Özkan, E., Chakraborty, C., Mulinyawe, S.B., Annis, D.S., Huberman, A.D., et al. (2009).

Gabapentin Receptor $\alpha 2\delta$ -1 Is a Neuronal Thrombospondin Receptor Responsible for Excitatory CNS Synaptogenesis. *Cell* 139, 380–392.

Ervasti, J.M., and Campbell, K.P. (1991). Membrane organization of the dystrophin-glycoprotein complex. *Cell* 66, 1121–1131.

Fairclough, R.J., Wood, M.J., and Davies, K.E. (2013). Therapy for Duchenne muscular dystrophy: renewed optimism from genetic approaches. *Nat. Rev. Genet.* 14, 373–378.

Fincham, J.R.S. (1966). Genetic complementation (W.A. Benjamin).

Finkel, R.S. (2010). Read-through strategies for suppression of nonsense mutations in Duchenne/ Becker muscular dystrophy: aminoglycosides and ataluren (PTC124). *J. Child Neurol.* 25, 1158–1164.

Finkel, R.S., Flanigan, K.M., Wong, B., Bönnemann, C., Sampson, J., Sweeney, H.L., Reha, A., Northcutt, V.J., Elfring, G., Barth, J., et al. (2013). Phase 2a Study of Ataluren-Mediated Dystrophin Production in Patients with Nonsense Mutation Duchenne Muscular Dystrophy. *PLoS ONE* 8, e81302.

Friede, R.L. (1972). Control of myelin formation by axon caliber. (With a model of the control mechanism). *J. Comp. Neurol.* 144, 233–252.

Goemans, N.M., Tulinius, M., van den Akker, J.T., Burm, B.E., Ekhart, P.F., Heuvelmans, N., Holling, T., Janson, A.A., Platenburg, G.J., Sipkens, J.A., et al.

(2011). Systemic Administration of PRO051 in Duchenne's Muscular Dystrophy. *N. Engl. J. Med.* *364*, 1513–1522.

Guyon, J.R., Goswami, J., Jun, S.J., Thorne, M., Howell, M., Pusack, T., Kawahara, G., Steffen, L.S., Galdzicki, M., and Kunkel, L.M. (2009). Genetic isolation and characterization of a splicing mutant of zebrafish dystrophin. *Hum. Mol. Genet.* *18*, 202–211.

Haffter, P., Granato, M., Brand, M., Mullins, M.C., Hammerschmidt, M., Kane, D.A., Odenthal, J., van Eeden, F.J., Jiang, Y.J., Heisenberg, C.P., et al. (1996). The identification of genes with unique and essential functions in the development of the zebrafish, *Danio rerio*. *Development* *123*, 1–36.

Haller, F.R., and Low, F.N. (1971). The fine structure of the peripheral nerve root sheath in the subarachnoid space in the rat and other laboratory animals. *Am. J. Anat.* *131*, 1–19.

Hodgkin, A.L. (1937). Evidence for electrical transmission in nerve. *J. Physiol.* *90*, 183–210.

Homolova, K., Zavadakova, P., Doktor, T.K., Schroeder, L.D., Kozich, V., and Andresen, B.S. (2010). The deep intronic c.903+469T>C mutation in the MTRR gene creates an SF2/ASF binding exonic splicing enhancer, which leads to pseudoexon activation and causes the cbIE type of homocystinuria. *Hum. Mutat.* *31*, 437–444.

Hörstadius, S.O. (1950). The neural crest: its properties and derivatives in the light of experimental research (London [u.a.]: Oxford University Press).

Huxley, A.F., and Stämpfli, R. (1949). Evidence for saltatory conduction in peripheral myelinated nerve fibres. *J. Physiol.* *108*, 315–339.

Hwang, W.Y., Fu, Y., Reyon, D., Maeder, M.L., Tsai, S.Q., Sander, J.D., Peterson, R.T., Yeh, J.-R.J., and Joung, J.K. (2013). Efficient genome editing in zebrafish using a CRISPR-Cas system. *Nat. Biotechnol.* *31*, 227–229.

Jaegle, M., Ghazvini, M., Mandemakers, W., Piirsoo, M., Driegen, S., Levavasseur, F., Raghoenath, S., Grosveld, F., and Meijer, D. (2003). The POU proteins Brn-2 and Oct-6 share important functions in Schwann cell development. *Genes Dev.* *17*, 1380–1391.

Jin, H., Tan, S., Hermanowski, J., Böhm, S., Pacheco, S., McCauley, J.M., Greener, M.J., Hinits, Y., Hughes, S.M., Sharpe, P.T., et al. (2007). The dystrotelin, dystrophin and dystrobrevin superfamily: new paralogues and old isoforms. *BMC Genomics* *8*, 19.

Jinek, M., Chylinski, K., Fonfara, I., Hauer, M., Doudna, J.A., and Charpentier, E. (2012). A Programmable Dual-RNA-Guided DNA Endonuclease in Adaptive Bacterial Immunity. *Science* *337*, 816–821.

Joseph, N.M., Mukoyama, Y., Mosher, J.T., Jaegle, M., Crone, S.A., Dormand, E.-L., Lee, K.-F., Meijer, D., Anderson, D.J., and Morrison, S.J. (2004). Neural crest stem cells undergo multilineage differentiation in developing peripheral

nerves to generate endoneurial fibroblasts in addition to Schwann cells. *Dev. Camb. Engl.* *131*, 5599–5612.

Kamei, M., Isogai, S., Pan, W., and Weinstein, B.M. (2010). Imaging blood vessels in the zebrafish. *Methods Cell Biol.* *100*, 27–54.

Karfunkel, P. (1973). The mechanisms of neural tube formation. *Int. Rev. Cytol.* *38*, 245–271.

Khelifi, M.M., Ishmukhametova, A., Khau Van Kien, P., Thorel, D., Méchin, D., Perelman, S., Pouget, J., Claustres, M., and Tuffery-Giraud, S. (2011). Pure intronic rearrangements leading to aberrant pseudoexon inclusion in dystrophinopathy: a new class of mutations? *Hum. Mutat.* *32*, 467–475.

Khurana, T.S., Watkins, S.C., Chafey, P., Chelly, J., Tomé, F.M.S., Fardeau, M., Kaplan, J.-C., and Kunkel, L.M. (1991). Immunolocalization and developmental expression of dystrophin related protein in skeletal muscle. *Neuromuscul. Disord.* *1*, 185–194.

Kinali, M., Arechavala-Gomez, V., Feng, L., Cirak, S., Hunt, D., Adkin, C., Guglieri, M., Ashton, E., Abbs, S., Nihoyannopoulos, P., et al. (2009). Local restoration of dystrophin expression with the morpholino oligomer AVI-4658 in Duchenne muscular dystrophy: a single-blind, placebo-controlled, dose-escalation, proof-of-concept study. *Lancet Neurol.* *8*, 918–928.

Knapik, E.W. (2000). ENU mutagenesis in zebrafish--from genes to complex diseases. *Mamm. Genome Off. J. Int. Mamm. Genome Soc.* *11*, 511–519.

Knapik, E.W., Goodman, A., Atkinson, O.S., Roberts, C.T., Shiozawa, M., Sim, C.U., Weksler-Zangen, S., Trolliet, M.R., Futrell, C., Innes, B.A., et al. (1996). A reference cross DNA panel for zebrafish (*Danio rerio*) anchored with simple sequence length polymorphisms. *Development* 123, 451–460.

Knapik, E.W., Goodman, A., Ekker, M., Chevrette, M., Delgado, J., Neuhaus, S., Shimoda, N., Driever, W., Fishman, M.C., and Jacob, H.J. (1998). A microsatellite genetic linkage map for zebrafish (*Danio rerio*). *Nat. Genet.* 18, 338–343.

Kobielak, A., Pasolli, H.A., and Fuchs, E. (2004). Mammalian formin-1 participates in adherens junctions and polymerization of linear actin cables. *Nat. Cell Biol.* 6, 21–30.

Krauss, S., Concordet, J.-P., and Ingham, P.W. (1993). A functionally conserved homolog of the *Drosophila* segment polarity gene *hh* is expressed in tissues with polarizing activity in zebrafish embryos. *Cell* 75, 1431–1444.

Kucenas, S., Takada, N., Park, H.-C., Woodruff, E., Broadie, K., and Appel, B. (2008). CNS-derived glia ensheath peripheral nerves and mediate motor root development. *Nat. Neurosci.* 11, 143–151.

Kucenas, S., Wang, W.-D., Knapik, E.W., and Appel, B. (2009). A Selective Glial Barrier at Motor Axon Exit Points Prevents Oligodendrocyte Migration from the Spinal Cord. *J. Neurosci. Off. J. Soc. Neurosci.* 29, 15187–15194.

- Kuhlbrodt, K., Herbarth, B., Sock, E., Hermans-Borgmeyer, I., and Wegner, M. (1998). Sox10, a novel transcriptional modulator in glial cells. *J. Neurosci. Off. J. Soc. Neurosci.* 18, 237–250.
- Lawler, J. (2002). Thrombospondin-1 as an endogenous inhibitor of angiogenesis and tumor growth. *J. Cell. Mol. Med.* 6, 1–12.
- Lederfein, D., Yaffe, D., and Nudel, U. (1993). A housekeeping type promoter, located in the 3' region of the Duchenne muscular dystrophy gene, controls the expression of Dp71, a major product of the gene. *Hum. Mol. Genet.* 2, 1883–1888.
- Leshchiner, I., Alexa, K., Kelsey, P., Adzhubei, I., Austin-Tse, C.A., Cooney, J.D., Anderson, H., King, M.J., Stottmann, R.W., Garnaas, M.K., et al. (2012). Mutation mapping and identification by whole-genome sequencing. *Genome Res.* 22, 1541–1548.
- Lidov, H.G.W. (1996). Dystrophin in the Nervous System. *Brain Pathol.* 6, 63–77.
- Lidov, H.G., Selig, S., and Kunkel, L.M. (1995). Dp140: a novel 140 kDa CNS transcript from the dystrophin locus. *Hum. Mol. Genet.* 4, 329–335.
- Liu, J., Supnet, C., Sun, S., Zhang, H., Good, L., Popugaeva, E., and Bezprozvanny, I. (2014). The role of ryanodine receptor type 3 in a mouse model of Alzheimer disease. *Channels Austin Tex* 8, 230–242.

Loewi, O., and Navratil, E. (1926). Über humorale Übertragbarkeit der Herznervenwirkung. *Pflüg. Arch. Für Gesamte Physiol. Menschen Tiere* 214, 678–688.

Lowery, L.A., and Sive, H. (2004). Strategies of vertebrate neurulation and a re-evaluation of teleost neural tube formation. *Mech. Dev.* 121, 1189–1197.

Lyons, D.A., Pogoda, H.-M., Voas, M.G., Woods, I.G., Diamond, B., Nix, R., Arana, N., Jacobs, J., and Talbot, W.S. (2005). *erbb3* and *erbb2* are essential for schwann cell migration and myelination in zebrafish. *Curr. Biol. CB* 15, 513–524.

Marques, M.J., Conchello, J.A., and Lichtman, J.W. (2000). From plaque to pretzel: fold formation and acetylcholine receptor loss at the developing neuromuscular junction. *J. Neurosci. Off. J. Soc. Neurosci.* 20, 3663–3675.

Martí, E., Bumcrot, D.A., Takada, R., and McMahon, A.P. (1995). Requirement of 19K form of Sonic hedgehog for induction of distinct ventral cell types in CNS explants. *Nature* 375, 322–325.

McDonald, C.M., Abresch, R.T., Carter, G.T., Fowler, W.M., Johnson, E.R., Kilmer, D.D., and Sigford, B.J. (1995). Profiles of neuromuscular diseases. Duchenne muscular dystrophy. *Am. J. Phys. Med. Rehabil. Assoc. Acad. Physiatr.* 74, S70–S92.

McElroy, S.P., Nomura, T., Torrie, L.S., Warbrick, E., Gartner, U., Wood, G., and McLean, W.H.I. (2013). A Lack of Premature Termination Codon Read-Through

Efficacy of PTC124 (Ataluren) in a Diverse Array of Reporter Assays. *PLoS Biol* 11, e1001593.

Meeker, N.D., Hutchinson, S.A., Ho, L., and Trede, N.S. (2007). Method for isolation of PCR-ready genomic DNA from zebrafish tissues. *BioTechniques* 43, 610, 612, 614.

Meyer, D., and Birchmeier, C. (1995). Multiple essential functions of neuregulin in development. *Nature* 378, 386–390.

Michelmore, R.W., Paran, I., and Kesseli, R.V. (1991). Identification of markers linked to disease-resistance genes by bulked segregant analysis: a rapid method to detect markers in specific genomic regions by using segregating populations. *Proc. Natl. Acad. Sci. U. S. A.* 88, 9828–9832.

Misgeld, T., Kummer, T.T., Lichtman, J.W., and Sanes, J.R. (2005). Agrin promotes synaptic differentiation by counteracting an inhibitory effect of neurotransmitter. *Proc. Natl. Acad. Sci. U. S. A.* 102, 11088–11093.

Monaco, A.P., Neve, R.L., Colletti-Feener, C., Bertelson, C.J., Kurnit, D.M., and Kunkel, L.M. (1986). Isolation of candidate cDNAs for portions of the Duchenne muscular dystrophy gene. *Nature* 323, 646–650.

Montgomery, A., and Swenarchuk, L. (1977). Dystrophic mice show age related muscle fibre and myelinated axon losses. *Nature* 267, 167–169.

Nasevicius, A., and Ekker, S.C. (2000). Effective targeted gene “knockdown” in zebrafish. *Nat. Genet.* 26, 216–220.

Nave, K.-A. (2010). Myelination and support of axonal integrity by glia. *Nature* 468, 244–252.

Nicoli, S., Gilardelli, C.N., Pozzoli, O., Presta, M., and Cotelli, F. (2005). Regulated expression pattern of gremlin during zebrafish development. *Gene Expr. Patterns* 5, 539–544.

Nishiyama, A., Lin, X.H., Giese, N., Heldin, C.H., and Stallcup, W.B. (1996). Co-localization of NG2 proteoglycan and PDGF alpha-receptor on O2A progenitor cells in the developing rat brain. *J. Neurosci. Res.* 43, 299–314.

Obholzer, N., Swinburne, I.A., Schwab, E., Nechiporuk, A.V., Nicolson, T., and Megason, S.G. (2012). Rapid positional cloning of zebrafish mutations by linkage and homozygosity mapping using whole-genome sequencing. *Dev. Camb. Engl.* 139, 4280–4290.

Olsson, Y. (1990). Microenvironment of the peripheral nervous system under normal and pathological conditions. *Crit. Rev. Neurobiol.* 5, 265–311.

Papan, C., and Campos-Ortega, J.A. (1994). On the formation of the neural keel and neural tube in the zebrafish *Danio (Brachydanio) rerio*. *Roux's Arch. Dev. Biol.* 203, 178–186.

Parkinson, D.B., Bhaskaran, A., Droggiti, A., Dickinson, S., D'Antonio, M., Mirsky, R., and Jessen, K.R. (2004). Krox-20 inhibits Jun-NH2-terminal kinase/c-Jun to control Schwann cell proliferation and death. *J. Cell Biol.* *164*, 385–394.

Parmantier, E., Lynn, B., Lawson, D., Turmaine, M., Namini, S.S., Chakrabarti, L., McMahon, A.P., Jessen, K.R., and Mirsky, R. (1999a). Schwann Cell-Derived Desert Hedgehog Controls the Development of Peripheral Nerve Sheaths. *Neuron* *23*, 713–724.

Parrinello, S., Napoli, I., Ribeiro, S., Wingfield Digby, P., Fedorova, M., Parkinson, D.B., Doddrell, R.D.S., Nakayama, M., Adams, R.H., and Lloyd, A.C. (2010). EphB signaling directs peripheral nerve regeneration through Sox2-dependent Schwann cell sorting. *Cell* *143*, 145–155.

Peltz, S.W., Morsy, M., Welch, E.M., and Jacobson, A. (2013). Ataluren as an agent for therapeutic nonsense suppression. *Annu. Rev. Med.* *64*, 407–425.

Peterson, S.M., and Freeman, J.L. (2009). RNA Isolation from Embryonic Zebrafish and cDNA Synthesis for Gene Expression Analysis. *J. Vis. Exp.*

Pfeiffer, S.E., Warrington, A.E., and Bansal, R. (1993). The oligodendrocyte and its many cellular processes. *Trends Cell Biol.* *3*, 191–197.

Pichavant, C., Aartsma-Rus, A., Clemens, P.R., Davies, K.E., Dickson, G., Takeda, S., Wilton, S.D., Wolff, J.A., Wooddell, C.I., Xiao, X., et al. (2011). Current Status of Pharmaceutical and Genetic Therapeutic Approaches to Treat DMD. *Mol. Ther.* *19*, 830–840.

- Plessis, D.G. Du, Mouton, Y.M., Muller, C.J., and Geiger, D.H. (1996). An ultrastructural study of the development of the chicken perineurial sheath. *J. Anat.* *189*, 631–641.
- Pringle, N.P., and Richardson, W.D. (1993). A singularity of PDGF alpha-receptor expression in the dorsoventral axis of the neural tube may define the origin of the oligodendrocyte lineage. *Dev. Camb. Engl.* *117*, 525–533.
- Ranvier, L.A. (1878). *Leçons sur l'histologie du système nerveux: Tome 2* (Adamant Media Corporation).
- Rathbone, M.P., Stewart, P.A., and Vetrano, F. (1975). Dystrophic spinal cord transplants induce abnormal thymidine kinase activity in normal muscles. *Science* *189*, 1106–1107.
- Richardson, W.D., Smith, H.K., Sun, T., Pringle, N.P., Hall, A., and Woodruff, R. (2000). Oligodendrocyte lineage and the motor neuron connection. *Glia* *29*, 136–142.
- Sadoulet-Puccio, H.M., and Kunkel, L.M. (1996). Dystrophin and its isoforms. *Brain Pathol. Zurich Switz.* *6*, 25–35.
- Sainath, R., and Granato, M. (2013). Plexin A3 and turnout regulate motor axonal branch morphogenesis in zebrafish. *PloS One* *8*, e54071.
- Schoenwolf, G.C., and Smith, J.L. (1990). Mechanisms of neurulation: traditional viewpoint and recent advances. *Development* *109*, 243–270.

- Scott-Drew, S., and French-Constant, C. (1997). Expression and function of thrombospondin-1 in myelinating glial cells of the central nervous system. *J. Neurosci. Res.* *50*, 202–214.
- Sepp, K.J., Schulte, J., and Auld, V.J. (2000). Developmental dynamics of peripheral glia in *Drosophila melanogaster*. *Glia* *30*, 122–133.
- Simon-Areces, J., Dopazo, A., Dettenhofer, M., Rodriguez-Tebar, A., Garcia-Segura, L.M., and Arevalo, M.-A. (2011). Formin1 mediates the induction of dendritogenesis and synaptogenesis by neurogenin3 in mouse hippocampal neurons. *PLoS One* *6*, e21825.
- Smith, C.J., Morris, A.D., Welsh, T.G., and Kucenas, S. (2014). Contact-Mediated Inhibition Between Oligodendrocyte Progenitor Cells and Motor Exit Point Glia Establishes the Spinal Cord Transition Zone. *PLoS Biol* *12*, e1001961.
- Söderfeldt, B., Olsson, Y., and Kristensson, K. (1973). The perineurium as a diffusion barrier to protein tracers in human peripheral nerve. *Acta Neuropathol. (Berl.)* *25*, 120–126.
- D'Souza, V.N., Nguyen, T.M., Morris, G.E., Karges, W., Pillers, D.A., and Ray, P.N. (1995). A novel dystrophin isoform is required for normal retinal electrophysiology. *Hum. Mol. Genet.* *4*, 837–842.
- Summerton, J. (1999). Morpholino antisense oligomers: the case for an RNase H-independent structural type. *Biochim. Biophys. Acta* *1489*, 141–158.

Tasaki, I., and Takeuchi, T. (1941). Der am Ranvierschen Knoten entstehende Aktionsstrom und seine Bedeutung für die Erregungsleitung. *Pflüg. Arch Ges Physiol* 244, 696–711.

Tasaki, I., and Takeuchi, T. (1942). Weitere Studien über den Aktionsstrom der markhaltigen Nervenfasern und über die elektrosaltatorische Übertragung des Nervenimpulses. *Pflüg. Arch Ges Physiol* 245, 764–782.

Tennyson, C.N., Klamut, H.J., and Worton, R.G. (1995). The human dystrophin gene requires 16 hours to be transcribed and is cotranscriptionally spliced. *Nat. Genet.* 9, 184–190.

Topilko, P., Schneidermanoury, S., Levi, G., Baronvanevercooren, A., Chenoufi, A., Seitanidou, T., Babinet, C., and Charnay, P. (1994). Krox-20 Controls Myelination in the Peripheral Nervous-System. *Nature* 371, 796–799.

Ugozzoli, L., and Wallace, R.B. (1991). Allele-specific polymerase chain reaction. *Methods* 2, 42–48.

Voz, M.L., Coppieters, W., Manfroid, I., Baudhuin, A., Von Berg, V., Charlier, C., Meyer, D., Driever, W., Martial, J.A., and Peers, B. (2012). Fast homozygosity mapping and identification of a zebrafish ENU-induced mutation by whole-genome sequencing. *PloS One* 7, e34671.

Webster, H. deF (1971). The Geometry of Peripheral Myelin Sheaths During Their Formation and Growth in Rat Sciatic Nerves. *J. Cell Biol.* 48, 348–367.

Welch, E.M., Barton, E.R., Zhuo, J., Tomizawa, Y., Friesen, W.J., Trifillis, P., Paushkin, S., Patel, M., Trotta, C.R., Hwang, S., et al. (2007). PTC124 targets genetic disorders caused by nonsense mutations. *Nature* 447, 87–91.

Weston, J.A. (1963). A radioautographic analysis of the migration and localization of trunk neural crest cells in the chick. *Dev. Biol.* 6, 279–310.

Windebank, A.J., Wood, P., Bunge, R.P., and Dyck, P.J. (1985). Myelination determines the caliber of dorsal root ganglion neurons in culture. *J. Neurosci. Off. J. Soc. Neurosci.* 5, 1563–1569.

Wyatt, R.M., and Balice-Gordon, R.J. (2003). Activity-dependent elimination of neuromuscular synapses. *J. Neurocytol.* 32, 777–794.

Xu, J., Xiao, N., and Xia, J. (2010). Thrombospondin 1 accelerates synaptogenesis in hippocampal neurons through neuroligin 1. *Nat. Neurosci.* 13, 22–24.

Zhang, J., Talbot, W.S., and Schier, A.F. (1998). Positional cloning identifies zebrafish one-eyed pinhead as a permissive EGF-related ligand required during gastrulation. *Cell* 92, 241–251.

Zhou, Q., and Anderson, D.J. (2002). The bHLH Transcription Factors OLIG2 and OLIG1 Couple Neuronal and Glial Subtype Specification. *Cell* 109, 61–73.

Zhou, F., Leder, P., Zuniga, A., and Dettenhofer, M. (2009). Formin1 disruption confers oligodactylism and alters Bmp signaling. *Hum. Mol. Genet.* 18, 2472–2482.

Zubrzycka-Gaarn, E.E., Bulman, D.E., Karpati, G., Burghes, A.H.M., Belfall, B., Klamut, H.J., Talbot, J., Hodges, R.S., Ray, P.N., and Worton, R.G. (1988). The Duchenne muscular dystrophy gene product is localized in sarcolemma of human skeletal muscle. *Nature* 333, 466–469.